

ACTIVITIES IN MOLTEN SILICATES

A thesis presented for the
Diploma of the Imperial College of Science and Technology

by

Ram Autar SHARMA

February, 1963

TABLE OF CONTENTS

ABSTRACT

I INTRODUCTION

General	1
Relevant Previous Work	
A. Sulphur in Aluminate and Silicate Melts	
(i) Sulphide capacities	3
(ii) Limiting solubilities of sulphur and activities in crystalline lime and lime-alumina and lime-silica melts.	9
B. Activities of Manganese Oxide in Aluminate and Silicate Melts.	14

II APPROACH ADOPTED IN THE PRESENT WORK

A. Sulphur Equilibrium Between the Melts and Gas Phase.	
(i) Sulphide capacities	19
(ii) Limiting solubilities of sulphur and activities in crystalline lime and lime-alumina and lime-silica melts.	21
B. Activities of Manganese Oxide in Aluminate and Silicate Melts.	26

III EXPERIMENTAL METHODS

1. Apparatus	28
2. Preparation of materials	35
3. Procedure	36
4. Analytical method	40
5. Note on thermal diffusion	42

Errors	44
IV <u>RESULTS</u>	
General	46
A. Sulphur in Aluminate and Silicate Melts and Crystalline Oxides.	
(i) Sulphide capacities	48
(ii) Limiting solubilities of sulphur and activities in crystalline lime and lime- alumina and lime-silica melts.	55
B. Activities of Manganese Oxide in Aluminate and Silicate Melts.	64
Activity Coefficients of Sulphides in Aluminate and Silicate Melts.	67
V <u>DISCUSSION</u>	
A. Sulphur in Aluminate and Silicate Melts and Crystalline Oxides.	
(i) Sulphide capacities.	73
(ii) Limiting solubilities of sulphur and activities in crystalline lime and lime- alumina and lime-silica melts.	85
B. Activities of Manganese Oxide in Aluminate and Silicate Melts.	106
Activity Coefficients of Sulphides in Aluminate and Silicate Melts.	110
Results in Relation to Ideal Mixing Theory of Silicate Melts.	114
<u>APPENDIX</u>	
Calculation of Partial Pressures of Gasses.	120
<u>ACKNOWLEDGEMENTS</u>	136
<u>REFERENCES</u>	137

Abstract

The Sulphide capacity, $C_s = \text{Wt. \% S} \left(\frac{P_{O_2}}{P_{S_2}} \right)^{\frac{1}{2}}$, has been determined for the melts, $\text{MnO} + \text{Al}_2\text{O}_3$, $\text{MgO} + \text{SiO}_2$, $\text{Al}_2\text{O}_3 + \text{SiO}_2$, $\text{MnO} + \text{MgO} + \text{SiO}_2$, $\text{MnO} + \text{SiO}_2 + \text{Al}_2\text{O}_3$, $\text{MgO} + \text{SiO}_2 + \text{Al}_2\text{O}_3$ and pure crystalline CaO , MgO , Al_2O_3 and SiO_2 , at 1650°C , by establishing the equilibrium between a gas phase of known oxygen and sulphur potentials and the sample. C_s was found to decrease with decreasing basic oxide concentration in the melt and at constant N_{SiO_2} , to decrease from one binary to the next in the order $\text{MnO} + \text{SiO}_2 > \text{MgO} + \text{SiO}_2 > \text{Al}_2\text{O}_3 + \text{SiO}_2$. The results obtained for the $\text{MnO} + \text{MgO} + \text{SiO}_2$ melts were used to check the validity of Flood's Equation which was supported by them in the range of composition studied.

Saturation limits of sulphur in crystalline lime at 1650°C and in lime-alumina and lime-silica melts at 1500°C were measured by equilibrium studies of the reaction:



The activity coefficient of calcium sulphide, calculated from the saturation limits, was found to be 1600 at N_{CaS} of 0.00063 in crystalline lime, while it ranges from 72.5 to 28.0 between 0.43 and 0.30 $N_{\text{Al}_2\text{O}_3}$ in the lime-alumina melts and from 8.5 to 17.3 between 0.58 and 0.42 N_{SiO_2} in lime-silica. The activities derived from the calcium

sulphide saturation limits in lime-alumina melts agree well with the free energies of formation of crystalline aluminates, and in lime silica melts with those of crystalline meta- and ortho-silicates. The free energies of formation, obtained from the activity data for lime-silica melts, together with those of $\text{MnO} + \text{SiO}_2$ and with those of $\text{FeO} + \text{SiO}_2$, were used to calculate the free energies of formation of silicates for the ternaries $\text{MnO} + \text{CaO} + \text{SiO}_2$ and $\text{FeO} + \text{CaO} + \text{SiO}_2$ respectively, using the ideal mixing theory. They were compared with experimental values. Good agreement in the meta-silicate region and negative deviation in the ortho-silicate region were observed.

Activity coefficients of sulphides in the melts $\text{MnO} + \text{Al}_2\text{O}_3$, $\text{MgO} + \text{SiO}_2$, $\text{MnO} + \text{SiO}_2 + \text{Al}_2\text{O}_3$ and $\text{CaO} + \text{SiO}_2 + \text{Al}_2\text{O}_3$ were also derived from the relevant activity and sulphide capacity data. The activity coefficient was seen to increase with decrease in integral free energy of formation of the melt and was maximum at the minimum in ΔG° curve.

The activity of manganese oxide in $\text{MnO} + \text{Al}_2\text{O}_3$ and $\text{MnO} + \text{SiO}_2 + \text{Al}_2\text{O}_3$ systems at 1650°C was measured by equilibration of manganese between the melt and a thin platinum coil embedded in it, in an atmosphere of known oxygen partial pressure. The activity in $\text{MnO} + \text{SiO}_2 + \text{Al}_2\text{O}_3$ melts was found to be constant at constant mole fraction of manganese oxide.

INTRODUCTION

General

Metallurgical slags, the most important solvents of the pyrometallurgist, play a significant role in the extraction and refining of metals. They are used to collect waste products in the former and extract impurities in the latter. The potential efficiency of these processes is dependent on the thermodynamic properties of these slags, the knowledge of which, therefore, is imperative and useful to obtain. The smelter or the refiner may also utilise this knowledge of thermodynamics, as an aid in process control, to predict the way in which his slag metal equilibria will be influenced by changes in composition, in temperature and in oxygen and sulphur partial pressures. The academic chemist may be guided for his atomic models by the measure of binding energy between two atoms or groups of atoms from enthalpy changes (ΔH), and by the distribution of these atoms or groups of atoms with respect to each other from the entropy changes (ΔS).

The present work was designed to study the thermodynamics of solutions of sulphides and oxides in aluminate and silicate melts. The simple binary and ternary melts were selected for study to gain the basic understanding upon which the chemistry of more complex systems such as metallurgical slags may be built.

The chemical behaviour of sulphur in iron and steel-making has long been a subject of research to better the control of sulphur in the finished product. A large amount of data has also been reported on the desulphurizing powers of slags, but most of this has been obtained from the measurement of the partition of sulphur between the metal and slag. Only recently the sulphur holding capacities of slags have been determined by studying the equilibrium between the melt and the gas phase (1 - 8). This technique has been employed here to derive the sulphur holding capacities of some slags over a wide range of compositions, the limiting solubilities of sulphur and activities in aluminate and silicate melts. The solid solubility of calcium sulphide in crystalline lime and the sulphur holding capacities of crystalline calcium, magnesium, aluminium and silicon oxides have also been measured.

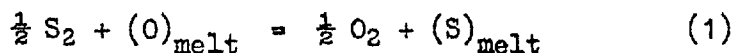
Relevant Previous Work

A. Sulphur in Aluminate and Silicate Melts.

(i) Sulphide capacities

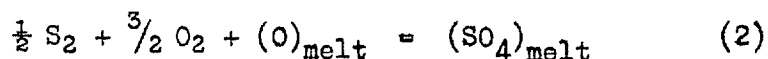
Fincham and Richardson^{1,2} studied the equilibrium of sulphur and oxygen between melts and the gas phase by the same technique as that used in this work. The melts used by these authors were mixtures of CaO + SiO₂, MgO + SiO₂, FeO + SiO₂ and CaO + Al₂O₃. They made a detailed study of the effects of temperature, oxygen potential in the gas phase and melt composition on the gas-slag equilibrium.

The main conclusions from this work were that, when the oxygen partial pressure is less than about 10⁻⁵ atm., a sulphur atom can only enter the melt by displacing a suitable oxygen atom. The sulphur is then held in the melt entirely as sulphide, its concentration being controlled by the equilibrium:-



This equilibrium moves to the right with increasing temperature.

However, when the oxygen pressure is greater than about 10⁻³ atm., the sulphur is held in the melt as sulphate according to the equilibrium:-



The equilibrium moves to the left with increasing temperature.

Davies³, using the same technique, investigated the equilibrium of oxygen and sulphur between the gas phase and silicate melts consisting of CaO + SiO₂, MgO + SiO₂, CaO + MgO + SiO₂, MnO + SiO₂ and CaO + MnO + SiO₂. His work also showed that, at oxygen partial pressures of approximately 10⁻⁶ to 10⁻⁷ atm., the transfer of sulphur proceeded according to the equilibrium reaction (1).

The sulphide capacities of binary MnO + SiO₂ and ternary CaO + MnO + SiO₂ melts determined at 1500°C, 1575°C and 1650°C, were found to increase with temperature. These results were also used to check the validity of Flood's equation.⁹ This equation is a relation between the equilibrium constants K'_{AB} , K'_A and K'_B for the reaction (1) at constant silica mole fraction for a ternary system AO + BO + SiO₂ and binary systems AO + SiO₂ and BO + SiO₂ respectively. AO and BO are basic oxides. Flood's derivation leads to the equation:

$$\log K'_{AB} = N_{A^{++}} \log K'_A + N_{B^{++}} \log K'_B$$

where $N_{A^{++}}$ and $N_{B^{++}}$ are the ionic fractions of the cations A⁺⁺ and B⁺⁺ in the melt. This equation involves the assumption that ΔS for the reaction (1) is independent of cation concentration, and

$$\Delta H = N_{A^{++}} \Delta H_A + N_{B^{++}} \Delta H_B$$

Reasonable agreement with the predictions of Flood's equation was found in the CaO + MgO + SiO₂ system, whereas little agreement was observed in the CaO + MnO + SiO₂ system.

Abraham,^{6,8} by a similar method, determined the sulphide capacities of the following mixtures: $\text{MnO} + \text{SiO}_2$, $\text{CaO} + \text{P}_2\text{O}_5$, $\text{CaO} + \text{SiO}_2 + \text{P}_2\text{O}_5$, $\text{CaO} + \text{Al}_2\text{O}_3 + \text{P}_2\text{O}_5$ and $\text{CaO} + \text{MgO} + \text{SiO}_2 + \text{Al}_2\text{O}_3$. The results for $\text{MnO} + \text{SiO}_2$ at 1500°C and 1650°C indicated that the sulphide capacity increased with increasing temperature and manganese oxide concentration and decreasing SiO_2 concentration in the melts.

Abraham also observed during the measurements of C_s in the melts containing P_2O_5 that the platinum cups are unsuitable as containers. Iridium cups are found satisfactory for these melts. The P_2O_5 volatilised from the melts at the temperature of the experiment. On account of this, measurements could be made with $\text{CaO} + \text{P}_2\text{O}_5$ mixtures containing up to 0.27 mole fraction P_2O_5 only; with the $\text{CaO} + \text{SiO}_2 + \text{P}_2\text{O}_5$ and $\text{CaO} + \text{Al}_2\text{O}_3 + \text{P}_2\text{O}_5$ mixtures the maximum was 0.07 mole fraction of P_2O_5 . By a comparison of the values of C_s for $\text{CaO} + \text{Al}_2\text{O}_3$, $\text{CaO} + \text{SiO}_2$ and $\text{CaO} + \text{P}_2\text{O}_5$ melts, it could be shown that on a mole for mole basis the addition of P_2O_5 to lime leads to much lower sulphide capacities than the addition of Al_2O_3 or SiO_2 . It was also observed from the sulphide capacities for the systems $\text{CaO} + \text{Al}_2\text{O}_3 + \text{SiO}_2$, $\text{CaO} + \text{SiO}_2 + \text{P}_2\text{O}_5$ and $\text{CaO} + \text{Al}_2\text{O}_3 + \text{P}_2\text{O}_5$ that the substitution of phosphorus pentoxide for silica or alumina greatly lowers the sulphide capacity, the effect being greater with silica than with Al_2O_3 .

The results obtained with $\text{CaO} + \text{SiO}_2$ and $\text{CaO} + \text{SiO}_2 + \text{P}_2\text{O}_5$ and with $\text{CaO} + \text{Al}_2\text{O}_3$ and $\text{CaO} + \text{Al}_2\text{O}_3 + \text{P}_2\text{O}_5$ indicated that one mole of P_2O_5 is equivalent to 2.2-2.3 mole of silica or 1.5 - 1.75 mole of alumina in lowering the sulphide capacity of a melt.

The results obtained for $\text{CaO} + \text{MgO} + \text{Al}_2\text{O}_3 + \text{SiO}_2$ melts at 1500°C showed that the substitution of MgO for CaO or of SiO_2 for Al_2O_3 (mole for mole) leads to lower sulphide capacities. This observation was at variance with the work of Osborn¹⁰ et al., who stated that the sulphur partitions are determined solely by the wt % ratio $\frac{\text{CaO} + \text{MgO}}{\text{SiO}_2 + \text{Al}_2\text{O}_3}$ and that, provided this ratio is constant, the sulphide capacities are unaffected by the alumina content. When the sulphide capacity of one of the slags of composition 30% SiO_2 , 43% CaO , 12% MgO and 15% Al_2O_3 by weight, was compared in the laboratory with that of a normal blast furnace type slag containing 31.8% SiO_2 , 42.2% CaO , 2.5% MgO and 19% Al_2O_3 by weight, the two C_s values were in ratio 2.2 : 1, while in practice the ratio of two partition ratios was 4 : 1. The explanation given for this was that the equilibrium distribution of sulphur is more closely approached on industrial scale with the high magnesia slags than with more ordinary types, possible because of their lower viscosity.

Carter and Macfarlane⁵ investigated the equilibrium between $\text{CO} + \text{CO}_2 + \text{SO}_2$ gas mixtures and melts consisting of lime-silica and lime-alumina at 1500°C . The C_s values calculated for their results are in agreement with those measured in the present work (see later).

St. Pierre and Chipman⁴ studied the effect of composition changes on the sulphur capacity of slags by equilibration with a gas mixture of SO_2 to CO ratio = 34.1. The compositions studied included pure iron oxide, iron oxide containing lime up to saturation and lime-silica-iron oxide slags with molar ratios of lime to silica of 2.24, 1.28 and 0.52. According to these workers, for a fixed silica content, the sulphide capacity is independent of the relative amounts of lime and iron oxide over the range of composition studied. Further, at high silica contents, the value is also independent of silica concentration. Abraham reports that the results in the $\text{MnO} + \text{CaO} + \text{SiO}_2$ melts³ are in disagreement with the findings of St. Pierre and Chipman in the region where comparison was possible.

Dewing and Richardson¹¹ gave a more reliable value for the dissociation energies of SO and S_2 than those used earlier by Fincham and Richardson¹ and Davies and Richardson³. Abraham used these new values for the calculation of P_{O_2} and P_{S_2} which were found to be significantly different from those of Fincham and Richardson and Davies and Richardson. As a result of this

he revised the C_s values reported earlier using these new values of P_{O_2} and P_{S_2} . The validity of Flood's equation⁹ was tested for the pseudo binaries $MnOSiO_2 + CaOSiO_2$ and $MgOSiO_2 + CaOSiO_2$. Agreement with prediction made by the equation was good for the pseudo binary $MgOSiO_2 + CaOSiO_2$ and approximate for $MnOSiO_2 + CaOSiO_2$.

(ii) Limiting solubilities of sulphur and activities in crystalline lime and lime-alumina and lime-silica melts.

(a) Solubility of sulphur in crystalline lime and lime-alumina and lime-silica melts.

St. Pierre and Chipman⁴ equilibrated two samples of powdered lime with a gas mixture containing $\text{SO}_2/\text{CO} = 34.1$ at 1550°C . One sample contained 8.9% sulphur by weight added as calcium sulphide, and the other had no sulphur initially. They reported a solid solubility of calcium sulphide of 1.42 mole percent in calcium oxide at 1550°C .

MacCaffery and Oesterle¹² measured the solubility of calcium sulphide in ternary lime-alumina-silica melts by constructing phase diagrams for the pseudo-binary systems calcium sulphide-oxide mixtures from cooling curves. They found that solubility is more dependent on temperature than on composition. At 1500°C the solubility corresponded to about 8% of sulphur for acid melts and 11% of sulphur for more basic melts.

Glaser¹³ found the solubility of calcium sulphide in a pure calcium meta silicate (CaSiO_3) melt to correspond to 5.5% of sulphur at 1500°C . A region of liquid immiscibility was found at higher sulphur contents and temperatures.

Filler and Darben¹⁴, using a blast furnace slag containing lime, magnesia, alumina and silica (with also a small amount of manganese oxide), found the solubility of calcium sulphide to correspond to between 3.5 - 4.5% of sulphur at 1500°C.

(b) Activities in lime-alumina melts

Activities in lime + alumina melts, estimated in different ways, have been reported by Fincham and Richardson¹, Carter and Macfarlane⁵ and Chipman¹⁵. In the first two methods use was made of measured sulphide capacities defined as

$$C_s = \text{wt \% S} \left(\frac{p_{O_2}}{p_{S_2}} \right)^{\frac{1}{2}}$$

In the third, the lime activities were deduced by combining thermal data for crystalline aluminates with the sulphide capacity data.

The uncertainties of all these estimates arise from a lack of knowledge of activity coefficients of calcium sulphide in the melts. Fincham and Richardson¹ assumed a value of 5 for the solid sulphide, in all the melts at 1650°C. Carter and Macfarlane⁵ found the C_s values at 1500°C for the slag 60.6 wt % CaO, 32.4 wt % Al₂O₃, 7 wt % SiO₂ and for a series of CaO + Al₂O₃ mixtures. From the CaO + Al₂O₃ + SiO₂ phase diagram¹⁶ it is known that the lime activity in the first melt is unity at 1500°C. If it is assumed that the activity coefficient of CaS is the same

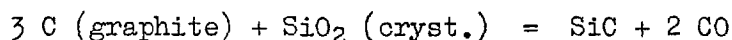
in all the melts investigated, one can write

$$a_{\text{CaO}} = \frac{C_s}{C_s^1}$$

where C_s denotes the sulphide capacity of the lime + alumina slag and C_s^1 that of the standard slag in which the lime activity is one. This assumption is almost certainly in error, for it has been shown recently⁷ that the activity coefficient of manganese sulphide in $\text{MnO} + \text{SiO}_2$ melts⁷ increases by a factor of at least 3 as the mole fraction of MnO falls from 0.72 to 0.48.

(c) Activities in lime-silica melts.

The published data on activities in the system lime + silica are conflicting. Kay and Taylor¹⁷ measured the activity of silica by means of the equilibrium

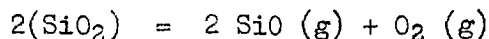


In the presence of both graphite and SiC, the activity of silica is proportional to the square of the pressure of carbon monoxide. They first measured the CO pressures in the presence of pure silica and then in slags of varying SiO_2 concentrations, making adequate correction for the partial pressure of SiO. The silica activities were obtained by the relation

$$a_{\text{SiO}_2} = \frac{(P_{\text{CO}}^2)^2}{(P_{\text{CO}}^1)^2}$$

where P_{CO}^1 and P_{CO}^2 are the partial pressures of CO in the presence of pure silica and over the melt respectively.

Young et al.¹⁸ determined the silica activities in the liquidus of the CaO + SiO₂ system at 1627°C, by using the effusion method for measuring the pressures of SiO and O₂ above the melt and above pure cristobalite. From the consideration of the equation

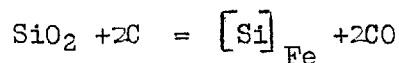


it can be seen that

$$a_{\text{SiO}_2} = \sqrt{p_{\text{SiO}}^2 p_{\text{O}_2} / p_{\text{SiO}}'^2 p_{\text{O}_2}'}$$

where primes refer to the pressures above pure cristobalite and absence of primes is above the melt in question. Allowance was made for oxygen atoms in the gas phase at the temperature of the experiment.

Langenberg, Kaplan and Chipman¹⁹ obtained the silica activities by the distribution of silicon between graphite-saturated Fe-C-Si alloys and slag containing silica. The following equilibrium was carried out in graphite crucibles in CO at one atmosphere:



where $[\text{Si}]_{\text{Fe}}$ is the amount of silicon in Fe-C-Si alloy. When the melts were made under one atmosphere CO, and were graphite-saturated, then the equilibrium constant K reduces to

$$K = \frac{a_{[\text{Si}]_{\text{Fe}}}}{a_{\text{SiO}_2}}$$

The activities of silica were obtained from the equilibrium data, the activity of silicon in Fe-C-Si alloys and the free energy change of the reaction.

Carter and Macfarlane²⁰ calculated the calcium oxide activities in CaO + SiO₂ melts at 1500°C by measuring the sulphide capacities of a standard lime saturated CaO + SiO₂ + Al₂O₃ slag and CaO + SiO₂ melts. They assumed the activity coefficient of calcium sulphide to be equal to 16 in the standard slag and 12 in all other melts. Lime activities obtained by the relation

$$a_{\text{CaO}} = \frac{12 C_s}{16 C_b}$$

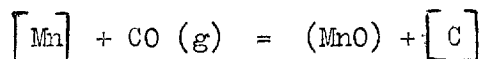
where C_s is the sulphide capacity of the standard slag and C_b is that of any other melt.

Richardson²¹ derived the activities in CaO + SiO₂ melts at 1600°C using the available thermodynamic data of the calcium silicates and CaO - SiO₂ phase diagram.

Sanbongi and Omori²² obtained the silica activities by the measurement of reversible e.m.f. in a double cell.

B. Manganese Oxide Activities in Aluminate and Silicate Melts.

Turkdogan²³ has calculated the activity coefficients of manganese oxide in quaternary $\text{CaO} + \text{Al}_2\text{O}_3 + \text{SiO}_2 + \text{MnO}$ melts from the experimental results of Stuckel and Cocubinsky²⁴, who determined the distribution of manganese between blast-furnace type slag and metal by equilibrating these two phases in a graphite crucible at one atmosphere of CO . If the activity of manganese in carbon-saturated iron is known, that of manganese oxide in the melt can be calculated from the available data on the free energy change of the reaction



$$K = \frac{a_{(\text{MnO})}}{a_{[\text{Mn}]}}$$

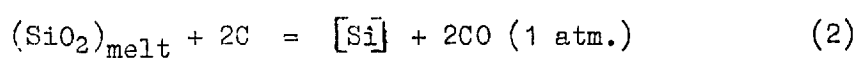
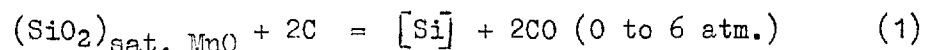
The activity coefficient of manganese in carbon-saturated iron was not known and so it was taken as being approximately equal to that of iron in carbon-saturated iron. It was also assumed that, in carbon-saturated Fe-Mn melts, small percentages of manganese would not affect the activity coefficient of iron.

Activity coefficients were calculated from the manganese oxide activities so obtained in the quaternary melts and plotted for the pseudo ternary system $\text{CaO} + \text{Al}_2\text{O}_3 + \text{SiO}_2$

containing 5% by weight of manganese oxide. The following conclusions were made from these plots:

- (i) For a given CaO content γ_{MnO} increases as alumina is replaced by SiO_2
- (ii) For a given SiO_2 content γ_{MnO} increases as alumina is replaced by lime
- (iii) For a given alumina content γ_{MnO} increases as SiO_2 ~~alumina~~ is replaced by lime at low CaO/ SiO_2 ratios, but at higher basicities, further increase in lime content of the slag at the expense of silica decreases γ_{MnO} .

Turkdogan and Hancock²⁵ determined the silica activities in the binary MnO + SiO_2 system by measuring the amounts of silica reduced into carbon-saturated manganese from the binary silicates at one atmosphere of CO, and from silica-saturated melts at CO pressures ranging from 0 to 6 atmospheres



$$a_{\text{SiO}_2} = \frac{P_2^2 \text{CO}}{P_1^2 \text{CO}}$$

where P_1^{CO} and P_2^{CO} are the pressures of CO in equilibrium with Mn-C-Si alloys of equal silicon concentration in the two cases. They determined the silica activities at 1350°C, 1400°C and 1450°C. The activities were seen to increase below and decrease above 0.49 mole fraction of silica with increase in temperature. In fact the activity curves were found to cross over at about 0.49 mole fraction.

Davies³ measured the activities of manganese oxide in binary MnO + SiO₂ and ternary CaO + MnO + SiO₂ melts at 1500°C, 1575°C and 1650°C. The activities in the binary MnO + SiO₂ melts showed a pronounced deviation from Raoult's law except at high manganese oxide contents. Silica activities, calculated by the application of Gibbs-Duhem equation, and the free energy of formation of binary manganous oxide-silica melts, derived from the activities, were also reported.

Davies, by correlating the manganese oxide activities in the ternary system with the sulphide capacities in these melts, found a definite connection between the metal oxide activity and the sulphide capacity of the melt.

Abraham⁶ redetermined the manganese oxide activities in the binary MnO + SiO₂ and the ternary MnO + CaO + SiO₂ melts at 1500°C and 1650°C. This was because Abraham and Barton^{26,27} disagreed on the data for pure manganese oxide, which were to be used in the calculation of manganese oxide activities described later. After necessary correction in the data for pure manganese oxide, Davies⁷ results agreed with those of Abraham. It was also observed, from the results of MnO + SiO₂ and CaO + MnO + SiO₂ melts, that the manganese oxide activities decreased with temperature, while Turkdogan reports that a_{MnO} in MnO + SiO₂ melts increases below and decreases above 0.049 mole fraction of silica with temperature.

The results of MnO + CaO + SiO₂ melts have been also used to test the validity of the ideal mixing theory²⁷ (see Discussion). Reasonable agreement between the calculated values and measured ones in the meta-silicate region and negative deviations in the orth-silicate region were observed.

Abraham³ also determined the manganese oxide activities at 1650°C in CaO + MnO + SiO₂ + Al₂O₃ melts in the range of compositions of interest to blast furnace and open hearth operators. γ_{MnO} was observed to be constant up to 8 wt % of MnO in these melts at constant ratios of CaO : SiO₂ : Al₂O₃ 52.0-30.0; 37.2-63.3; 10.8-6.7. The following conclusions were drawn from the results obtained for the melts, each of which contained 5 wt % MnO.

- (i) For a given CaO content, γ_{MnO} decreased as Al₂O₃ was replaced by SiO₂.
- (ii) For a given SiO₂ content, γ_{MnO} increased as Al₂O₃ was replaced by CaO.
- (iii) For a given Al₂O₃ content, γ_{MnO} increased as SiO₂ was replaced by CaO at all CaO/SiO₂ ratios.
- (iv) At low lime-silica ratios, the addition of alumina at constant CaO/SiO₂ ratios, increased the MnO activity coefficients, whereas, when this ratio is about one, the addition of Al₂O₃ to the melt, did not have any appreciable effect on the activity coefficient.

The conclusions (i), (iii) and (iv) are in disagreement with those of Turkdogan²³. The values of the MnO activity coefficients also differed by a factor of ten from those reported by Turkdogan.

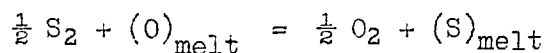
Filer and Darken¹⁴ measured the partition of manganese between blast-furnace slag and metal by bringing the two into equilibrium in the presence of carbon. The slag compositions were 0.11-0.46 wt % MnO, 2-6 wt % MgO, 31-34 wt % SiO₂ and 13-15 wt % Al₂O₃. The activity coefficient of manganese oxide, calculated on the assumption that γ_{Mn} is equal to γ_{Fe} in carbon-saturated iron was in reasonable agreement with that obtained by Abraham from his results.

Approach Adopted in the Present Work

A. Sulphur Equilibrium Between the Melt and Gas Phase.

(i) Sulphide capacities

Fincham and Richardson¹ have shown that, when a silicate melt is equilibrated with a gas phase of known oxygen and sulphur partial pressures, if the oxygen partial pressure is less than 10^{-5} atm. then the sulphur atom enters the melt by displacing a suitable oxygen atom. The sulphur atom is held as sulphide according to the equation



$$K = \frac{(S) P_{O_2}^{\frac{1}{2}}}{(O) P_{S_2}^{\frac{1}{2}}}$$

It can be assumed that the activity of replaceable oxygen in the melt is not significantly altered by the substitution of small amounts of sulphur and that for low concentrations of sulphur the activity of sulphur (S) is proportional to the sulphur concentration, then the quantity $\text{wt } \% S (P_{O_2}/P_{S_2})^{\frac{1}{2}}$ defined as sulphide capacity C_s of a melt remains constant at given temperature.

The experimental technique consisted of bringing the melts, contained in platinum cups, into equilibrium with a gas phase of known oxygen and sulphur potentials at the desired temperature. The sulphur in the melt, after quenching, was analysed at the end of the experiment. The gas phase was made

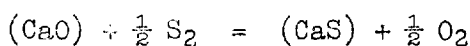
by mixing nitrogen, carbon dioxide, hydrogen and sulphur dioxide in calculated proportions. This mixture established the required sulphur and oxygen pressures at the temperature of the experiment. The calculations for p_{O_2} and p_{S_2} are given in the Appendix. Details of the apparatus used and experimental procedure are given later.

In the present work the sulphide capacities of the melts $MnO + Al_2O_3$, $MgO + SiO_2$, $Al_2O_3 + SiO_2$, $MnO + Al_2O_3 + SiO_2$, $MnO + MgO + SiO_2$, $MgO + SiO_2 + Al_2O_3$ and pure CaO , MgO , SiO_2 and Al_2O_3 were determined at $1650^\circ C$ by the technique described above.

II Limiting Solubilities of Sulphur and Activities
in Crystalline Lime and Lime-alumina and Lime-
silica Melts.

(a) Crystalline lime and lime-alumina melts

The limiting solubilities of sulphur in crystalline lime and lime-alumina melts could be determined by considering the equation



$$K = \frac{a_{\text{CaS}}}{a_{\text{CaO}}} \left(\frac{p_{\text{O}_2}}{p_{\text{S}_2}} \right)^{\frac{1}{2}} \quad (1)$$

when $(\frac{p_{\text{S}_2}}{p_{\text{O}_2}})^{\frac{1}{2}}$ is increased, a_{CaS} or wt % sulphur in crystalline lime or in the melt should also increase (provided a_{CaO} does not change appreciably). Beyond this limit, when a_{CaS} is unity, if $(\frac{p_{\text{S}_2}}{p_{\text{O}_2}})^{\frac{1}{2}}$ is slightly increased, wt % sulphur will increase markedly. This will continue to increase until the a_{CaO} has been sufficiently lowered to establish equilibrium again. This happens because CaO is consumed in conversion to CaS in the melt. If log wt % sulphur in the melt is plotted against $(\frac{p_{\text{S}_2}}{p_{\text{O}_2}})^{\frac{1}{2}}$, a smooth curve with a sudden discontinuity (Fig. 8) is obtained. The discontinuity is caused by the formation of CaS in the second phase. This point of discontinuity will give the sulphur in the melt at saturation at that particular $(\frac{p_{\text{S}_2}}{p_{\text{O}_2}})^{\frac{1}{2}}$ ratio.

In the actual procedure, the ratio $\frac{P_{H_2(i)}}{P_{CO_2(i)}}$ is plotted against log wt % sulphur (Fig. 8), since this is directly related to $(P_{S_2}/P_{O_2})^{\frac{1}{2}}$ (see Appendix).

The saturation limits of sulphur in crystalline lime at 1650°C and in lime-alumina melts at 1500°C were obtained by this technique. The gas mixture used consisted of N₂, H₂, CO₂ and SO₂. More details of the procedure are given on page 85.

Lime activities in CaO + Al₂O₃ melts, saturated with sulphur, can be derived from the relation (1) using the experimental values of $(P_{S_2}/P_{O_2})^{\frac{1}{2}}$ and the value of K derived from the data.^{28, 29, 30} The activities in the binary CaO + Al₂O₃ melts were obtained from the corresponding values in the ternary on the assumption that a_{CaO} is dependent only on CaO to Al₂O₃ ratio when only a small amount of CaS is present. Further details are given on page 87.

(b) Lime-silica melts

Lime-silica melts, unlike the lime-alumina melts, under the conditions described in the previous section, did not show sharp increases in wt % sulphur or N_{CaS} when the limits of CaS solubility were exceeded. This was because the activities of lime in the silicates are much lower than in the corresponding aluminates and fall more rapidly as CaS is produced by the sulphurizing gas mixture at the expense

of CaO. Thus, even when the ratio P_{S_2}/P_{O_2} for the gas substantially exceeds that for equilibrium with both melt and free CaS, the melt does not need to lose much of its lime as solid sulphide before its lime activity becomes sufficiently low for the equilibrium with free CaS and gas to be re-established.

The gas mixture N_2 , H_2 , CO_2 and SO_2 did not produce sufficiently high sulphur to oxygen potential ratios to saturate the $CaO + SiO_2$ melts with sulphur. A different gas mixture of N_2 , H_2 , CO_2 and H_2S was found and used. This gas mixture gave the required sulphur to oxygen partial pressure ratios for all the melts studied.

The gas mixtures used herein were more reducing than those previously used. SiO_2 was reduced into the platinum cups, giving low melting alloys of Pt-Si, and thus making platinum an unsuitable material for containers. Iridium cups were therefore used; they behaved well under experimental conditions.

Sulphur saturation limits in these melts were obtained by a graphical method as follows:

The compositions of the melts, after the experiment, having the constituents CaO , SiO_2 and CaS were plotted on a ternary graph. Consider the relation (1) again. In a homogeneous melt, along any line of constant CaO to SiO_2 ratio

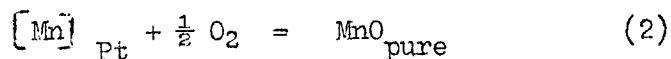
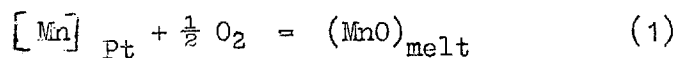
on this ternary diagram N_{CaS} should increase with the increase in $(P_{S_2}/p_{O_2})^{\frac{1}{2}}$ ratio. Calculations based on the thermodynamical data for CO_2 , H_2S , H_2O , S_2 and $S^{28, 31}$ have shown that the $(P_{S_2}/p_{O_2})^{\frac{1}{2}}$ ratio is proportional to P_{H_2S}/p_{CO_2} as shown in Figure 38. Thus, for a melt of constant lime to silica ratio, N_{CaS} should increase with P_{H_2S}/p_{CO_2} , being zero when P_{H_2S} is zero. At and beyond the point where free CaS is produced, the composition of the remaining melt, and hence of the gas, should remain constant. Now along this line of constant lime to silica ratio the plot of $\frac{P_{H_2S}}{p_{CO_2}}$ against N_{CaS} increases at first and then becomes constant; the point at which this change occurs will give the N_{CaS} in the melt at saturation at that particular P_{H_2S}/p_{CO_2} ratio. Due to the difficulty of getting the final compositions along the constant lime to silica ratio, the actual experiments were conducted to get the final compositions along constant mole fraction of silica in the melt. Further details of the procedure by which the compositions of the melts along a constant lime to silica ratio were obtained from the above experimental results by interpolations and the derivation of the subsequent solubility limits from them are given on page 94.

Activities of lime in the ternary $CaO + SiO_2 + CaS$ melts at CaS saturation were determined by the relation (1) from the value of K obtained from the data^{28, 29, 30} and the

experimental values of $(P_{S_2}/P_{O_2})^{1/2}$. The lime activities in the binary CaO + SiO₂ melts were obtained from them on the assumption that γ_{CaO} remains constant with constant lime to silica ratio. More details are given on page 96.

B Manganese Oxide Activities in Aluminate and Silicate Melts.

The activity of manganese oxide in each of the aluminate and silicate melts was determined from the amount of manganese reduced into a thin platinum coil embedded in the melt, when the latter reached equilibrium with the coil at a given oxygen pressure and temperature. Consider the following reactions:



From (1) and (2)

$$a(\text{MnO}) = \frac{a'[\text{Mn}]_{\text{Pt}} p_{\text{O}_2}'^{\frac{1}{2}}}{a[\text{Mn}]_{\text{Pt}} p_{\text{O}_2}^{\frac{1}{2}}}$$

The primes refer to the activity and oxygen partial pressure for the melt and the absence of primes to those for pure manganese oxide.

$$a(\text{MnO}) = \frac{p_{\text{O}_2}'^{\frac{1}{2}}}{p_{\text{O}_2}^{\frac{1}{2}}}$$

when the compositions of Mn-Pt alloys are the same in both the cases.

Manganese oxide activities in the binary $\text{MnO} + \text{Al}_2\text{O}_3$ and ternary $\text{MnO} + \text{Al}_2\text{O}_3 + \text{SiO}_2$ melts at 1650°C were calculated by determining the compositions of Mn-Pt alloys for the various melts at oxygen partial pressure of 10^{-5} atm. The oxygen partial pressure of 10^{-5} atm. was obtained from a gas mixture of nitrogen, hydrogen and carbon dioxide in calculated proportions. (Calculations in Appendix). The required oxygen partial pressures corresponding to these Mn-Pt alloys in equilibrium with pure oxide were obtained from the relationship between equilibrium oxygen partial pressures and Mn-Pt alloy compositions for pure manganese oxide.⁶ (The actual plot is given in Appendix).

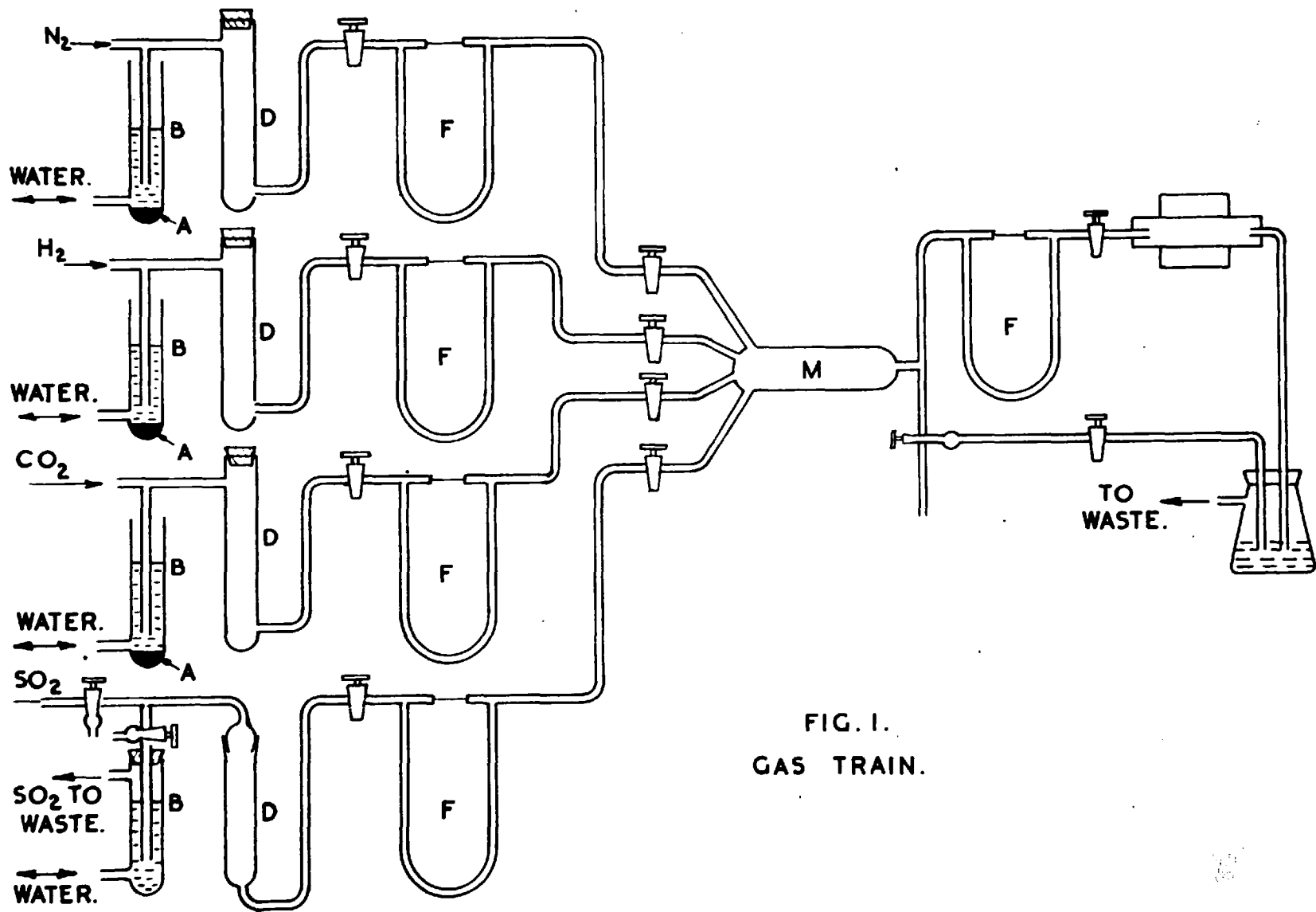


FIG. 1.
 GAS TRAIN.

III EXPERIMENTAL METHODS

1. Apparatus:

The apparatus used in all the experiments has been the same. Differences in technique will be discussed under "Procedure".

(a) Gas Train

(i) The gas train is shown diagrammatically in Fig. 1. It consists of four standard flow meters (F) for admitting the gases to the system. The gases came from cylinders and were maintained at constant pressure by means of "blow offs" (B) fitted on the in-going side of the flow meters. The "blow offs", in the preliminary experiments, contained water which was later on replaced by n-dibutyl phthalate. The gases passed through the drying towers (D). Carbon dioxide was dried by anhydrous magnesium perchlorate (anhydrone), and sulphur dioxide by anhydrous calcium chloride. When H_2S was used, it was purified by passing over iodine and then passing four times through water and drying again with $CaCl_2$. The drying towers for nitrogen and hydrogen contained "Sofnolite" (sodium hydroxide plus an indicator supported on an inert base) followed by anhydrone. The Sofnolite was meant to remove CO_2 . The gases after passing through the mixing chamber (M) (filled with pieces of broken glass) were led into the equilibrium furnace at a constant flow rate of 500 cc per minute and then to waste through a bubbler (O). The flow rates of the individual gases could

be varied by altering the heads of liquid in the "blow offs" (B). Each "blow off" except that for sulphur dioxide had a pool of mercury (A) in the bottom and could be raised, when not in use, to dip the tip of the inlet tube under the surface of mercury. This was done to stop the liquid being sucked back into the apparatus. The sulphur dioxide "blow off" was sealed off from the atmosphere to allow the "blow off" gas to be sent to the fume cupboard. A three way stop cock was incorporated which enabled the "blow off" to be isolated from the rest of the system. The number of joints was kept to a minimum and all joints and leads were made with pressure rubber tubing. The apparatus was regularly tested for gas tightness.

(ii) Gases:

Commercial gases of high purity were used. The (oxygen free) nitrogen and hydrogen contained 99.95% of N_2 and H_2 respectively, after drying and less than ten volumes per million of oxygen³¹. The carbon dioxide contained on the average 99.5% of CO_2 , the remainder being mainly air. The amount of air, however, could be as much as 1% in some cases³². The sulphur dioxide was about 99.8% pure. . While the H_2S used³³ in place of SO_2 was of initial 98.5% purity Its purity, checked by analysis, increased to more than 99% after purification.

(iii) Flow Meters:

Four capillary flow-meters (F) of the conventional pattern were used. Their manometers contained n-dibutyl phthalate. Each of them was calibrated by means of a "soap bubble" flow-meter by noting the time taken for the gas to sweep a soap film through a known volume. The reproducibility of the method was better than $\pm \frac{1}{2}\%$. However, it is not considered that the absolute accuracy of the flow meters so calibrated was better than $\pm 1\%$. The calibrations of the flow-meters were checked and necessary corrections were made before each experiment.

(b) Furnace:

A horizontal molybdenum wound furnace (Fig. 2) was used in all the experiments. The heating element (K) was molybdenum tape, 0.02 inch thick and $\frac{1}{8}$ inch wide. It was wound at approximately six turns per inch on recrystallised alumina tube (A) of about two feet long and two inches in diameter. The total resistance was nearly 0.6 ohm when cold. This tube (A) was sealed into the steel furnace casing (P) by means of a gland at either end, packed with asbestos string impregnated with graphite oil. The furnace case was filled with the alumina powder (L) for insulation. A slow stream of "forming" gas (90% N₂, 10% H₂) or cracked ammonia was passed through it to protect the molybdenum tape from oxidation. All joints and electrical leads (M) were

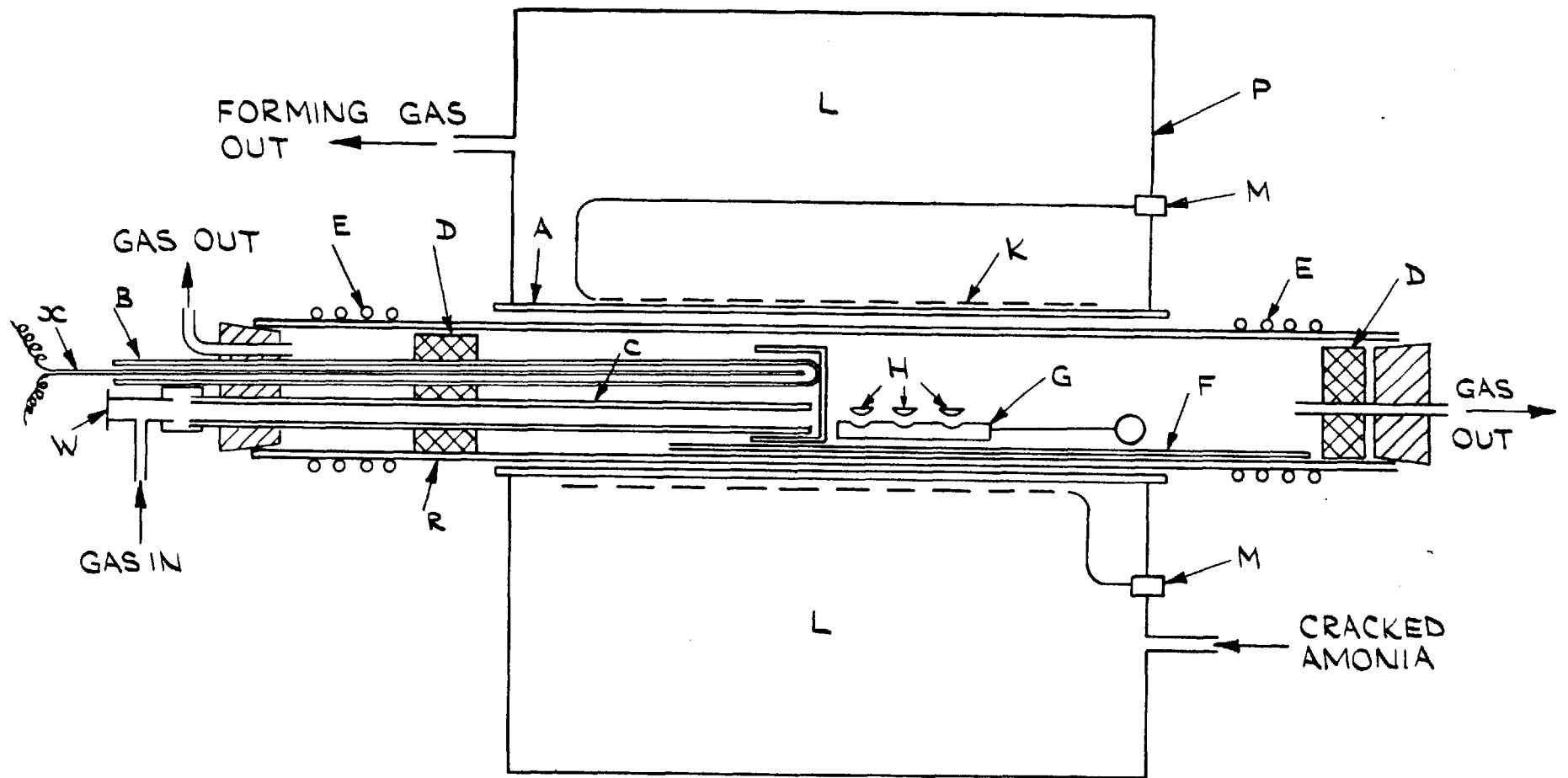


FIG.2. ARRANGEMENT IN EQUILIBRIUM FURNACE.

sealed with a calcium fluoride-sodiumsilicate. The reaction tube (R) of recrystallised alumina, three feet long and 1.3 inch diameter, was held in position in the furnace tube (A) by asbestos wool between the tubes, and by Jobilee clips on both ends. The ends were cooled by passing water through coils of compo tubing (E). The rubber bungs were protected by radiation shields (D) made of silica insulating brick. The furnace had a zone of 1.5 inch . over which the temperature was constant to within 5°C at 1500° - 1650°C.

The samples were contained in platinum or iridium cups (H) supported on an alumina tray (G). A platinum wire loop attached to one end of this tray, or a vertical hole on this end, enabled the tray to be pulled out of the hot zone along the alumina gutter (F). The gutter was a strip cut longitudinally from an alumina tube. It was designed to protect the main reaction tube, from being cracked, due to thermal shock during introduction and removal of the specimens. The gutter (F) was made of two equal halves. At the end of the experiment one half in the cooler part of the reaction tube was removed, cleaned together with the tube, and was placed back into the position. This was done to avoid the error in melt composition during quenching from the condensed sulphur in the cooler part of the reaction tube. The gases were led into the furnace through an alumina tube (C) of $\frac{1}{4}$ inch in diameter in order to minimise thermal diffusion errors.

A small alumina crucible (I) was placed over one end of tube (C). At the other end was attached a standard B₁₀ cone over which a T tube can be fitted. Through one limb of T, the mixed gas entered the furnace. A glass disc (W) was cemented on to the other end as shown in the diagram. This served as a window through which an optical pyrometer could be sighted down to the base of the crucible (I) placed within the even temperature zone of the furnace. Alongside of the sighting tube, an alumina sheath (B) $\frac{1}{4}$ inch in diameter was placed. This was used for inserting thermo-couple (x) to measure the temperature. Current to the furnace was supplied from a "Variac" auto-transformer.

(c) Temperature Measurement and Control

The temperature was measured by sighting a Leeds and Northrup disappearing filament optical pyrometer on to the base of the crucible (I) through the window (W). The pyrometer was calibrated against a 5% Rh-Pt : 20 Rh-Pt thermocouple by placing the junction of the thermocouple in the even temperature zone of the furnace and taking simultaneous readings of the pyrometer and the thermocouple. The calibration was made up to 1650°C. The temperature observed by the optical pyrometer was also frequently checked by a 5% Rh-Pt : 20 Rh-Pt thermocouple (X) placed in the alumina sheath (B) during the experiment.

The temperature of the furnace was controlled automatically by a Kelvin and Hughes electronic controller of the proportional type operating a mercury relay, which interrupted the whole of the furnace current. The control thermocouple was inserted between the furnace tube and the reaction tube. The hot junction was placed at a point $100^{\circ} - 150^{\circ}\text{C}$ lower than the temperature of the even zone, in order to prevent the too rapid deterioration which occurs at temperatures above 1600°C . With this arrangement, the fluctuation was maintained within 2°C at 1650°C .

(d) Sample Holding Assemblies

(i) Platinum and iridium cups:

The samples were held in small platinum cups of roughly hemispherical shapes, with diameters of about $\frac{1}{4}$ inch. They were made from a platinum sheet (0.005 inch thick) by cutting out a circular disc of 0.6 inch diameter with a punch and then pressing these discs into cups with a small press.

Platinum cups were found unsuitable for holding melts in reducing atmospheres of oxygen partial pressure of 10^{-8} atm. and below it. Iridium cups were therefore used. They were made in the same way as platinum cups except that the press was heated to approximately 800°C before use. They were 0.3 inches in diameter and 0.2 inches deep. They were able to hold 0.3 gm. of melt.

(ii) Alumina supports:

Alumina trays for holding the cups were made from alumina blocks by drilling a number of depressions. These depressions were so spaced that when the tray was in position, all the cups would be within the even temperature zone of the furnace. This allowed only six platinum cups or four iridium cups in the furnace at a time.

The blocks used for making trays were made from alumina cement, which consisted of alumina powder with a small proportion of an organic binder. The cement was made into a paste with water and allowed to set in a flat mould (usually a filter paper box) and then dried at 100°C for 24 hours. The blocks were then cut out and shaped with a file. The depressions on it were made with a drill. The blocks were fired at 1500°C before use. This treatment made them hard and quite resistant to thermal shock.

Those melts which had a high manganese oxide content, crept out of the cups during the experiment. This was avoided by using a special support to hold the cups, made of platinum wires on an alumina boat.

2. Preparation of Materials

(i) Calcium oxide was prepared by igniting Analar calcium carbonate at 1000°C for 2 hours in a platinum dish and cooling in a desiccator.

(ii) Silica was obtained from clear mineral quartz. This was crushed to powder, washed several times with dilute hydrochloric acid to remove traces of iron, and finally washed with water. It was then dried at 110°C.

(iii) Alumina was obtained by igniting Analar aluminium oxide at 1000°C for two hours in a platinum dish and then cooling in a desiccator.

(iv) Magnesia was obtained by igniting fused magnesia (98% MgO) powder at 1000°C for 2 hours in a platinum dish and cooling in a desiccator.

(v) Manganese oxide was prepared from 99.99% pure electrolytic manganese. The metal was dissolved in concentrated nitric acid and the solution so obtained was evaporated to dryness. The manganese dioxide so formed was reduced in a stream of hydrogen at 1100°C for two hours. Green manganous oxide was formed.

The samples were prepared by weighing out the calculated amounts of the constituents and mixing them together in an agate mortar. The quantity of sample taken for the experiment was approximately 0.4 gm., but in the case of

$\text{Al}_2\text{O}_3 + \text{SiO}_2$ and $\text{MgO} + \text{SiO}_2$ melts, and pure oxides for most of the samples it was 0.8 - 1 gm. taken in four different cups.

3. Procedure:

A. Sulphur in aluminate and silicate melts:

The procedure adopted for the measurements of sulphide capacities and limiting solubilities of sulphur in lime-alumina, lime-silica melts and pure crystalline CaO , was the same. First of all the molybdenum furnace, generally at 1200°C when not in use, was brought to the required temperature. The Kelvin and Hughes proportional controller was adjusted to keep the furnace at this temperature for the duration of the experiment. The furnace was flushed with nitrogen. The cups containing the samples of desired compositions, were placed on the alumina tray and this was pushed slowly into the even temperature zone of the furnace over a period of ten to fifteen minutes. The furnace was then closed. The passage of nitrogen was continued for a further fifteen minutes, during which time the samples attained the required temperature. The mixed gases from the flow meter system, adjusted to the required composition, were then passed through the furnace at a flow rate of 500 cc per minute. The flow meter readings were checked at regular intervals and adjusted if necessary.

The temperature was measured regularly by optical pyrometer and also by a thermocouple. Under similar experimental conditions, Fincham³⁴ found, by plotting the weight percent sulphur in the melt against the time, that equilibrium was attained in about five hours. He also checked the equilibrium time by approaching the equilibrium from the higher sulphur side. In the present work, experiments were usually conducted for eight hours, although in the measurements of sulphur in pure oxides and in some of the other experiments to check the equilibrium time, the duration was increased to 24 hours.

At the end of the experiment, the mixed gases were turned off and only nitrogen was kept flowing. One half of the gutter was removed, cleaned together with the reaction tube, and was placed back into position. The alumina tray with the samples, was quickly pulled from the hot zone into the cold end of the reaction tube. This was done by means of a silica rod having a small right angle hook at its one end, which hooked the platinum loop attached to the tray or the vertical hole on its end. Because of their small size, the samples cooled rapidly. Under these conditions, Fincham³⁴ has shown that no significant loss of sulphur, as sulphur dioxide, takes place during quenching.

After quenching, the melts were crushed out of the cups and analysed for sulphur. The melts containing manganese oxide, because of the alteration in composition arising from reduction of MnO into the platinum, were analysed for manganese oxide at the end of experiment in addition to the sulphur analysis. The process of determining the sulphide capacities and the limiting solubilities of sulphur in lime-alumina, lime-silica melts and crystalline calcium oxide, and derivation of the activities in these systems from them, have been described on pages 21 - 25.

B. Activities of manganese oxide in aluminate and silicate melts.

The method followed herein has been described by Davies³ and Abraham⁶. The theory has been described on pages 26 and 27.

The experimental procedure was almost the same as outlined in the previous section. However, in this case, a small platinum coil, 0.002 inch thick and 0.1 inch wide, was embedded in each of the samples of the powdered melts before pushing into the furnace. The gaseous mixture consisted of nitrogen, hydrogen and carbon dioxide only. As described in the previous section, the gases from the flow meters were turned on after putting the samples in the even hot zone of the furnace. The manganese oxide from the melt was reduced at

the low oxygen pressure prevailing in the furnace and dissolved in the platinum coil. The manganese platinum alloy forming in this way, reached equilibrium with the melt and gaseous phase in about 5-6 hours. This has also been observed by Davies⁵ and Abraham⁶, who reported six hours as a sufficient period for the attainment of equilibrium.

The hydrogen and carbon dioxide were turned off after the samples had been in the furnace for eight hours. The samples were then pulled quickly into the cooler end of the reaction tube and allowed to cool in the nitrogen atmosphere.

The solidified melts and the platinum coils were removed from the cups and then were separated from each other. The coils so obtained were cleaned with emery paper and examined under a binocular microscope to make sure that no speck of manganese oxide was adhering to them. Both the melts and the alloys were then analysed for manganese.

As mentioned earlier, the composition of the melt changed due to the reduction of manganese oxide from the melt into the platinum cup. This made the prediction of the final composition of the melt from its initial composition impossible. However, by the following procedure it was possible to know the activity of manganese oxide in a given composition. The sample of the desired composition was prepared. To the different portions of this sample, various extra amounts of

pure manganese oxide were added. The experiment was then carried out in the usual way. After the experiment, these samples contained varying proportions of manganese oxides, some more and some less than the desired composition. The activities of manganese oxides in all these samples were calculated in the usual way and the activity in the desired composition could be obtained by interpolation.

4. Analytical Methods:

A. Sulphur

Sulphur in the melts was determined by the stoichiometric combustion method³⁵. In most cases about 0.3 gm. of the powdered sample in an aluminous porcelain combustion boat (preheated to drive off any sulphur present) was placed in a stream of carbon dioxide at about 1450°C. However, in the case of $\text{Al}_2\text{O}_3 + \text{SiO}_2$, $\text{MgO} + \text{SiO}_2$ melts, and CaC , MgO , Al_2O_3 and SiO_2 , the quantity taken for analysis was about 0.8 gm. CaO to $\text{Al}_2\text{O}_3 + \text{SiO}_2$, Al_2O_3 to $\text{MgO} + \text{SiO}_2$, $(\text{SiO}_2 + \text{Al}_2\text{O}_3)$ to CaO and to MgO , $(\text{CaO} + \text{SiO}_2)$ to Al_2O_3 and $(\text{CaC} + \text{Al}_2\text{O}_3)$ to SiO_2 were also added in suitable proportions, before analysis, to bring down the m.p. of the respective samples. The combustion was carried out in a recrystallised alumina reaction tube, heated by platinum wound electric resistance furnace. The sulphur in the sample was converted to sulphur dioxide, which was absorbed into distilled water. The sulphurous acid formed was estimated by titration with standard iodine solution

using starch as an indicator. The titration was performed while the sulphur dioxide was being evolved. It took 2 hours for the manganese oxide containing melts to evolve all the sulphur, whereas the other melts gave up within 3 hours. Corrections were made for small traces of sulphur dioxide present in the carbon dioxide. The sulphur analysis was standardised by analysing Analar calcium sulphate as described by Fincham and Richardson,³⁵

B. Manganese oxide

About 0.15 gm. of the sample was weighed accurately and fused with potassium bisulphate in a platinum dish. After cooling, the product was dissolved in a mixture of 5 cc of 40% Hydrofluoric acid and 5 cc of 50% sulphuric acid in the same platinum dish. The solution was then heated to fumes and almost evaporated to dryness. This ensured the removal of silica as silicon tetrafluoride. After cooling the solution was carefully diluted and made up to a litre. A known volume of this solution was pipetted out (the volume depending on the manganese content of the melt) and the manganese was oxidized to permanganate by potassium periodate. The oxidised solution was made to 250 ml. The manganese was determined colourimetrically using a Unicam SP 600 Spectrophotometer set at 525 Angstroms.

C. Manganese in Mn-Pt alloys

The coil of Mn-Pt alloy was cleaned thoroughly from the adhering manganese oxide with emery paper. About 10-20 mgm of the alloy was weighed accurately and dissolved in aqua-^eregia. The solution was evaporated to dryness. The residue was treated with concentrated sulphuric acid and heated to fumes to remove chloride and nitrate ions. The solution was diluted. Manganese was oxid^{ised} to permanganate by potassium periodate and estimated colourimetrically as earlier.

5. Note on thermal diffusion:

The equilibrium studies of the present types involve flowing gaseous mixtures and condensed phases. The thermal diffusion can be a serious problem. Alcock and Richardson³⁶, using hydrogen and hydrogen sulphide mixtures, measured the extent of thermal diffusion in their apparatus at varying flow rates and showed that in a static system, an error up to 100% could occur at 1200°K.

To avoid significant error due to thermal diffusion, the gas flow rate should be such that (i) it is fast enough to overcome the thermal diffusion in the ingoing temperature gradient, and (ii) slow enough to allow the gases to reach the equilibrium temperature before coming into contact with the condensed phase. There is thus an optimum range of flow

rates where thermal diffusion is a minimum. Fincham³⁴ varied the gas flow rate from 1.5 cc to 17.3 cc per sec. at S.T.P. and found no significant difference in the experimental results. According to this, the flow rate of 500 cc per minute in the present work, should not involve any appreciable error due to thermal diffusion.

Estimates of Errors

Errors, in the experimental results, will be considered here, while those in D_{O_2} and D_{N_2} are discussed in the "Appendix 1". Errors in the calculated data will be given along with their respective discussion.

A. Temperature

In the experiments up to 1650°C, where a thermocouple as well as an optical pyrometer was used, the stated temperatures are accurate to within $\pm 5^\circ\text{C}$ ($\pm 3^\circ\text{C}$ thermocouple error, $\pm 2^\circ\text{C}$ fluctuations in furnace temperature). Where only an optical pyrometer calibrated by a thermocouple was used, the uncertainty became $\pm 8^\circ\text{C}$. Finchan³⁴ has shown that these errors in the temperature measurements did not cause significant errors in the measured sulphur for a given composition of the ingoing gas. These should also not lead to the serious errors in the activities data, as the temperature co-efficients of activities are not great. (i.e. the activity is not expected to change more than 10% for 100°C).

B. Gas mixtures

Each of the flow meters had a maximum error of $\pm 1\%$. This would cause a maximum error of $\pm 2\%$ in the proportion of any one constituent. A possible error of $\pm \frac{1}{2}\%$ in the proportions of carbon dioxide and nitrogen, due to the presence of up to 1% (average $\frac{1}{2}\%$) of air in the carbon dioxide, is also included in this.

C. Sulphur analysis

For sulphur contents above 0.10% the error is $\pm 2\%$.
Below about 0.05% sulphur, the accuracy is low.

D. Manganese analysis

An error of $\pm 1\%$ is estimated in the analysis of manganese in the melts. The analysis of manganese in the Mn-Pt alloys should also be accurate to within $\pm 1\%$ where the manganese content is between 4.5% to 5.5%. But the accuracy becomes low in the alloys of higher concentration of manganese.

RESULTS

General

(a) The results are presented in tabular form. The quantities, calculated from measured results, have been marked by asterisks. The tables have been divided into the following main sections.

A. Sulphur in Aluminate and Silicate Melts
and Crystalline Oxides.

(i) Sulphide capacities

(ii) Limiting solubilities of sulphur
and activities in crystalline lime
and lime-alumina and lime-silica
melts.

B. Activities of Manganese Oxide in Aluminate
and Silicate Melts

Activity Coefficients of Sulphides in
Aluminate and Silicate Melts.

(b) Melt compositions are clearly shown in the tables. The mole fraction is indicated by the symbol N . Sulphur content in the melt in weight percentage is indicated as wt % S.

(c) Reproducibility of the measurements is expressed in terms of maximum deviation from the best line drawn through the experimental results,

(d) The samples were normally kept inside the furnace under the experimental conditions for eight hours, but in the measurements of sulphur in $\text{Al}_2\text{O}_3 + \text{SiO}_2$, $\text{MgO} + \text{SiO}_2$ melts and in pure oxides, they were kept for 24 hours.

(e) Each of the partial pressures is denoted in atmospheres by a small p with subscript. e.g. p_{O_2} means oxygen partial pressure in atmospheres. A subscript (i) indicates the partial pressure of the gas in the ingoing gas mixture, e.g. $p_{\text{H}_2(i)}$ is the partial pressure of hydrogen, in atmospheres, in the ingoing gas mixture.

(f) p_{O_2} and p_{S_2} are the calculated values of the oxygen and sulphur partial pressures at the temperature of the experiment. (Details in Appendix 1). No corrections have been made for variations in atmosphere (total) pressure. p_{S_2} for a given gas composition and temperature varies with the total pressure, but the necessary corrections are insignificant in comparison with the uncertainties in the thermodynamic data used in the calculations. p_{O_2} is independent of total pressure when obtained from a gas mixture of H_2 , CO_2 and N_2 . Since it is determined by the equilibrium constants

$$K_1 = \frac{p_{\text{CO}}}{p_{\text{CO}_2}} p_{\text{O}_2}^{\frac{1}{2}} ; \quad K_2 = \frac{p_{\text{H}_2\text{O}}}{p_{\text{H}_2}} \frac{p_{\text{CO}}}{p_{\text{CO}_2}}$$

A. Sulphur in Aluminate and Silicate Melts and Crystalline Oxides

(i) Sulphide capacities

TABLE I

Binary MnO + Al₂O₃ melts. Temperature 1650°C

$$\begin{aligned}
 P_{N_2(i)} &= 0.5 & P_{H_2(i)} &= 0.154 \\
 P_{CO_2(i)} &= 0.526 & P_{SO_2(i)} &= 0.02 \\
 P_{O_2} &= 1.115 \times 10^{-6} & P_{S_2} &= 1.839 \times 10^{-4}
 \end{aligned}$$

<u>Wt % MnO</u>	<u>N_{MnO}</u>	<u>Wt % S</u>	<u>-log C_s</u>
56.6	0.653	0.211	1.786
62.5	0.705	0.349	1.567
64.0	0.720	0.405	1.450
67.0	0.745	0.540	1.380
69.5	0.765	0.689	1.272
71.0	0.780	0.676	1.280
71.5	0.782	0.521	1.392
76.7	0.825	1.025	1.098
77.0	0.828	0.813	1.20
79.5	0.847	0.915	1.147
80.0	0.852	0.670	1.284
84.0	0.882	0.545	1.350
86.7	0.904	0.517	1.396
87.0	0.905	0.735	1.243
87.7	0.910	0.553	1.367
91.5	0.940	0.314	1.630
94.0	0.956	0.15	1.930

Maximum deviation \pm 8%

TABLE II

Binary MgO + SiO₂ melts. Temperature 1650°C

$$\begin{aligned} P_{N_2(i)} &= 0.50 & P_{H_2(i)} &= 0.364 \\ P_{CO_2(i)} &= 0.116 & P_{SO_2(i)} &= 0.02 \\ P_{O_2} &= 1.038 \times 10^{-8} & P_{S_2} &= 2.958 \times 10^{-5} \end{aligned}$$

<u>Wt % MgO</u>	<u>N_{MgO}</u>	<u>Wt % S</u>	<u>-log U_S</u>
30.0	0.39	0.0349	4.19
30.7	0.40	0.0398	4.127
35.0	0.44	0.0350	4.180
36.0	0.46	0.0410	4.114
39.5	0.49	0.0516	4.015
40.0	0.50	0.042	4.103
45.3	0.53	0.0566	3.99

Maximum deviation $\pm 8\%$

TABLE III

Binary Al₂O₃ + SiO₂ melts, Temperature 1650°C

$$P_{N_2(i)} = 0.50 \qquad P_{H_2(i)} = 0.364$$

$$P_{CO_2(i)} = 0.116 \qquad P_{SO_2(i)} = 0.02$$

$$P_{O_2} = 1.038 \times 10^{-8} \qquad P_{S_2} = 2.958 \times 10^{-3}$$

<u>Wt % Al₂O₃</u>	<u>N_{Al₂O₃}</u>	<u>Wt % S</u>	<u>-log Cs</u>
3.4	0.020	0.0183	4.466
3.7	0.025	0.0207	4.412
6.7	0.040	0.0310	4.26
7.0	0.040	0.0341	4.195
9.0	0.056	0.0343	4.191
10.0	0.066	0.0527	4.00
16.0	0.09	0.0360	4.17
16.2	0.09	0.0261	4.31
20.0	0.128	0.027	4.30
22.0	0.14	0.0378	4.24
29.6	0.20	0.0325	4.22
39.5	0.28	0.0335	4.26

Accuracy within $\pm 10\%$

TABLE IV

Ternary MnO + Al₂O₃ + SiO₂ melts. Temperature 1650°C

$$P_{N_2(i)} = 0.5 \qquad P_{H_2(i)} = 0.154$$

$$P_{CO_2(i)} = 0.326 \qquad P_{SO_2(i)} = 0.02$$

$$P_{O_2} = 1.115 \times 10^{-6} \qquad P_{S_2} = 1.839 \times 10^{-4}$$

<u>N_{MnO}</u>	<u>N_{SiO₂}</u>	<u>N_{Al₂O₃}</u>	<u>Wt % S</u>	<u>-log C_s</u>
.656	.257	.087	0.269	1.68
.525	.371	.104	0.0610	2.323
.633	.262	.105	0.115	2.049
.445	.462	.092	0.04	2.507
.503	.290	.210	0.387	2.522
.388	.484	.128	0.0314	2.613
.785	.078	.137	0.0479	1.43
.590	.146	.264	0.1464	1.95
.510	.315	.175	0.0586	2.37
.716	.070	.214	0.320	1.604
.565	.103	.335	0.403	2.504
.709	.104	.187	0.3313	1.539
.424	.206	.368	0.0379	2.530
.610	.110	.280	0.1958	1.817
.588	.247	.164	0.0403	1.936
.765	.141	.094	0.7752	1.220
.764	.166	.0704	0.790	1.210
.610	.380	.210	0.0376	2.577

Maximum deviation \pm 8%

TABLE V

Ternary MnO + MgO + SiO₂ melts. Temperature 1650°C

$$\begin{aligned}
 P_{N_2(i)} &= 0.5 & P_{H_2(i)} &= 0.154 \\
 P_{CO_2(i)} &= 0.326 & P_{SO_2(i)} &= 0.02 \\
 P_{O_2} &= 1.115 \times 10^{-6} & P_{S_2} &= 1.839 \times 10^{-4}
 \end{aligned}$$

<u>N_{MnO}</u>	<u>N_{MgO}</u>	<u>N_{SiO₂}</u>	<u>Wt % S</u>	<u>-log C_s</u>
.626	.077	.297	0.2765	1.667
.537	.096	.367	0.1214	2.025
.525	.185	.290	0.2327	1.742
.390	.238	.372	0.0554	2.366
.141	.334	.525	0.0586	3.426
.190	.420	.390	0.1180	3.123
.114	.460	.426	0.0723	3.321
.339	.342	.319	0.9363	2.222
.264	.382	.354	0.40	2.59
.648	.198	.767	0.349	2.651
.214	.306	.480	0.1103	3.151
.430	.275	.743	0.278	2.750
.298	.144	.558	0.178	2.944
.271	.223	.506	0.121	3.110
.358	.195	.447	0.217	2.857
.147	.388	.465	0.60	3.407
.197	.366	.437	0.868	3.258

$$\begin{aligned}
 P_{N_2} &= 0.5 & P_{H_2} &= 0.364 \\
 P_{CO_2} &= 0.116 & P_{SO_2} &= 0.02 \\
 P_{O_2} &= 1.038 \times 10^{-8} & P_{S_2} &= 2.958 \times 10^{-3}
 \end{aligned}$$

.033	.379	.59	0.0581	3.963
.023	.46	.517	0.0837	3.805

Maximum deviation $\pm 10\%$

TABLE VI

Ternary MgO + SiO₂ + Al₂O₃ melts. Temperature 1650°C

$$\begin{aligned}
 P_{N_2(i)} &= 0.50 & P_{H_2(i)} &= 0.364 \\
 P_{CO_2(i)} &= 0.116 & P_{SO_2(i)} &= 0.02 \\
 P_{O_2} &= 1.038 \times 10^{-3} & P_{S_2} &= 2.958 \times 10^{-3}
 \end{aligned}$$

N_{MgO}	N_{SiO_2}	$N_{Al_2O_3}$	Wt % S	$-\log C_s$
.184	.786	.0295	0.0228	4.369
.337	.639	.024	0.0347	4.187
.453	.527	.020	0.0389	4.137
.536	.447	.017	0.0563	3.977
.533	.423	.043	0.0672	3.900
.456	.493	.051	0.0571	3.97
.356	.583	.061	0.0353	4.179
.207	.718	.075	0.0326	4.215
.542	.383	.075	0.0688	3.890
.431	.476	.093	0.0574	3.969
.308	.579	.113	0.0351	4.183
.173	.692	.135	0.0262	4.310
.156	.641	.203	0.0240	4.347
.308	.525	.166	0.0442	4.082
.538	.350	.111	0.0733	3.862
.433	.430	.136	0.0562	3.978
.285	.543	.172	0.0366	4.165
.252	.469	.279	0.0388	4.140
.273	.489	.236	0.03263	4.210
.399	.406	.196	0.0586	3.970
.229	.454	.317	0.0325	4.216
.280	.499	.220	0.0389	4.138
.105	.832	.064	0.0207	4.411
.096	.872	.032	0.0115	4.668
.082	.767	.150	0.0155	4.54

Accuracy within $\pm 15\%$

TABLE VII

Crystalline CaO, MgO, SiO₂ and Al₂O₃. Temperature 1650°C

$$\begin{aligned}
 P_{N_2(i)} &= 0.5 & P_{H_2(i)} &= 0.364 \\
 P_{CO_2(i)} &= 0.116 & P_{SO_2(i)} &= 0.02 \\
 P_{O_2} &= 1.038 \times 10^{-8} & P_{S_2} &= 2.958 \times 10^{-3}
 \end{aligned}$$

MgO		Al ₂ O ₃		SiO ₂		CaO	
Wt % S	-log Cs	Wt % S	-log Cs	Wt % S	-log Cs	Wt % S	-log Cs
0.0069	4.89	0.0265	4.304	0.0107	4.70	36.6	-
0.0080	4.82	0.0265	4.304	0.00927	4.76		
0.0074	4.86	0.0265	4.304				

$$\begin{aligned}
 P_{N_2(i)} &= 0.5 & P_{H_2(i)} &= 0.260 \\
 P_{CO_2(i)} &= 0.22 & P_{SO_2(i)} &= 0.02 \\
 P_{O_2} &= 1.112 \times 10^{-7} & P_{S_2} &= 2.709 \times 10^{-3}
 \end{aligned}$$

0.00380	4.613	0.00265	4.77	0.0227	3.837
0.00668	4.37			0.0287	3.736
0.00794	4.29			0.0308	3.704
				0.0245	3.81
				0.0227	3.84

(ii) Limiting solubilities of sulphur and activities in crystalline lime and lime-alumina and lime-silica melts.

TABLE VIII

(a) Sulphur in crystalline calcium oxide. Temperature 1650°C.

$$P_{N_2(i)} = 0.5$$

$$P_{SO_2(i)} = 0.02$$

$$P_{CO_2(i)} + P_{H_2(i)} = 0.48$$

$\log \frac{P_{H_2}}{P_{CO_2}}$	$\frac{1}{2} \log \frac{P_{O_2}}{P_{S_2}}$	Wt % S	Original Sulphur
0.0726	2.1933	0.0259	Zero
0.0726	2.1933	0.0308	36.6%
^x 0.1315	2.290	0.0604	36.6%
^x 0.1315	2.290	0.0241	Zero
0.1315	2.290	0.034	26.6%
0.1315	2.290	0.0294	Zero
0.146	2.32	0.0353	Zero
0.1685	2.37	12.00	Zero
0.4966	2.7274	36.60	Zero
0.16*	2.35*	0.36*	Theoretical

x Duration of experiment was six hours.

Maximum deviation $\pm 13\%$

TABLE IX

Sulphur saturation limits and Cs values for CaO + Al₂O₃ melts.

Temperature 1500°C.

<u>N₂ CaO before experiment</u>	<u>Wt% sulphur at Saturation</u>	<u>Activity Coefficient of CaS</u>	<u>Sulphide Capacity Cs x 10³</u>
0.57	0.58	72.5	0.32
0.59	0.77	55.3	0.50
0.63	1.07	40.7	0.89
0.66	1.38	32.2	1.86
0.70	1.62	28.0	3.42
^x 1.0	0.036	1586	0.016

x For pure CaO the temperature of experiment was 1650°C.

TABLE X

Activities and free energies in CaO + Al₂O₃ melts relative to pure solid CaO and Al₂O₃. Temperature 1500°C.

<u>N_{CaO}</u>	<u>a_{CaO}</u>	<u>a_{Al₂O₃*}</u>	<u>-ΔG Kcal</u>
0.58	0.21	0.150	6.04
0.60	0.25	0.115	5.99
0.62	0.30	0.085	5.92
0.64	0.38	0.060	5.81
0.66	0.50	0.040	5.66
0.68	0.67	0.025	5.44
0.71	1.00	0.007	5.03

(c) Lime-silica melts.

TABLE XI

Sulphur in lime-silica melts at 1500°C.

$$P_{N_2} = 0.50 \quad P_{H_2S} = 0.08 \quad P_{CO_2} + P_{H_2} = 0.42$$

<u>N_{CaO}</u>	<u>N_{SiO₂}</u>	<u>N_{CaS}</u>	<u>Wt % S</u>	<u>3 P_{H₂S}/P_{CO₂}</u>
0.4557	0.3834	0.1608	8.56	9.441
0.4684	0.3934	0.1383	7.40	9.441
0.4713	0.4032	0.1257	6.741	9.441
0.4641	0.4131	0.1029	5.552	9.441
0.5003	0.231	0.0766	4.160	11.27
0.4352	0.3836	0.1813	9.60	11.27
0.4478	0.3934	0.1588	8.45	11.27
0.4508	0.4032	0.1462	7.80	11.27
0.4536	0.4133	0.1332	7.13	11.27
0.4737	0.4230	0.1031	5.56	11.27
0.4072	0.3836	0.2093	11.00	13.49
0.4195	0.4133	0.1680	8.90	13.49
0.4415	0.4231	0.1352	7.23	13.49
0.4081	0.4231	0.159	8.95	16.14
0.4323	0.5027	0.065	3.52	16.14
0.4176	0.3832	0.1993	10.50	11.80
0.4418	0.4033	0.155	8.25	11.80
0.4551	0.4133	0.1317	7.05	11.80
0.4751	0.423	0.102	5.50	11.80
0.4239	0.3733	0.2027	10.69	11.80
0.4482	0.4232	0.130	6.95	12.79
0.4210	0.4033	0.176	9.30	12.79
0.4006	0.3838	0.2154	11.30	12.79
0.4512	0.3347	0.2140	11.27	4.21
0.4955	0.3737	0.1308	7.025	4.21
0.5084	0.4627	0.0289	3.584	4.21
0.375	0.6137	0.0112	0.610	4.21
0.429	0.558	0.013	0.700	4.21
0.5284	0.4232	0.0486	2.660	4.21
0.4604	0.3779	0.1618	3.530	6.237
0.4138	0.3346	0.2524	13.11	6.237
0.3739	0.6137	0.0123	0.670	6.237
0.4244	0.5582	0.0176	0.960	6.237
0.5000	0.463	0.0373	2.040	6.237
0.5202	0.4232	0.0568	3.100	6.237
0.3700	0.6140	0.016	0.8816	8.61
0.4182	0.5578	0.0240	1.311	8.61
0.4870	0.4630	0.0504	2.750	8.61

TABLE XI continued

<u>N_{CaO}</u>	<u>N_{SiO₂}</u>	<u>N_{CaS}</u>	<u>Wt % S</u>	<u>$\frac{P_{H_2S}}{P_{CO_2}}$</u>
0.4968	0.423	0.0802	4.34	8.61
0.4628	0.5027	0.0346	1.89	8.61
0.3620	0.614	0.024	1.32	14.62
0.4082	0.5581	0.0338	1.845	14.62
0.4672	0.4628	0.070	3.80	14.62
0.4763	0.4232	0.1003	5.40	14.62
0.350	0.614	0.037	2.00	17.78
0.394	0.558	0.048	2.606	17.78
0.4531	0.4631	0.084	4.536	17.78
0.395	0.424	0.183	9.650	17.78
0.3424	0.6135	0.0437	2.360	26.61
0.3807	0.5581	0.0611	3.300	26.61
0.4246	0.4628	0.1128	6.050	26.61
0.3402	0.6135	0.0459	2.480	25.12
0.3855	0.5581	0.0563	3.047	25.12
0.4330	0.4628	0.1042	5.60	25.12
0.3866	0.4233	0.1904	10.03	25.12
0.4067	0.5029	0.0906	4.874	27.54
0.4442	0.4686	0.08906	4.941	27.54
0.3317	0.6137	0.0548	2.955	27.54
0.3655	0.5584	0.0762	4.100	27.54
0.4161	0.4624	0.1214	6.500	27.54
0.3308	0.6137	0.0556	3.00	34.28
0.3573	0.5581	0.0845	4.540	34.28
0.3076	0.6137	0.0786	4.214	44.87
0.3583	0.558	0.084	4.510	44.87
0.3208	0.4624	0.2165	11.30	44.87
0.3615	0.4828	0.1556	8.240	44.87
0.3933	0.5027	0.1036	5.570	44.87
0.4067	0.3738	0.2192	11.50	14.62
0.3681	0.3737	0.2580	13.40	24.27
0.4329	0.5024	0.0647	3.50	25.12
0.400	0.533	0.0664	3.587	25.12
0.4158	0.5328	0.0514	2.788	17.78
0.4352	0.5027	0.0621	3.361	17.78
0.3950	0.5326	0.07185	3.880	26.61
0.4164	0.5027	0.0808	4.360	26.61
0.4941	0.3738	0.1323	7.10	4.90
0.5077	0.4628	0.0300	1.62	4.90
0.4462	0.3344	0.2200	11.54	4.90
0.5274	0.4231	0.0494	2.70	4.90

P.S. Partial pressures given above are
in the ingoing gas mixture.

TABLE XII

Sulphur in lime-silica melts at 1550°C.

$$P_{N_2} = 0.5 \quad P_{H_2S} = 0.074 \quad P_{CO_2 + H_2} = 0.426$$

<u>N_{CaO}</u>	<u>N_{SiO₂}</u>	<u>N_{CaS}</u>	<u>Wt % S</u>	<u>3 x P_{H₂S}/P_{CO₂}</u>
0.3725	0.614	0.014	0.7565	7.00
0.425	0.558	0.0172	0.94	7.00
0.4763	0.5027	0.0209	1.145	7.00
0.5289	0.4233	0.0481	2.63	7.00
0.368	0.6138	0.0136	2.273	15.34
0.5488	0.4033	0.048	2.629	13.34
0.4544	0.4032	0.1422	7.6	13.34
0.424	0.4033	0.1734	9.181	16.8
0.398	0.4031	0.1987	10.46	20.65
0.4236	0.5581	0.0183	1.0	13.34
0.4715	0.5027	0.0258	1.41	13.34
0.4729	0.4231	0.104	5.6	13.34
0.3548	0.6141	0.0313	1.7	16.80
0.3967	0.5581	0.04533	2.46	16.80
0.4416	0.5025	0.0554	3.01	16.80
0.4363	0.423	0.1407	7.51	16.80
0.3526	0.6135	0.0338	1.831	20.65
0.3906	0.5581	0.0513	2.782	20.65
0.3667	0.4032	0.230	12.00	25.41
0.5168	0.4031	0.08	4.34	7.00
0.4345	0.5028	0.0627	3.40	20.65
0.4192	0.4232	0.1537	8.38	20.65
0.3368	0.6137	0.0493	2.66	25.41
0.3767	0.5581	0.0652	3.51	25.41
0.4184	0.5027	0.0789	4.257	25.41
0.3829	0.4231	0.1937	10.20	25.41

P.S. Partial pressures given above are
in the ingoing gas mixture.

TABLE XIII

Saturation limits and activity coefficients
of CaS for CaO + SiO₂ Melts. Temperature 1500°C.

<u>N_{CaO}</u>	<u>N_{CaS} at Saturation</u>	<u>Activity Coefficient of CaS</u>
0.40	0.116	8.45
0.44	0.107	9.40
0.48	0.097	10.65
0.52	0.083	12.45
0.56	0.066	15.30
0.58	0.055	17.80

TABLE XIV

Activities and molar free energies of formation
for CaO + SiO₂ melts relative to pure
solid CaO & SiO₂. Temperature 1500°C.

<u>N_{CaO}</u>	<u>N_{SiO₂}</u>	<u>a_{CaO}</u>	<u>a_{SiO₂}*</u>	<u>-ΔG Kcal*</u>
0.37	0.63	0.0017	1.00	8.2
0.41	0.59	0.0022	0.85	9.2
0.42	0.58	0.0024	0.62	10.2
0.46	0.54	0.0033	0.62	10.2
0.50	0.50	0.0055	0.39	10.8
0.52	0.48	0.0074	0.29	11.1
0.55	0.45	0.012	0.16	11.4
0.58	0.42	0.024	0.069	11.6

B. Activities of Manganese Oxide in Aluminate and Silicate Melts.

TABLE XV

Binary MnO + Al₂O₃ melts. Temperature 1650°C.

$$P_{N(i)} = 0.50 \quad P_{H(i)} = 0.08$$

$$P_{CO_2(i)} = 0.420 \quad P_{O_2(i)} = 10^{-5}$$

<u>Wt % MnO</u>	<u>N_{MnO}</u>	<u>Wt % Mn in Mn-Pt alloy</u>	<u>a_{MnO}</u>
54.20	0.63	4.72	0.537
56.31	0.65	4.73	0.54
59.05	0.675	4.787	0.55
60.12	0.68	4.77	0.543
61.27	0.695	5.146	0.634
62.95	0.71	5.145	0.634
63.04	0.71	5.113	0.672
64.25	0.72	5.264	0.733
65.63	0.733	5.21	0.716
66.06	0.737	5.277	0.741
67.42	0.748	5.561	0.86
67.04	0.748	5.348	0.767
67.7	0.752	5.546	0.79
68.3	0.755	5.624	0.891
69.08	0.762	5.58	0.87
70.01	0.77	5.613	0.89
74.03	0.804	5.58	0.834
79.07	0.844	6.04	1.0
76.08	0.82	5.80	1.0
80.04	0.852	5.801	1.0
88.00	0.911	5.91	1.0
84.53	0.987	5.80	1.0

Maximum deviation ± 5%

TABLE XVI

Alumina activities and molar free energies of formation
for MnO + Al₂O₃ melts relative to
pure solid oxides. Temperature 1650°C.

<u>N_{MnO}</u>	<u>N_{Al₂O₃}</u>	<u>a_{Al₂O₃}[*]</u>	<u>-ΔG Kcal[*]</u>
0.67	0.33	1.0	1.58
0.70	0.30	0.59	1.61
0.75	0.25	0.37	1.54
0.80	0.20	0.24	1.34
0.84	0.16	0.17	1.09

TABLE XVII

Ternary MnO + SiO₂ + Al₂O₃ melts. Temperature 1650°C.

$$\begin{aligned}
 P_{N_2(i)} &= 0.50 & P_{H_2(i)} &= 0.08 \\
 P_{CO_2(i)} &= 0.42 & P_{O_2} &= 10^{-5}
 \end{aligned}$$

<u>N_{MnO}</u>	<u>N_{SiO₂}</u>	<u>a_{Al₂O₃}</u>	<u>Wt % Mn in Mn-Pt alloy</u>	<u>a_{MnO}</u>
0.565	0.384	0.051	3.419	0.231
0.529	0.368	0.102	3.327	0.218
0.624	0.322	0.054	4.495	0.457
0.731	0.191	0.078	5.33	0.759
0.621	0.205	0.174	4.667	0.513
0.576	0.181	0.243	4.287	0.398
0.535	0.368	0.098	3.249	0.208
0.588	0.313	0.099	3.956	0.320
0.643	0.257	0.101	4.441	0.450
0.695	0.201	0.104	5.13	0.676
0.755	0.137	0.108	5.273	0.738
0.808	0.081	0.111	5.733	0.962
0.441	0.465	0.094	2.477	0.116
0.489	0.416	0.095	2.875	0.157
0.744	0.053	0.173	5.591	0.881
0.786	0.160	0.055	5.498	0.832
0.828	0.110	0.062	5.88	1.0
0.799	0.069	0.133	5.906	1.0
0.524	0.274	0.202	3.495	0.241
0.443	0.354	0.203	2.818	0.15
0.582	0.221	0.197	4.201	0.386
0.618	0.127	0.255	4.617	0.513
0.695	0.052	0.253	5.117	0.673
0.695	0.107	0.199	5.099	0.665
0.658	0.124	0.219	4.662	0.513
0.486	0.257	0.257	3.416	0.229
0.475	0.477	0.051	2.271	0.104
0.540	0.409	0.051	2.819	0.150
0.611	0.339	0.051	3.719	0.282
0.423	0.223	0.354	2.41	0.111
0.523	0.143	0.334	3.01	0.172

Maximum deviation ± 7%

Activity Coefficients of Sulphides in Aluminate and Silicate Melts

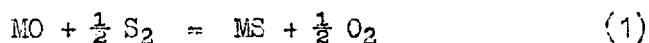
The activity coefficients of sulphides with respect to pure solids in the systems $MnO + Al_2O_3$, $MnO + SiO_2 + Al_2O_3$ and $MgO + SiO_2$ at $1650^\circ C$ have been calculated by using the measured sulphide capacities and activity data in these systems, by means of the following relation

$$\gamma_{MS} = \frac{a_{MO} \cdot 32 \cdot N \cdot K}{C_s}$$

which can be obtained from the equation

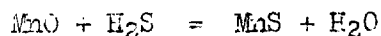
$$K = \frac{a_{MS}}{a_{MO}} \left(\frac{P_{O_2}}{P_{S_2}} \right)^{\frac{1}{2}}$$

for the reaction



where γ_{MS} is the activity coefficient of the sulphide MS
 a_{MO} is the activity of the oxide MO in the melt
 a_{MS} is the activity of the sulphide MS in the melt
 N is the number of gm. moles per 100 gm. of the slag
 $C_s = \text{wt \% S} \left(\frac{P_{O_2}}{P_{S_2}} \right)^{\frac{1}{2}}$ is the sulphide capacity
 K is the equilibrium constant for the reaction (1)

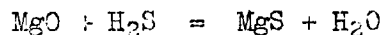
γ_{MnS} in the systems $\text{MnO} + \text{Al}_2\text{O}_3$ and $\text{MnO} + \text{Al}_2\text{O}_3 + \text{SiO}_2$ at 1650°C has been calculated using the C_s and a_{MnO} values measured in the present work and K value calculated from the free energy data³⁷ for the reaction



after slight extrapolation and combining the free-energy data for H_2S ²⁹ and H_2O ³⁰. The results are submitted for the binary $\text{MnO} + \text{Al}_2\text{O}_3$ in Table XVIII and Fig. 28, and for $\text{MnO} + \text{Al}_2\text{O}_3 + \text{SiO}_2$ in Table XX and Fig. 29. The γ_{MnS} in the ternary $\text{MnO} + \text{Al}_2\text{O}_3 + \text{SiO}_2$ at N_{SiO_2} to $N_{\text{Al}_2\text{O}_3}$ equal to 0.5 is also shown in Fig. 28.

It is considered that the a_{MnO} are correct to ± 8 , $K \pm 10\%$ and $C_s \pm 8\%$, so the values of γ_{MnS} are accurate to $\pm 15\%$.

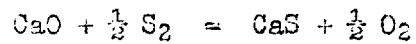
γ_{MgS} has been calculated at 1650°C using the value of C_s measured here, a_{MgO} ⁵⁸ and K value from the free energy data³⁷ for the reaction



after slight extrapolation and by combining with the free energy data on H_2S ²⁹ and H_2O ³⁰. The results are given in Table XIX and Fig. 28

It is suggested that a_{MgO} is correct to $\pm 10\%$,
Cs to $\pm 10\%$ and K to $\pm 10\%$, so the values are accurate to
 ± 17 .

The γ_{CaS} in the system $CaO + SiO_2 + Al_2O_3$ calculated
at $1600^\circ C$, by using Cs, a_{CaO} ¹⁷ and the equilibrium constant
of the reaction



has been presented in Fig. 29.

Activity Coefficients of Sulphides in Aluminate and Silicate melts.

TABLE XVIII

Activity coefficient of MnS for
MnO + Al₂O₃ melts at 1650°C.

<u>N_{MnO}</u>	<u>N_{Al₂O₃}</u>	<u>Activity coefficient of MnS*</u>
0.60	0.40	1.49
0.65	0.35	2.18
0.68	0.32	2.04
0.75	0.25	2.00
0.825	0.175	1.15

TABLE XIX

Activity coefficient of MgS for
MgO + SiO₂ melts at 1650°C.

<u>N_{MgO}</u>	<u>N_{SiO₂}</u>	<u>Activity Coefficient of MgS*</u>
0.39	0.61	1.2
0.45	0.55	2.15
0.54	0.46	3.47
0.57	0.43	3.42
0.60	0.40	3.0

TABLE XX

Activity coefficient for MnS for
MnO + SiO₂ + Al₂O₃ melts at 1650°C.

<u>N_{MnO}</u>	<u>Activity Coefficient of MnS at SiO₂ : Al₂O₃;</u>		
	1	0.44/0.66	0.7/0.3
0.42	3.49	3.41	3.73
0.46	3.92		
0.50	4.36	4.10	4.39
0.60	3.47	3.30	3.63
0.70	1.94	1.19	2.02
0.80	0.83	0.906	0.885

DISCUSSION

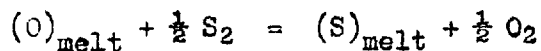
The results given in the previous chapter will be discussed section by section, as they were presented.

A. Sulphur in Aluminate and Silicate Melts and Crystalline Oxides.

(i) Sulphide capacities

The results, given in this section, were obtained with the object of showing the effect of melt composition on the sulphur holding capacity of the melt under the experimental conditions. The sulphur holding capacity, defined as sulphide capacity "Cs" by Fincham and Richardson¹, is a measure of the de-sulphurizing power of the melt under equilibrium conditions. Cs therefore, is an important property of metallurgical slags used in iron and steel production.

Under the experimental conditions of the measurements, at oxygen potentials ranging from 10^{-6} to 10^{-8} atm., the sulphur is held as sulphide according to the equation



As shown earlier, the sulphide capacity is

$$C_s = \text{wt \% S} (P_{O_2}/P_{S_2})^{\frac{1}{2}}$$

(a) Binary MnO + Al₂O₃ melts

Table I gives the measured sulphide capacities in these melts at 1650°C. The results are plotted in Fig. 3. It may be seen from the figure that the sulphide capacity of the melt increases with increasing manganese oxide content. The sulphide capacity in MnO + SiO₂ melts at 1650°C reported by Abraham and Richardson⁷ are also given in this figure. The upper points ● are the measurements done in the present work.

It may be seen that, in these binary melts (MnO + Al₂O₃ and MnO + SiO₂), the Cs values are the same below N_{MnO} equal to 0.625, but above this mole fraction the Cs values in MnO + Al₂O₃ melts are smaller than their corresponding Cs values in MnO + SiO₂. This would be expected, since the Cs value is dependent on the basic oxide activity and it is greater when the latter is greater. Above N_{MnO} equal to 0.625, a_{MnO} in MnO + Al₂O₃ melt is smaller than in the corresponding MnO + SiO₂ at the same mole fraction of manganese oxide. In Fig. 3, Cs values in MnO + Al₂O₃ melts are also observed to decrease from $N_{\text{MnO}} = 0.82$ to pure manganese oxide. This might be due to the formation of solid MnO whose concentration may increase continuously with increasing mole fraction of MnO while that of liquidus may decrease. The conjunction of the two curves at N_{MnO} equal to 0.82 thus suggests that the saturation limit of MnO

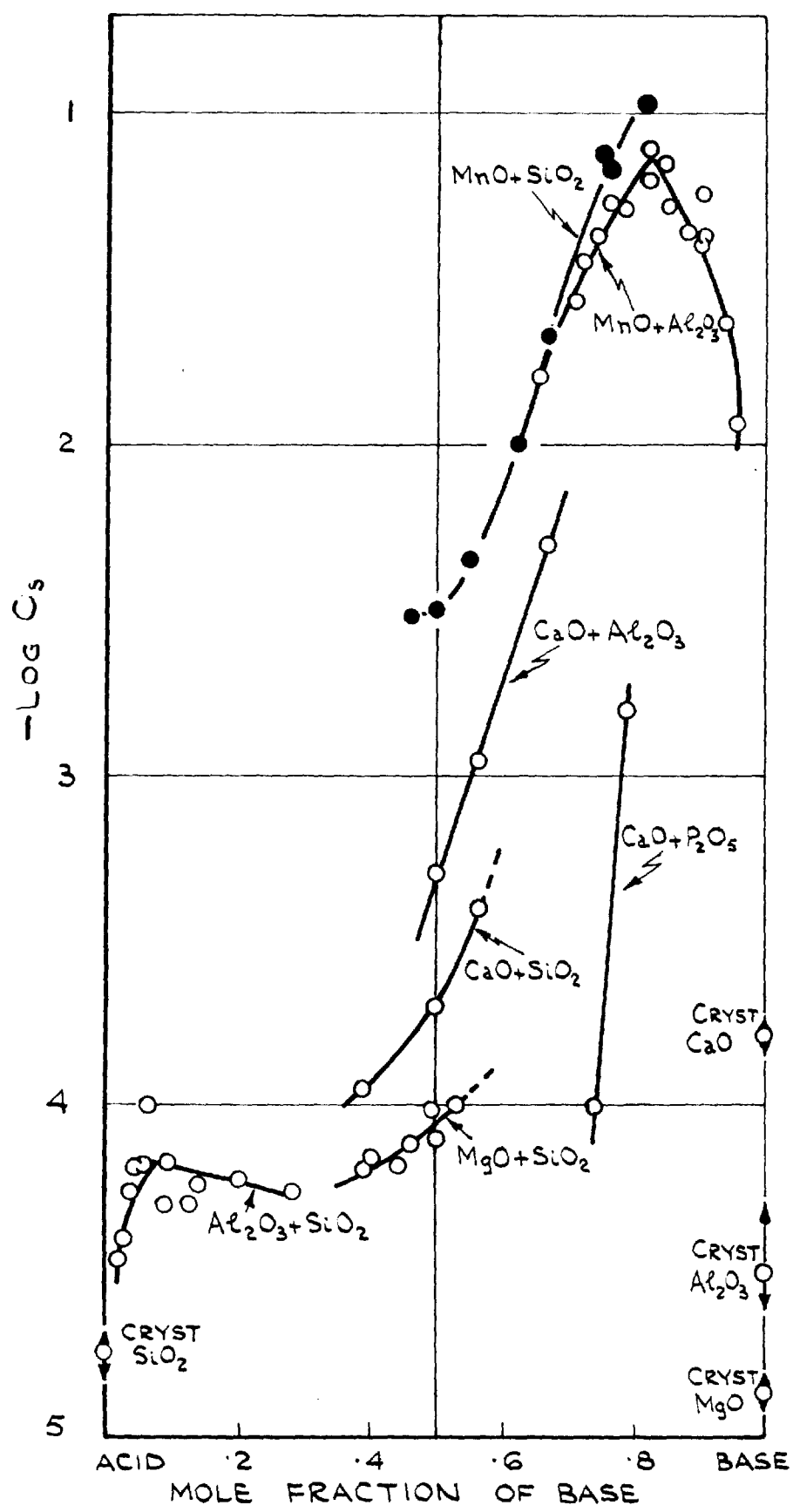
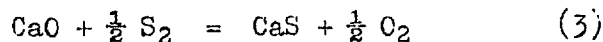
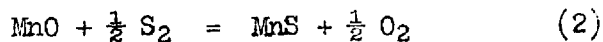
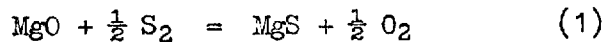


FIG.3. SULPHIDE CAPACITIES at 1650°C

in the melt has been reached. This saturation limit is in agreement with the activity data presented later.

(b) Binary MgO + SiO₂ melts

Sulphide capacities measured at 1650°C in these melts are given in Table II, and Fig. 3. It may be seen from this figure that the values of the sulphide capacity are very low and, at the same mole fraction of silica, they are smaller than the corresponding ones in MnO + SiO₂ or CaO + SiO₂ melts. This may be due to the fact that the equilibrium constants^{27, 28, 29, 30} of the reactions (2) and (3) equal to 2.1×10^{-3} and 4.46×10^{-3} are greater than that of (1), which is 2.4×10^{-5} at 1650°C.

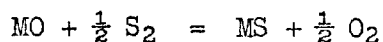


The C_s values in MgO + SiO₂ should be 200 times less than those in CaO + SiO₂ according to the difference in their K values. They are, however, higher than this would predict because the MgO activities are greater than the corresponding ones of CaO.

(c) Binary Al₂O₃ + SiO₂ melts

Sulphide capacities have been measured at 1650°C between 0.02 to 0.28 mole fractions of alumina in these melts. Results are given in Table III, and Fig. 3. Though the maximum deviation observed is $\pm 25\%$, it reduces to $\pm 10\%$ when the results of the experiments with one gm. samples are considered. It may be seen from this figure that the C_s decreases on either side of alumina mole fraction equal to 0.074. When alumina is greater than this, the decrease in C_s may be due to the formation of solid mullite, i.e. the melt may be saturated with mullite at $N_{Al_2O_3} = 0.074$. This is in agreement with the recent phase diagram given by Aramaki and Roy,³⁹ but in disagreement with the phase diagram reported by Tromel⁴⁰. C_s , plotted against alumina mole fraction, was observed to decrease progressively with decrease in alumina concentration and to extrapolate to zero for supercooled liquid silica. This indicates that sulphur may be dissolved in the melt on account of alumina.

The sulphide capacity in any melt is expected to be dependent on the concentration of the basic oxide or its activity and the equilibrium constant K for the reaction



i.e. the greater the concentration or activity and the equilibrium constant, the higher will be the value of the sulphide

capacity. Accordingly, it may be seen from Fig. 3 that sulphide capacity increases with basic component concentration in MnO + SiO₂,⁷ MnO + Al₂O₃, CaO + SiO₂, MgO + SiO₂, CaO + P₂O₅,⁸ and Al₂O₃ + SiO₂ melts. The Cs values decreasing in the order of MnO + SiO₂ > CaO + SiO₂ > MgO + SiO₂ at 0.50 mole fraction of silica is also in accordance with the equilibrium constants.

(d) Ternary MnO + SiO₂ + Al₂O₃ melts.

Results obtained in these melts at 1650°C are given in Table VI and Fig. 4. It is apparent from this figure that the sulphide capacity remains approximately constant at a constant mole fraction of manganese oxide. This is in accordance with expectation, since for these melts a_{MnO} has been observed to be approximately constant at constant mole fraction of MnO in this region of compositions (Fig. 26).

(e) Ternary MnO + MgO + SiO₂ melts.

Table V and Fig. 5 contain the results of the measurements of Cs in these melts at 1650°C. It may be seen from this figure that at constant ratio of $\frac{N_{\text{MgO}}}{N_{\text{SiO}_2}}$, the Cs increases with the manganese oxide concentration, and the increase is greater with increase in $\frac{N_{\text{MgO}}}{N_{\text{SiO}_2}}$ ratio. Along the constant mole fraction of silica line, the Cs is found to increase as MgO is replaced by MnO. This also is as would be expected

FIG. 4.
 SULPHIDE CAPACITIES
 ($-\log C_s$) in $MnO+Al_2O_3+SiO_2$
 AT 1650 °C.

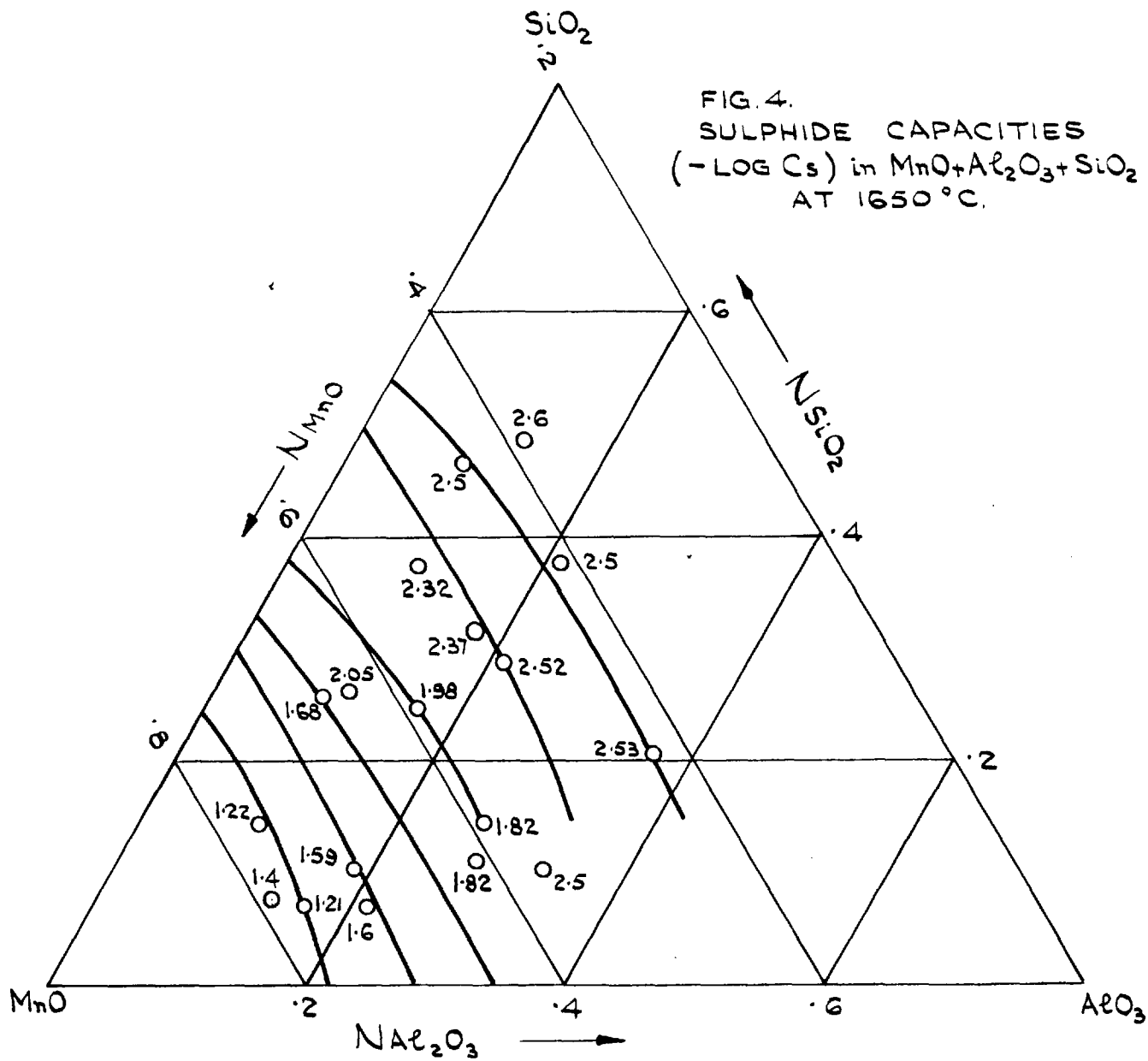
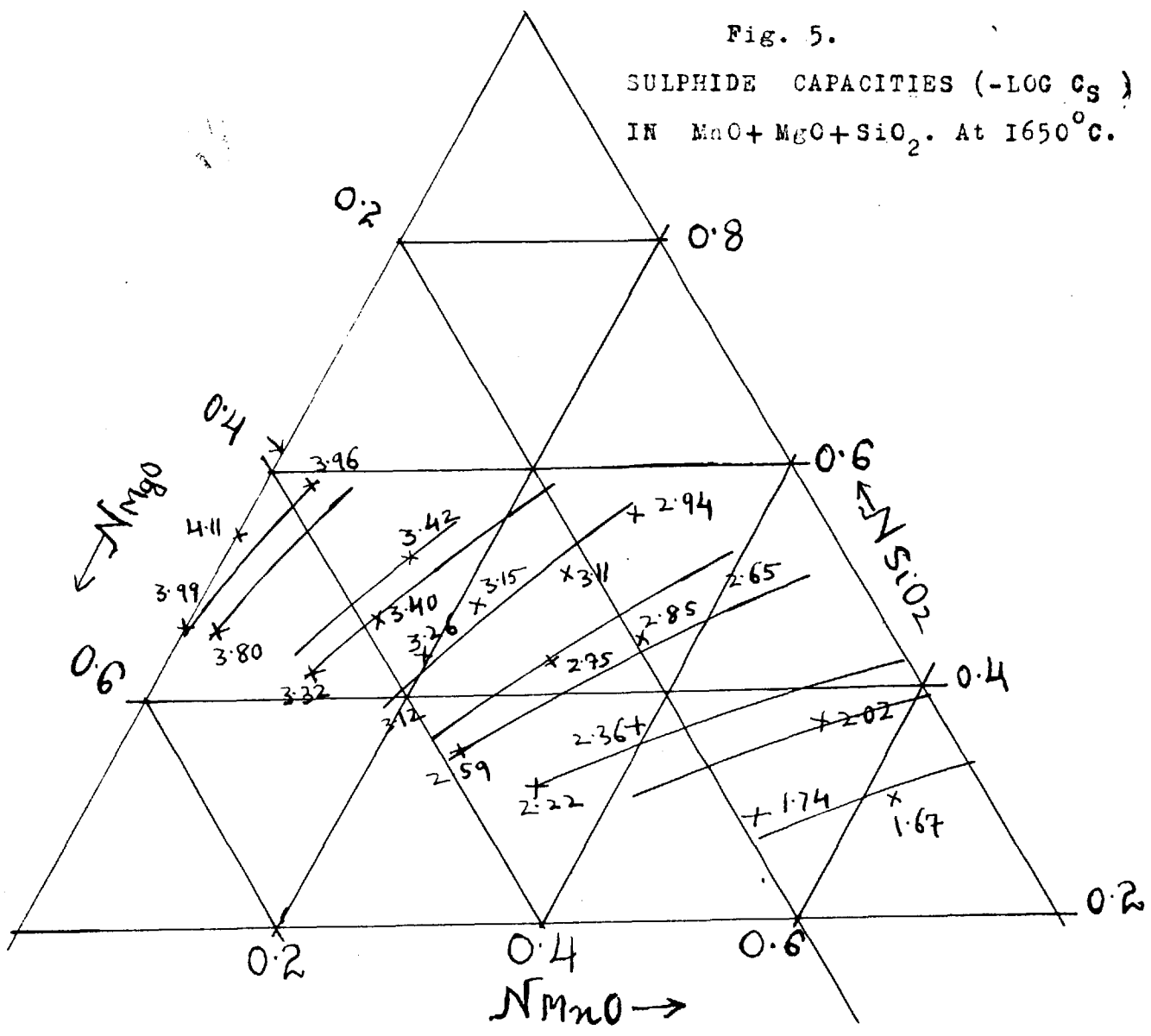
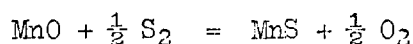


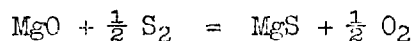
Fig. 5.
SULPHIDE CAPACITIES ($-\log C_S$)
IN $MnO + MgO + SiO_2$. At $1650^\circ C$.



since, firstly, a_{MnO} is always greater than a_{MgO} in these melts, and, secondly, the equilibrium constant for the reaction



is greater than that of



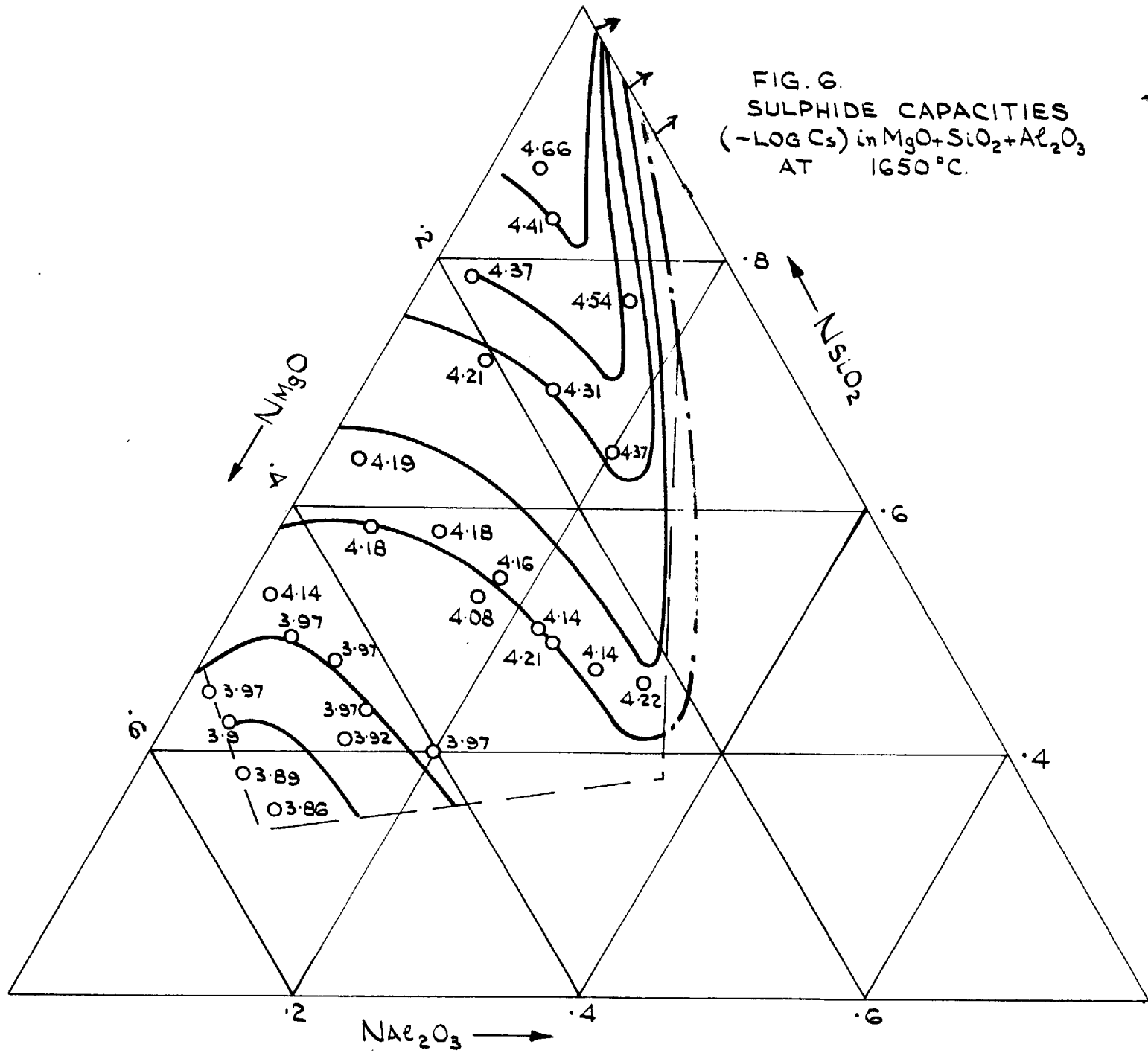
at this temperature.

(f) Ternary MgO + SiO₂ + Al₂O₃ melts.

Sulphide capacity measurements for these melts at 1650°C are given in Table VI and Fig. 6. It may be seen from the figure that the sulphide capacity increases with increasing alumina concentration along the line of constant $N_{\text{MgO}}/N_{\text{SiO}_2}$ ratio. The initial increase is greater as the $N_{\text{MgO}}/N_{\text{SiO}_2}$ ratio becomes larger.

Small amount of alumina added to SiO₂ may give rise to aluminium cations (Al³⁺), and added to a basic oxide such as MgO, to anions, (AlO₂⁻, AlO₃²⁻). In the case of a silicate mixture such as MgO + SiO₂, the behaviour should change from cationic to anionic as one proceeds from the silica side to the MgO. When the alumina concentration is high, it may partly give rise to anions, even in the silica rich region. It is also likely, as has been reported by Kozakevitch⁴¹ in CaO + SiO₂ + Al₂O₃ melts, that at $N_{\text{MgO}}/N_{\text{Al}_2\text{O}_3} \gg 1$ aluminum in the melts may have a coordination number of four and form

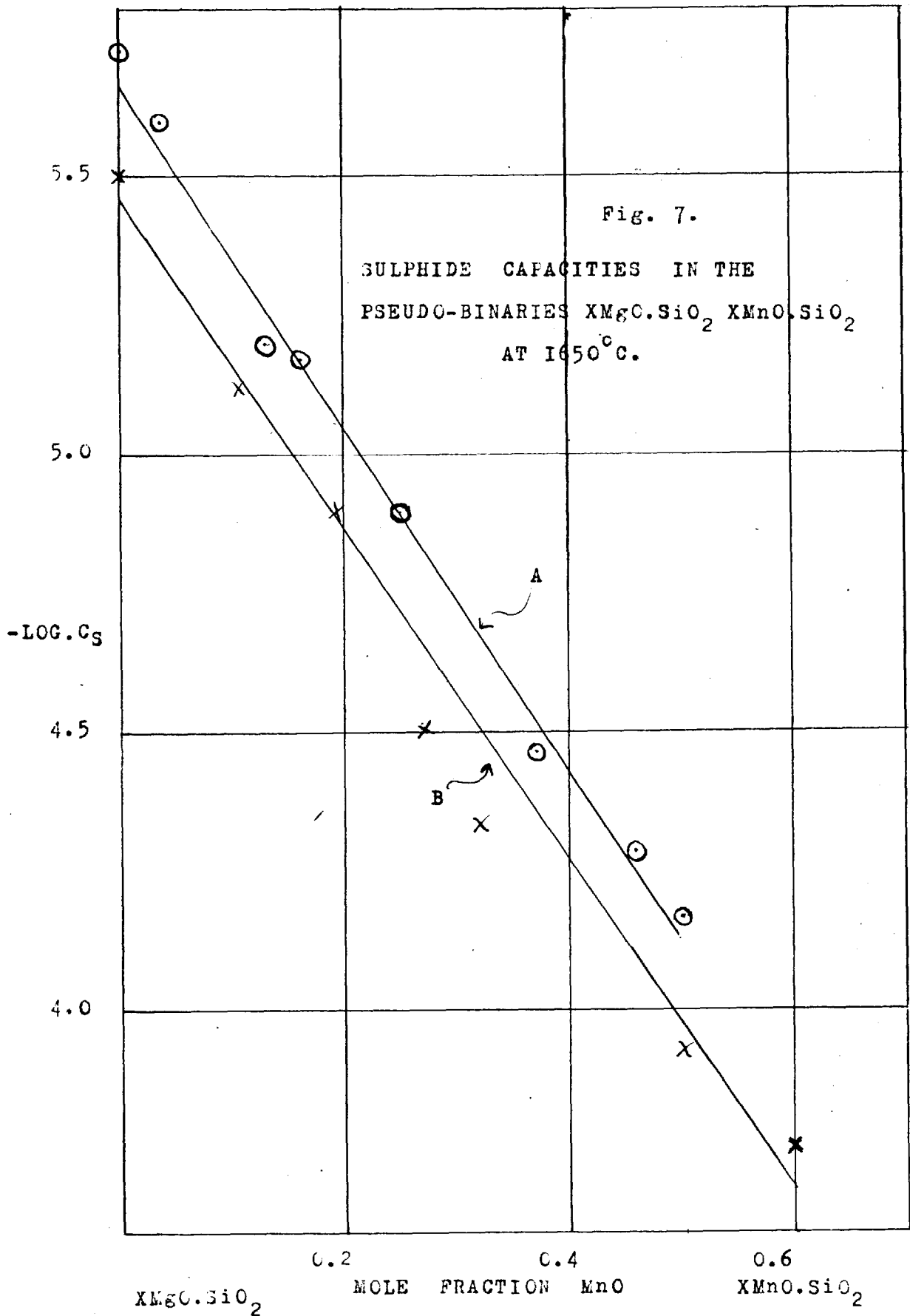
FIG. 6.
 SULPHIDE CAPACITIES
 ($-\log C_s$) in $MgO + SiO_2 + Al_2O_3$
 AT 1650°C.



6L

a tetrahedral structural unit AlO_4^{5-} in the silica network. This type of behaviour of alumina appears from the curves in Fig. 6. For example, the curve representing $-\log C_s = 4.37$ indicates that C_s first increases, then remains constant and finally decreases along the constant ratio of N_{MgO}/N_{SiO_2} , suggesting that the alumina might first have given rise to cations and then both cations and anions and finally more anions. The curve changes its direction upward at composition:- $MgO = 0.16$, $Al_2O_3 = 0.22$ and $SiO_2 = 0.62$ and beyond $N_{MgO}/N_{Al_2O_3} = 1$. This suggests that in this range alumina may give rise to anions with a tetrahedral structural unit AlO_4^{5-} in the silica network giving silica-like structure.

This peculiar behaviour of alumina may be one of the reasons for the difficulty found in the prediction of the desulphurizing power of complex slags.



Results in relation to Flood's Equation

Flood's equation⁹ has already been described in the Introduction (page 4). The results obtained in the present work provide a direct means of checking the validity of that equation which, when considering the sulphide capacities of silicate melts, may be written in the modified form:-

$$\log Cs'_{(A+B)} = N_A \log Cs'_{(A)} + N_B \log Cs'_{(B)}$$

where N_A and N_B are the mole fractions of cations A^{++} and B^{++} , i.e. are equal to $\frac{N_{AO}}{N_{AO} + N_{BO}}$ and $\frac{N_{BO}}{N_{AO} + N_{BO}}$

respectively. $Cs'_{(A)} = N_{S(A)} \left(\frac{P_{O_2}}{P_{S_2}} \right)^{\frac{1}{8}}$ in the presence

of cations A^{++} where $N_{S(A)}$ etc., are the mole fractions of sulphur instead of wt % S in the melt containing A^{++} cations and so on. This has been used to avoid the effects of differing atomic weights of cations.

Fig. 7 has been constructed from the results obtained in the systems $MnO + MgO + SiO_2$, $MnO + SiO_2$,⁶ and $MgO + SiO_2$ at 1650°C reported earlier. This figure gives plots ^{B+A} of $\log Cs'$ against the composition of the melt for the mole fractions 0.4 and 0.5 of silica. The linear relationship between $\log Cs'$ and the composition of the melt at constant mole fraction of silica is apparent from these plots,

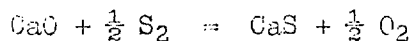
and thus supports the validity of the modified Flood's equation for the sulphide capacities in the ternary melt MnO + MgO + SiO₂ in this composition range at 1650°C.

Sulphur in Crystalline Oxides

The results in Table VII which indicates the equilibrium sulphur and sulphide capacities in crystalline CaO, MgO, Al₂O₃ and SiO₂ at 1650°C, shown in Fig. 3, are discussed below for each of the oxides separately.

CaO:

The way in which the results presented in Table VIII and Fig. 8A have been used to derive the saturation limit of sulphur in crystalline CaO, is given later. The saturated sulphur is equal to 0.036% when $(P_{C_2}/P_{S_2})^{\frac{1}{2}}$ is equal to 4.46×10^{-3} at 1650°C. The results confirm the value of the equilibrium constant $K^{\frac{23}{2}}$ for the reaction

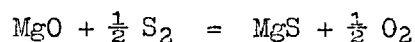


as shown later. If it is assumed that the sulphur at saturation at 1650°C is not appreciably different from that at 1550°C then the present finding disagrees substantially with that of St. Pierre and Chipman⁴ who reported a sulphur solubility in CaO of 0.78% at 1550°C. The equilibrium constant for the above reaction, calculated using the partial pressures of sulphur and oxygen reported by them, is equal to 0.16.

This also is very different from the value obtained from Rosenqvist's data,²⁸ which is equal to 3.27×10^{-3} . The activity coefficient of CaS in CaO calculated from the present data is equal to 1586 at N_{CaS} of 0.00063.

MgO:

The equilibrium sulphur in magnesium oxide equal to 0.008% (Table XI), was obtained for $(P_{\text{O}_2}/P_{\text{S}_2})^{\frac{1}{2}} = 1.87 \times 10^{-3}$ at 1650°C. Using the value for the equilibrium constant K (given earlier) for the reaction



$a_{\text{MgO}} = 0.013$ and $\gamma_{\text{MgS}} = 130$ at $N_{\text{MgO}} = 0.0001$, was calculated.

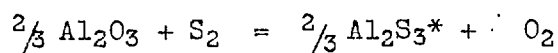
Unfortunately it has not been possible to measure the limiting solubility of sulphur in this oxide, because the gas mixture used here could not give the $(P_{\text{S}_2}/P_{\text{O}_2})^{\frac{1}{2}}$ ratio required for saturation. However, assuming that Henry's Law is obeyed from 0.008% S by weight up to that at saturation, and using the Cs value given in Table VII, the sulphur at saturation can be calculated. This is equal to 0.568%, which is greater than that found for CaO.

Al₂O₃:

The equilibrium sulphur in this oxide was 0.0265% and 0.0006% for $(P_{\text{O}_2}/P_{\text{S}_2})^{\frac{1}{2}}$ equal to 1.87×10^{-3} and 6.3×10^{-3}

at 1650°C. The sulphide capacities were 5.0×10^{-5} and 5.9×10^{-5} .

Rough calculation based on the available data^{42, 43} gave a value for the equilibrium constant K equal to 1.58×10^{-11} at 1650°C for the reaction



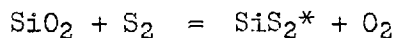
Using this value of K and experimental values of $(p_{\text{S}_2}/p_{\text{O}_2})^{\frac{1}{2}}$ $a_{\text{Al}_2\text{S}_3} = 2.4 \times 10^{-10}$ and 9.6×10^{-9} and $\gamma_{\text{Al}_2\text{S}_3} = 3.7 \times 10^{-6}$ and 2.7×10^{-5} at $N_{\text{Al}_2\text{S}_3} = 6.4 \times 10^{-5}$ and 2.8×10^{-4} were obtained. These values of $\gamma_{\text{Al}_2\text{S}_3}$ are comparable with the values 5.75×10^{-10} and 7.8×10^{-8} obtained on the basis of ideal behaviour (which might be possible in these very dilute solutions) where sulphur atoms are assumed to be randomly distributed on the oxygen lattice.

SiO₂:

The equilibrium sulphur 0.01% and 0.00265% were obtained in crystalline SiO₂ at 1650°C for $(p_{\text{O}_2}/p_{\text{S}_2})^{\frac{1}{2}}$ equal to 6.3×10^{-3} and 1.87×10^{-3} . The sulphide capacities were 2.0×10^{-5} and 1.7×10^{-5} . $a_{\text{SiS}_2} = 1.48 \times 10^{-8}$ and

* The free energy of formation of Al₂S₃ used in the above calculation was extrapolated from 25°C to 1650°C.

1.26×10^{-8} , and $\gamma_{\text{SiS}_2} = 1.6 \times 10^{-4}$ and 5.07×10^{-4} at
 $N_{\text{SiS}_2} = 9.0 \times 10^{-5}$ and 2.5×10^{-5} were calculated from
the experimental values of $(P_{\text{S}_2}/P_{\text{O}_2})^{\frac{1}{2}}$ and that of equilibrium
constant K for the reaction



which, on rough calculation from the available data,^{42, 43}
was found to be 4.76×10^{-14} . The values of γ_{SiS_2} , though
they appear very low, are comparable with $\gamma_{\text{SiO}_2} = 9.0 \times 10^{-5}$
and 2.5×10^{-5} obtained on the assumption of ideal solid
solution (which may not be unlikely at such a low concentration
of solute) in which sulphur atoms are randomly distributed
on the oxygen lattice.

* The free energy of formation of SiS_2 used in the calculation was extrapolated from 25° to 1650°C .

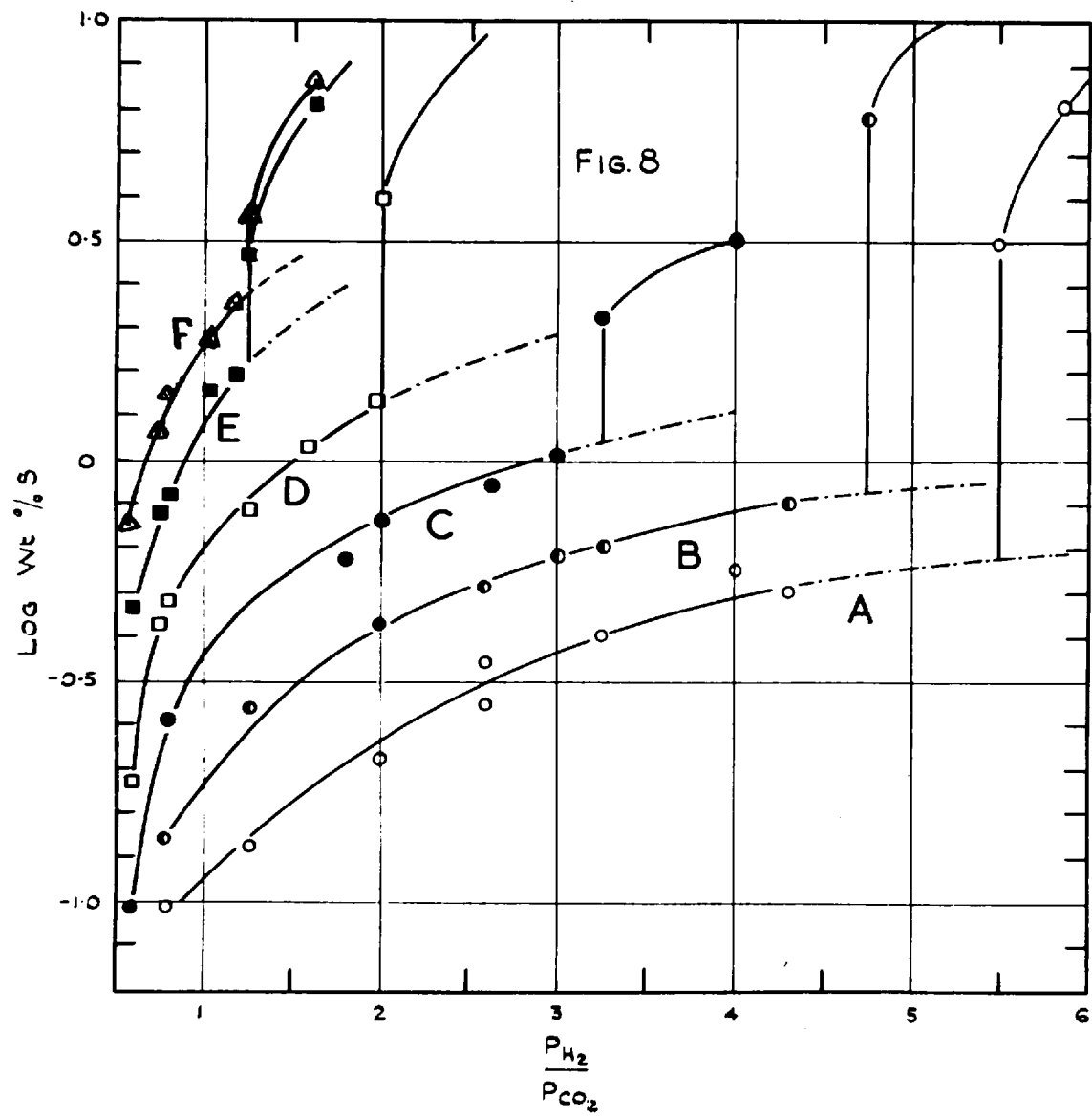
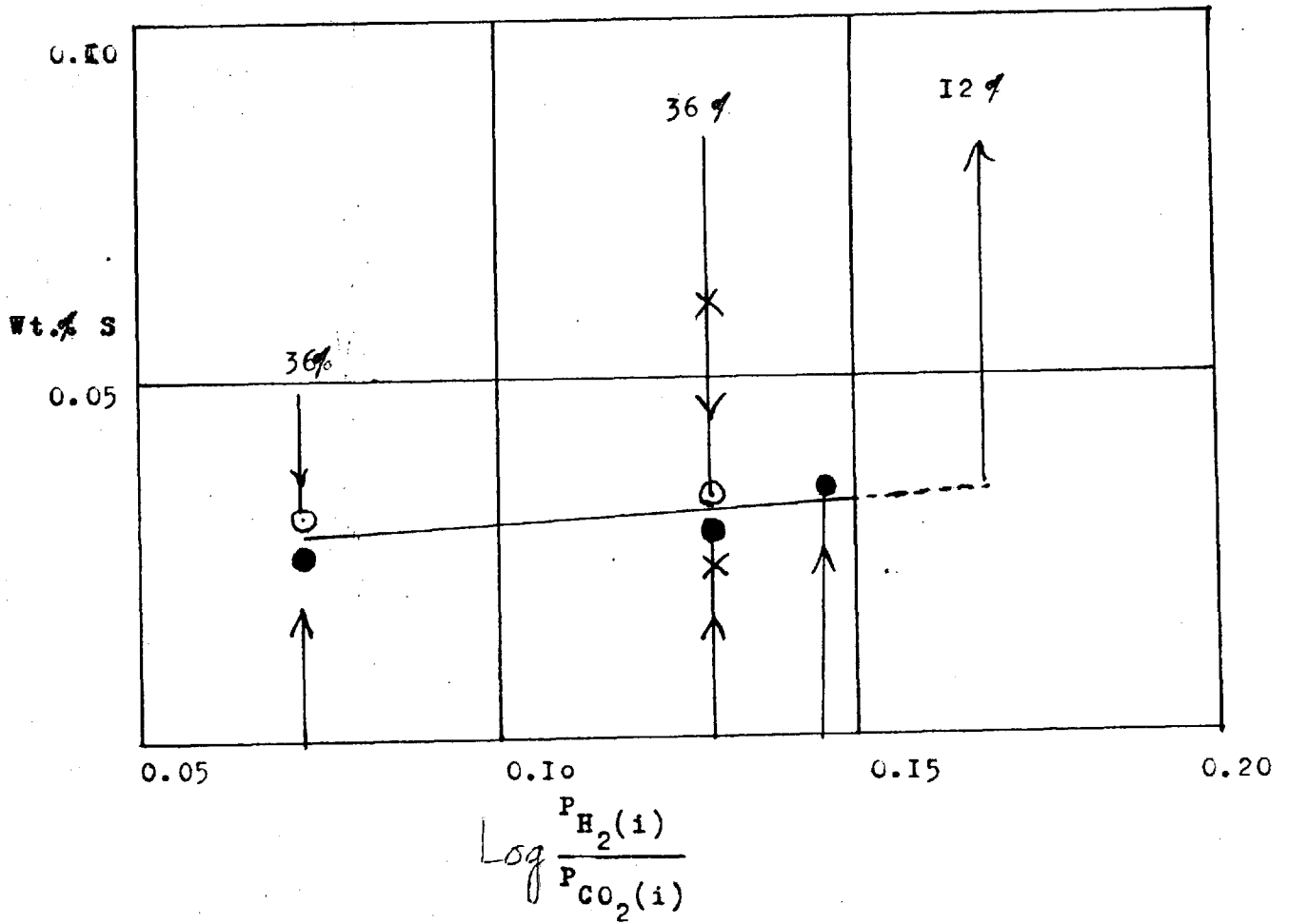


Fig. 8A.

Sulphur in Crystalline CaO. Temp. 1650°C.



(ii) Limiting solubilities of Sulphur and lime-activities in crystalline lime and lime-alumina and lime-silica melts.

(a) Lime + alumina melts and crystalline lime

(a₁) Solubility limits of CaS

The experimental results, at 1500°C for CaO + Al₂O₃ melts of six initial compositions with CaO (A) 42%, (B) 45%, (C) 48.2%, (D) 52%, (E) 56% and (F) 60.6% + 7% SiO₂ are given in Table VIIIA and Fig. 8. Those of crystalline lime at 1650°C are shown in Table VIII and Fig. 8A. In Fig. 8, log wt % S in the melts and in Fig. 8A, wt % S in crystalline lime have been plotted against $P_{H_2(i)}/P_{CO_2(i)}$. In Fig. 8A the solid points and circles represent the final percentages of sulphur obtained from the initial zero and 36.6% sulphur respectively. The saturation limit for any of the melts or CaO (described earlier) has been obtained by a sharp discontinuity in an otherwise smooth curve (Figs. 8 and 8A). The saturation limits so obtained have been shown in Table IX and Fig. 9. In this figure wt % S has been plotted as a function of the mole fraction of the lime present in the melt before sulphur pick up; further, the lower point for each composition is the last experimental point before saturation was reached, the upper solid point is that obtained from the intersection of the dotted extrapolation and the full vertical line (see Fig. 8). The full line in Fig. 9A

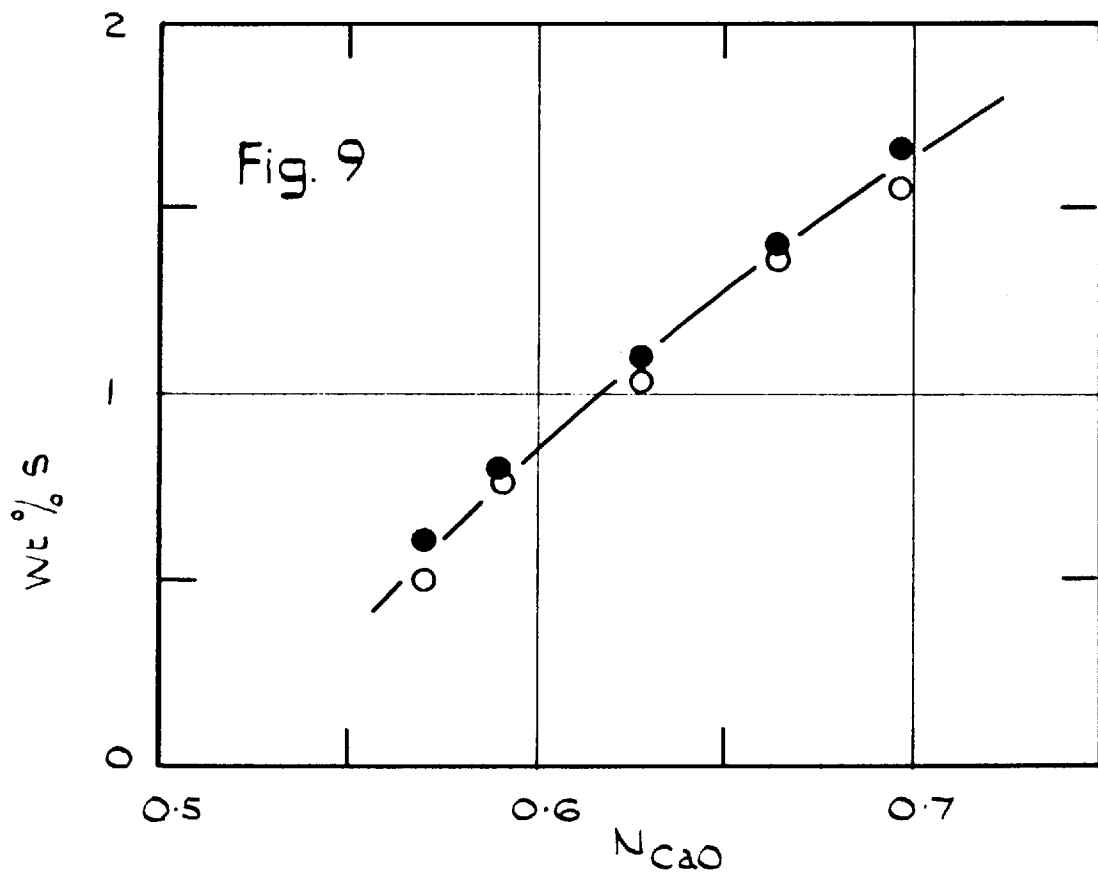
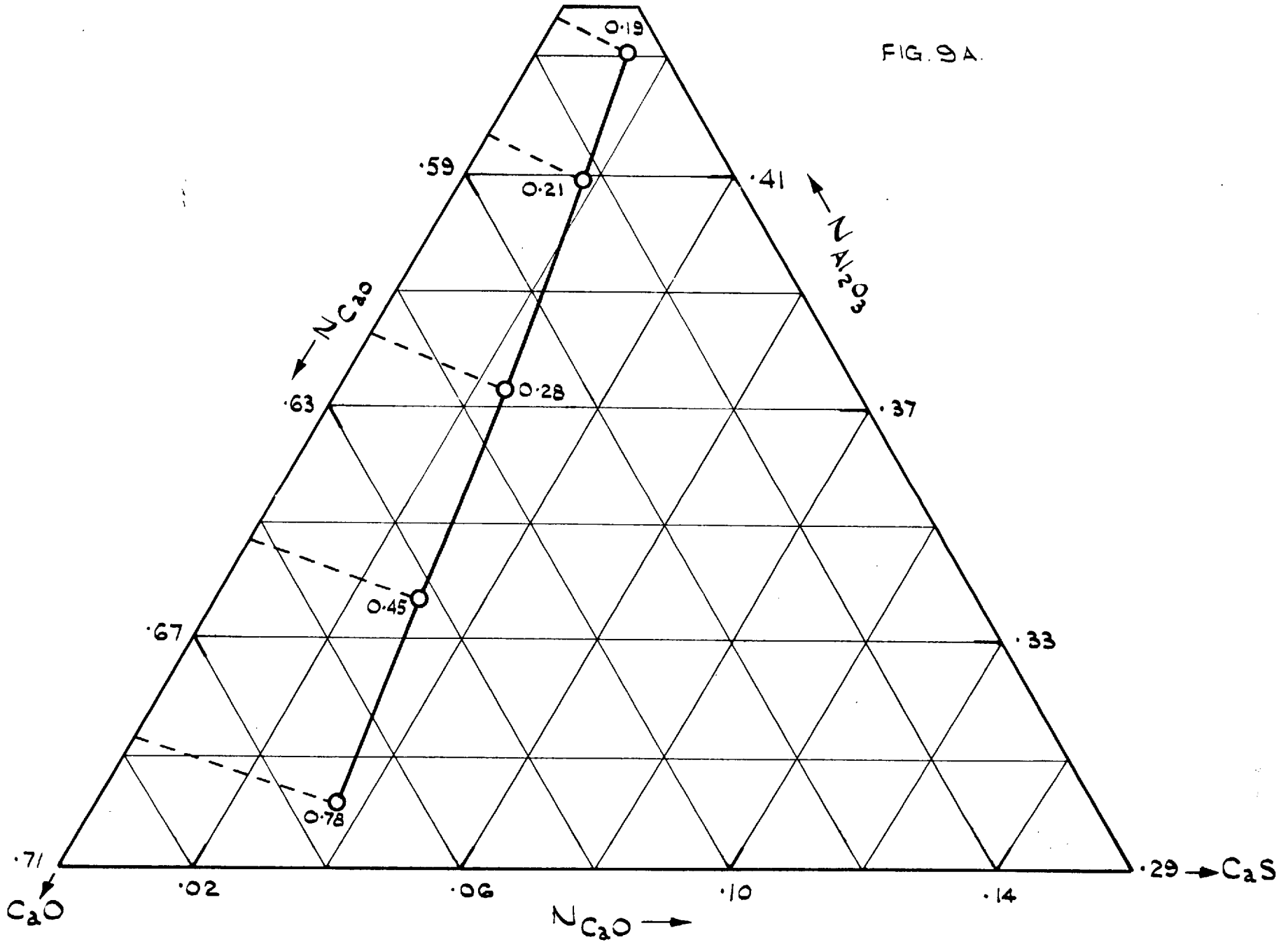


FIG. 9A.



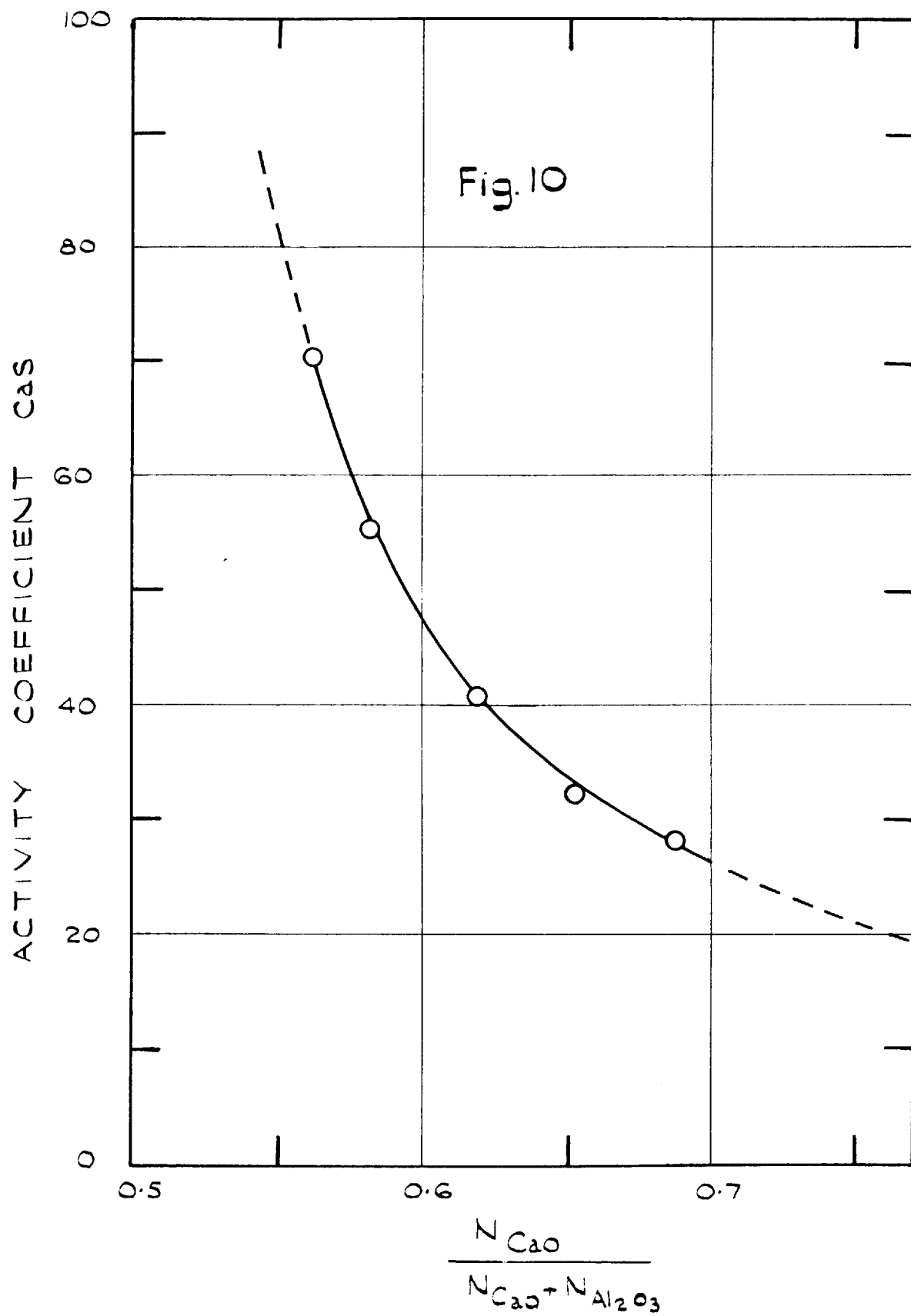
shows the saturation limits on the ternary composition diagram.

The values of the activity coefficient of CaS relative to the pure solid CaS are shown in Table IX and Fig. 10. The activity coefficient changes from 72.5 to 28.0 with change in N_{CaO} from 0.57 to 0.72 in the original melt. The variation is comparable with that already found for MnS in MnO + SiO₂ melts.⁷ In view of the large variations in activity coefficient of sulphide, this function should never be assumed to be constant over a wide range of composition, even for approximate calculation of lime activities from sulphide capacities.

The activity coefficient of solid CaS is expected to extrapolate (when N_{CaO} is equal to one) to a value given by the equation

$$1773 R \ln \gamma_{CaS} = (T_M - 1773) \Delta S_f$$

where T_M is the melting point of CaS and ΔS_f is its entropy of fusion. T_M is not known and there are no reports of CaS having been melted. Analogy with other sulphides suggests that ΔS_f must be about 5 cal.deg.⁻¹mole⁻¹, thus the curve for γ_{CaS} , which could be extrapolated to a value of 5 or 10 is compatible with a not unreasonable value of 2600° - 3100°C for the m.p.

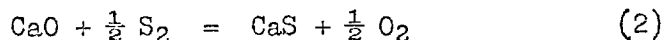


(a₂) Activities of calcium oxide in lime-alumina melts.

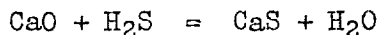
The relationship between the activities of lime and calcium sulphide in any slag is given by the equation

$$K = \frac{a_{\text{CaS}} \left(\frac{p_{\text{O}_2}}{p_{\text{S}_2}} \right)^{\frac{1}{2}}}{a_{\text{CaO}}} \quad (1)$$

where K is the equilibrium constant at 1500°C for the pure phase reaction



This has been accurately established by Rosenqvist²⁸ who studied the equilibrium



between 750° - 1425°C. A small extrapolation of his results enables one to calculate a value of 2.75×10^{-3} for K at 1500°C for reaction (2), after introducing thermodynamic data for H₂O²⁹ and H₂S.³⁰ The activities of lime calculated from equation (1) for the melts saturated with CaS are shown by the numbers in Fig. 9A.

There is no way of using these results for calculating the activities of lime in the absence of CaS, without making some assumptions. There are two simple alternatives, which lead to slightly different results. The simpler is to assume that in the presence of small amounts of CaS (here always less

than 0.04 mole fraction) a_{CaO} is dependent only on the ratio of lime to alumina. The lime activities with respect to pure CaO as standard state calculated in this way are shown by the full line in Fig. 11 and Table X. The other is to assume that γ_{CaS} is independent of N_{CaS} up to saturation. The lime activities calculated on this assumption, using the following relation, are slightly smaller than those obtained by the first method.

$$a_{CaO} = \frac{\gamma_{CaS} \cdot Cs}{32 N \cdot K} \quad (3)$$

where γ_{CaS} = activity coefficient of CaS

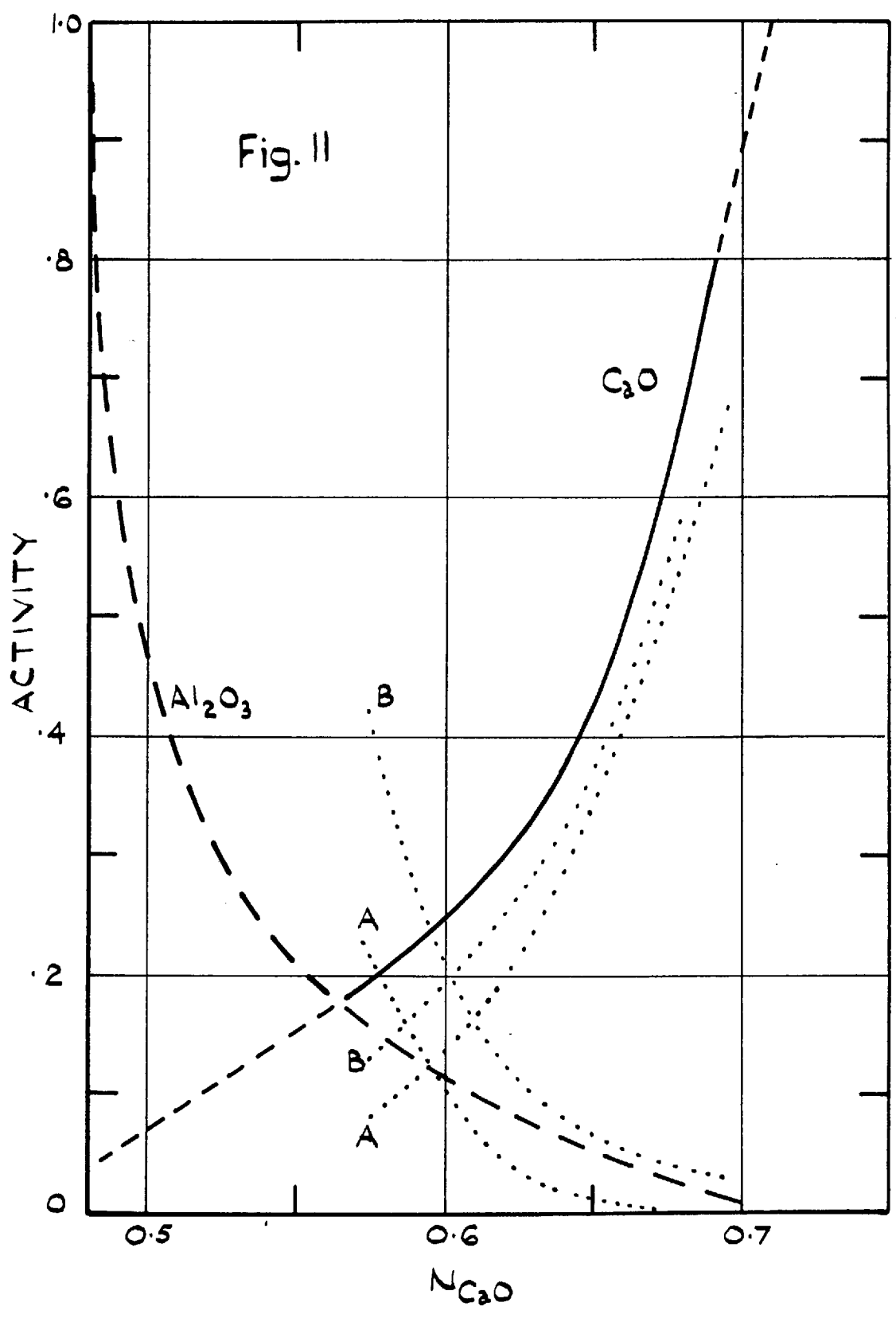
Cs = sulphide capacity

N = the number of gm. moles (CaO + Al₂O₃ + CaS)
in 100 gm. slag

K = the equilibrium constant for the pure phase
reaction (2)

32 = the atomic weight of sulphur.

The value of K can be checked from the sulphide capacity data, $Cs = \text{wt \% S} (P_{O_2}/P_{S_2})^{\frac{1}{2}}$ which can be calculated from the results of Carter and Macfarlane⁵ at 1500°C for the slag: CaO, 0.71; SiO₂, 0.08 and Al₂O₃, 0.21 mole fractions. According to the phase diagram,¹⁶ this melt is saturated with lime at 1500°C and so its activity is unity. The values of Cs (calculated with the newer and more reliable gas equilibrium



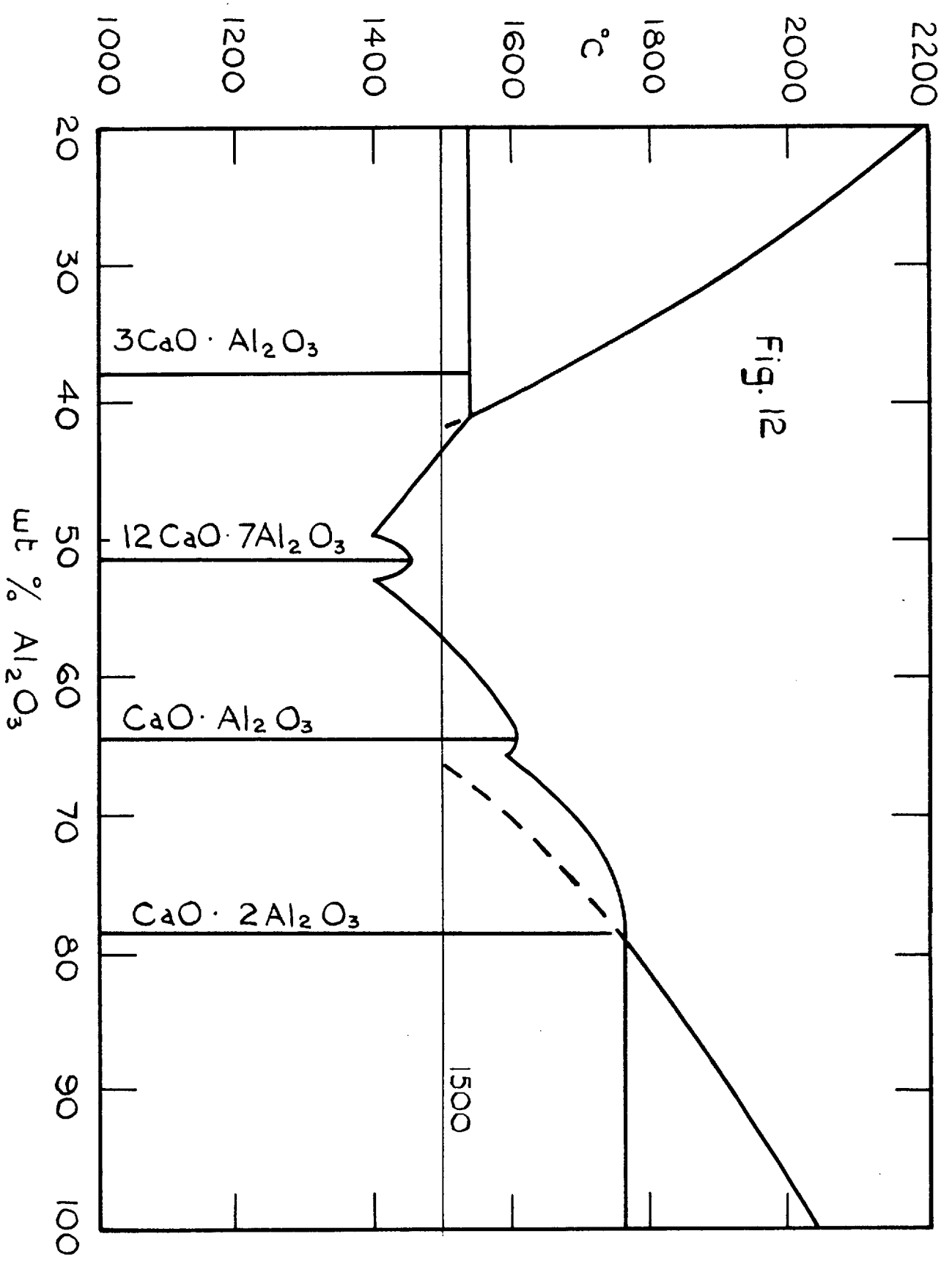
data) are 5.89×10^{-3} and 5.85×10^{-3} . Taking the mean (5.86×10^{-3}) and using equation (3), γ_{CaS} is found to be 22.7. The value of γ_{CaS} obtained in the present work for somewhat similar slag: CaO, 0.66; CaS, 0.055; SiO₂, 0.08 and Al₂O₃, 0.21 mole fractions with CaS at saturation, is equal to 18 ± 1 . Thus K is reasonably confirmed.

Again, by considering relation (1) for CaO saturated with sulphur, which is equal to 0.036% by weight at 1650°C,

$$K = (P_{\text{O}_2}/P_{\text{S}_2})^{\frac{1}{2}} = 4.46 \times 10^{-3}$$

whereas the value derived from the free energy data at 1650°C^{28, 29, 30} is equal to 4.53×10^{-3} . The agreement between these figures which is fortuitously remarkable, since their difference is well within the probable limits of error, provides a further confirmation of the K value; the doubts about this expressed on the basis of CaO + CaS solid solution formation by Fisher⁴⁴ and Shenck⁴⁵, are thereby not substantiated.

Taylor and Stobo⁴⁶ have suggested that, in slags of the composition 28 wt % CaO, 26 wt % SiO₂, 46 wt % Al₂O₃, γ_{CaS} may decrease by a factor of 4 or 5 as the concentration of CaS rises from zero to about 1% by weight. However, these authors' results require that the sulphide capacities, as defined



here, should increase markedly as sulphur displaces oxygen in the slag, whereas it has been found in this work that C_s is almost independent of sulphur concentration. (Table VIIIA). The conclusion of Taylor and Stobo concerning the change of γ_{CaS} with sulphur concentration is thus in doubt, at least in so far as melts of $CaO + Al_2O_3 + CaS$ are concerned. Since C_s is independent of sulphur concentration along any horizontal composition line in Fig. 9A, i.e. as sulphur displaces oxygen in a $CaO + Al_2O_3$ mixture, the ratio a_{CaO}/γ_{CaS} must be constant. This follows from equation (3) where both N and C_s remain nearly constant. Since a_{CaO} must almost certainly decrease along such a composition line, it follows that γ_{CaS} also decreases. The change, however, is not likely to be great.

The value of K appears to be accurate to $\pm 5\%$ and that of $(P_{O_2}/P_{S_2})^{\frac{1}{2}}$ at saturation is also probably accurate to $\pm 5\%$ and the assumption concerning the constancy of a_{CaO} at constant lime to alumina ratio is correct to $\pm 5\%$. Therefore the derived activities should be accurate to about $\pm 10\%$

The lime and alumina phase diagram is shown in Fig. 12. It is based on the work of Rankin and Wright,⁴⁷ as revised by Chipman¹⁵ in the light of more recent studies

of calcium aluminates. From this it can be inferred that, were it not for the formation of crystalline $3 \text{ CaO Al}_2\text{O}_3$, saturation with lime would occur at 1500°C at a mole fraction of 0.72 ± 0.01 . It can be seen from Fig. 11 that the lime activity curve extrapolates satisfactorily to unity at about this composition.

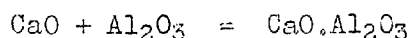
(a₃) Alumina activities in lime-alumina melts.

The alumina activities have been computed from the lime activities by means of the following modified Gibbs-Duhem equation, in which activity coefficient instead of activity is used.

$$\int_{N_{\text{CaO}} = X_1}^{N_{\text{CaO}} = X} d \log \gamma_{\text{Al}_2\text{O}_3} = - \int_{N_{\text{CaO}} = X_1}^{N_{\text{CaO}} = X} \frac{N_{\text{CaO}}}{N_{\text{Al}_2\text{O}_3}} d \log \gamma_{\text{CaO}} \quad (4)$$

X is the mole fraction of CaO corresponding to the composition at which the alumina activity is required and X_1 is the mole fraction of CaO at which the melt is saturated with $\text{CaO} \cdot \text{Al}_2\text{O}_3$. The alumina activity at $N_{\text{Al}_2\text{O}_3}$ equal to 0.42 at which the melt is saturated with $\text{CaO} \cdot \text{Al}_2\text{O}_3$ was obtained as follows:

From the heat of formation of $\text{CaO} \cdot \text{Al}_2\text{O}_3$ measured by Coughlin⁴⁸ and from relevant heat capacity data^{49, 50}, $\Delta G^\circ = -12220 \pm 700$ Cal at 1500°C , was calculated for the pure phase reaction



Thus, in equilibrium with crystalline aluminate at

$$N_{\text{Al}_2\text{O}_3} = 0.42$$

$$a_{\text{CaO}} \cdot a_{\text{Al}_2\text{O}_3} = (3.12 \pm 0.7) \times 10^{-2}$$

and with a_{CaO} equal to 0.21 from the Fig. 11, $a_{\text{Al}_2\text{O}_3}$ is found to be 0.15 ± 0.03 . The alumina activities for melts in which $N_{\text{Al}_2\text{O}_3}$ is less than 0.42 have been derived from the $a_{\text{Al}_2\text{O}_3}$ at 0.42 and the measured lime activities using the relation (4). The integration was carried out graphically. The phase diagram in Fig. 12 indicates that, were it not for the formation of crystalline aluminates, the melt would become saturated with alumina at a mole fraction of 0.5 (\pm about 0.02). The alumina activity thus rises to unity at about this concentration from the value of 0.15 at $N_{\text{Al}_2\text{O}_3} = 0.42$. The lime activity must therefore fall simultaneously from its value of 0.21 to about 0.04 at alumina saturation. In the light of the lime activity values the best compromise seems to be to set this saturation limit at 0.48 for N_{CaO} . The alumina activities so obtained are shown in Fig. 11 and Table X. The activities reported by Carter and Macfarlane⁵ and by Chipman¹⁵ have also been shown in Fig. 11 by A dotted and B dotted lines respectively. The difference between the present results and those

of these authors is due to the fact that their calculations involve the wrong assumption that a_{CaS} remains constant with change in the composition of the melt. The present results can be checked at two points as follows: It can be calculated from the available free energy data^{48, 49, 50} on $3 \text{ CaO} \cdot \text{Al}_2\text{O}_3$, that when the melt is in equilibrium with this crystalline solid at 1500°C at N_{CaO} equal to 0.70

$$a_{\text{CaO}}^3 a_{\text{Al}_2\text{O}_3} = (1.18 \pm 0.63) \times 10^{-2}$$

The alumina activity calculated from a_{CaO} with this equation is 0.016 ± 0.009 , compared with 0.010 derived from the Gibbs-Duhem equation. When the melt has the composition $12 \text{ CaO} \cdot 7 \text{ Al}_2\text{O}_3$ ($N_{\text{CaO}} = 0.63$), it can be calculated from the free energy data^{48, 49, 50} and an estimated entropy of fusion of $5.0 \text{ cal. deg.}^{-1}$ per mole of oxide, that

$$a_{\text{CaO}} a_{\text{Al}_2\text{O}_3}^{7/12} = 0.070 \pm 0.024$$

The alumina activity calculated from a_{CaO} with this equation is 0.068 ± 0.024 compared with 0.070 by the Gibbs-Duhem calculation. In both cases the agreement is satisfactory.

(a₄) The integral free energies of formation of the binary $\text{CaO} + \text{Al}_2\text{O}_3$ melts.

The partial molar free energies $\overline{\Delta G}$ of lime and alumina were calculated from the relation $\overline{\Delta G} = RT \ln a$. The integral molar free energies were then calculated from the partial molar free energies by the equation:

Fig. 13

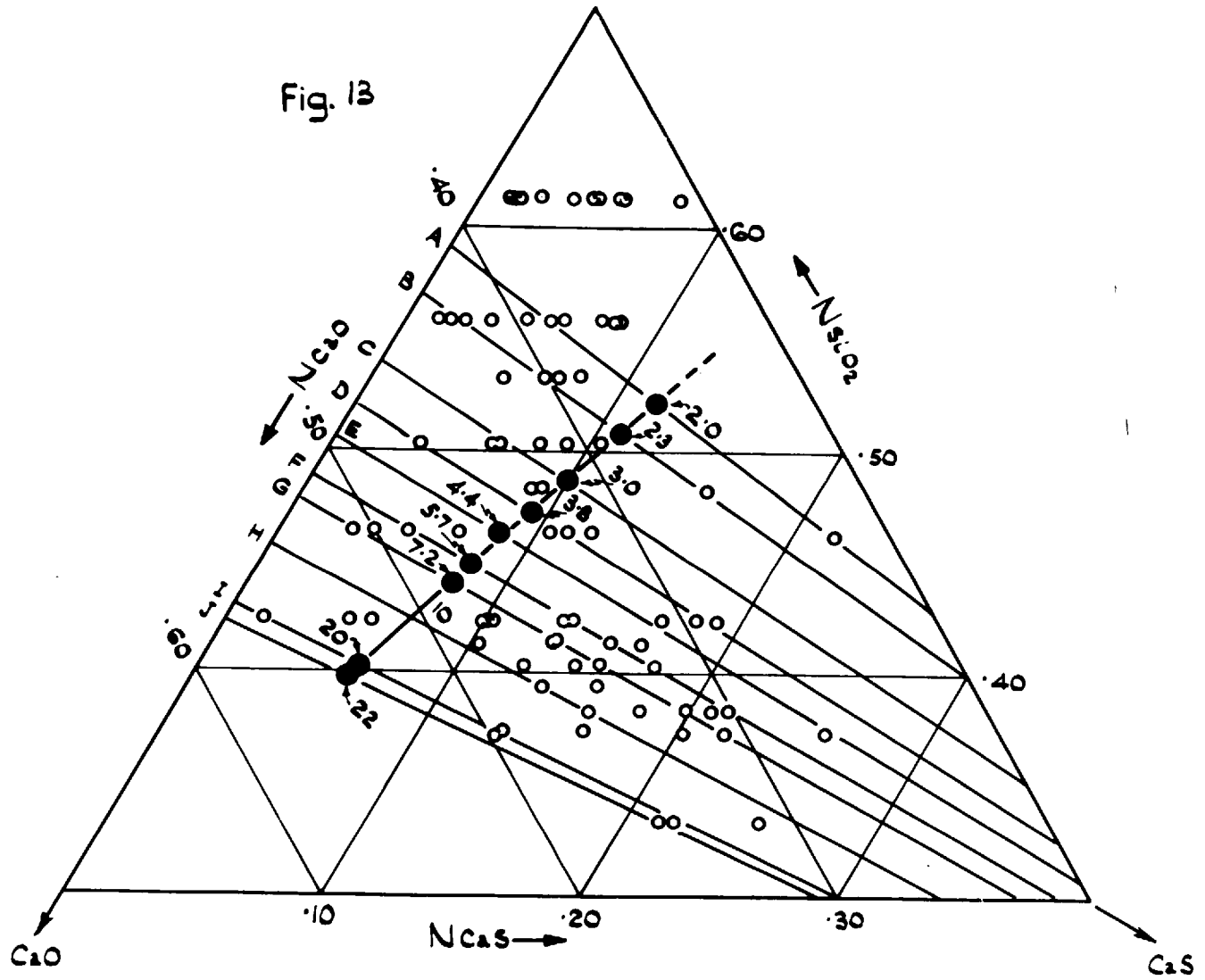
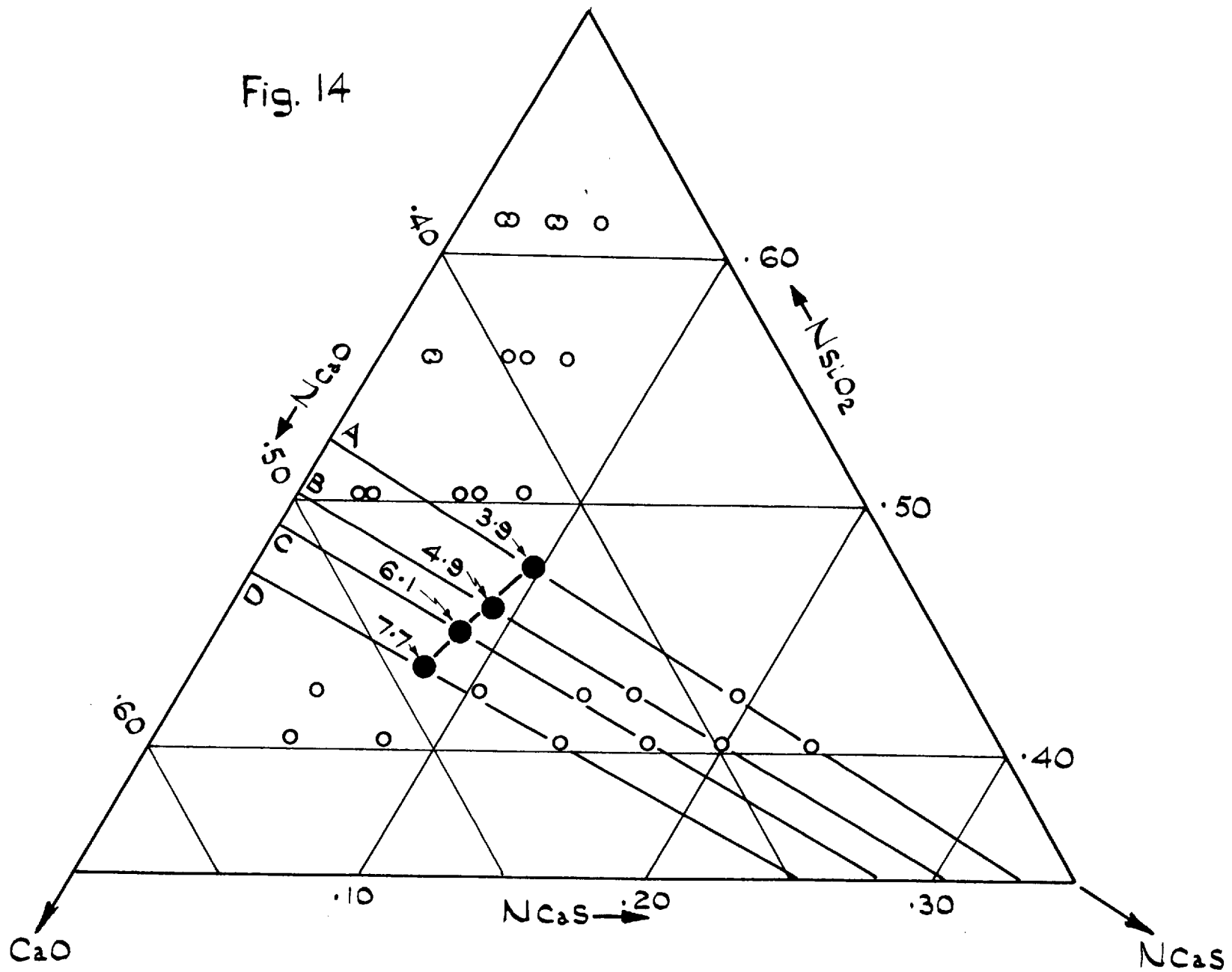
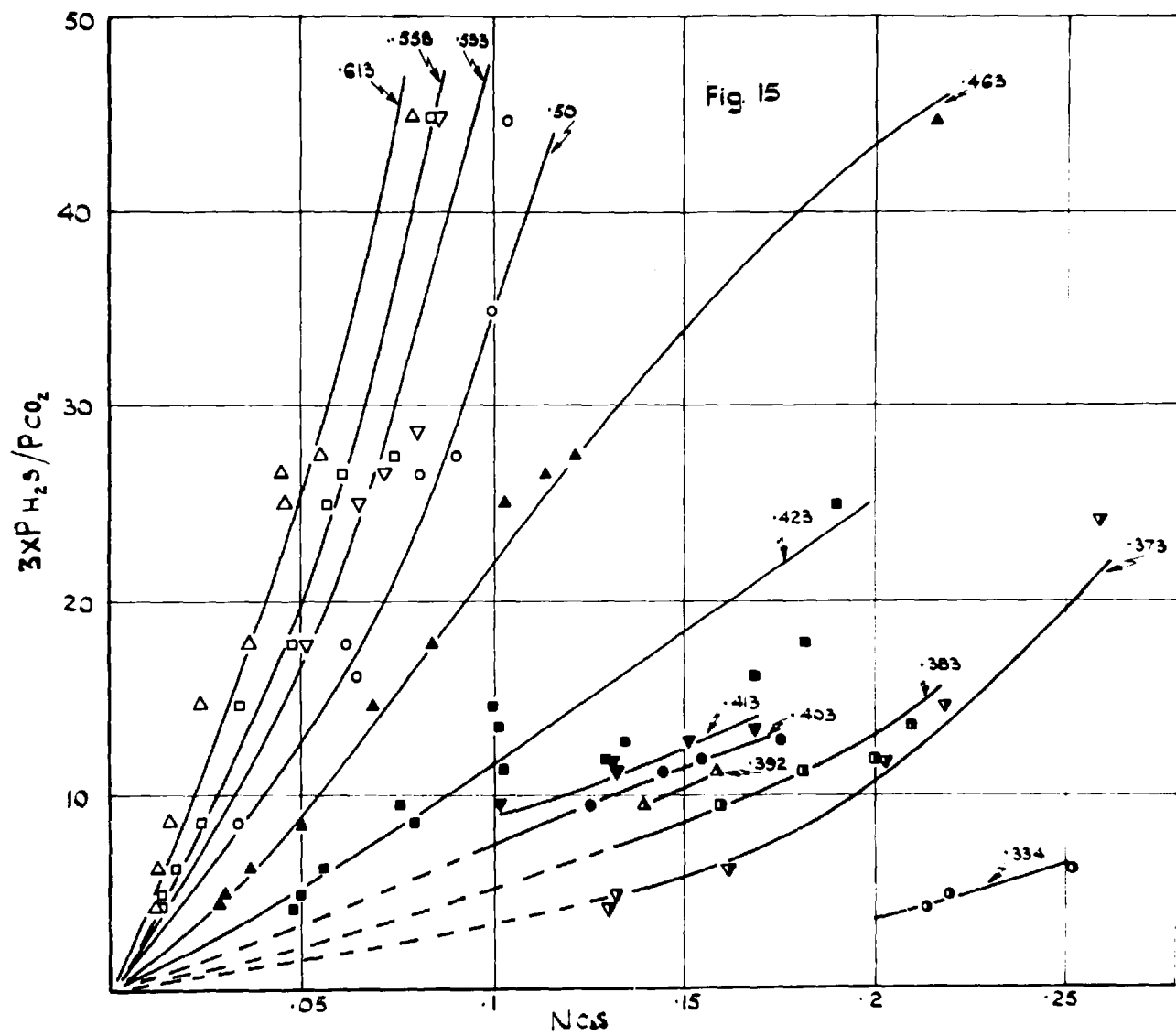
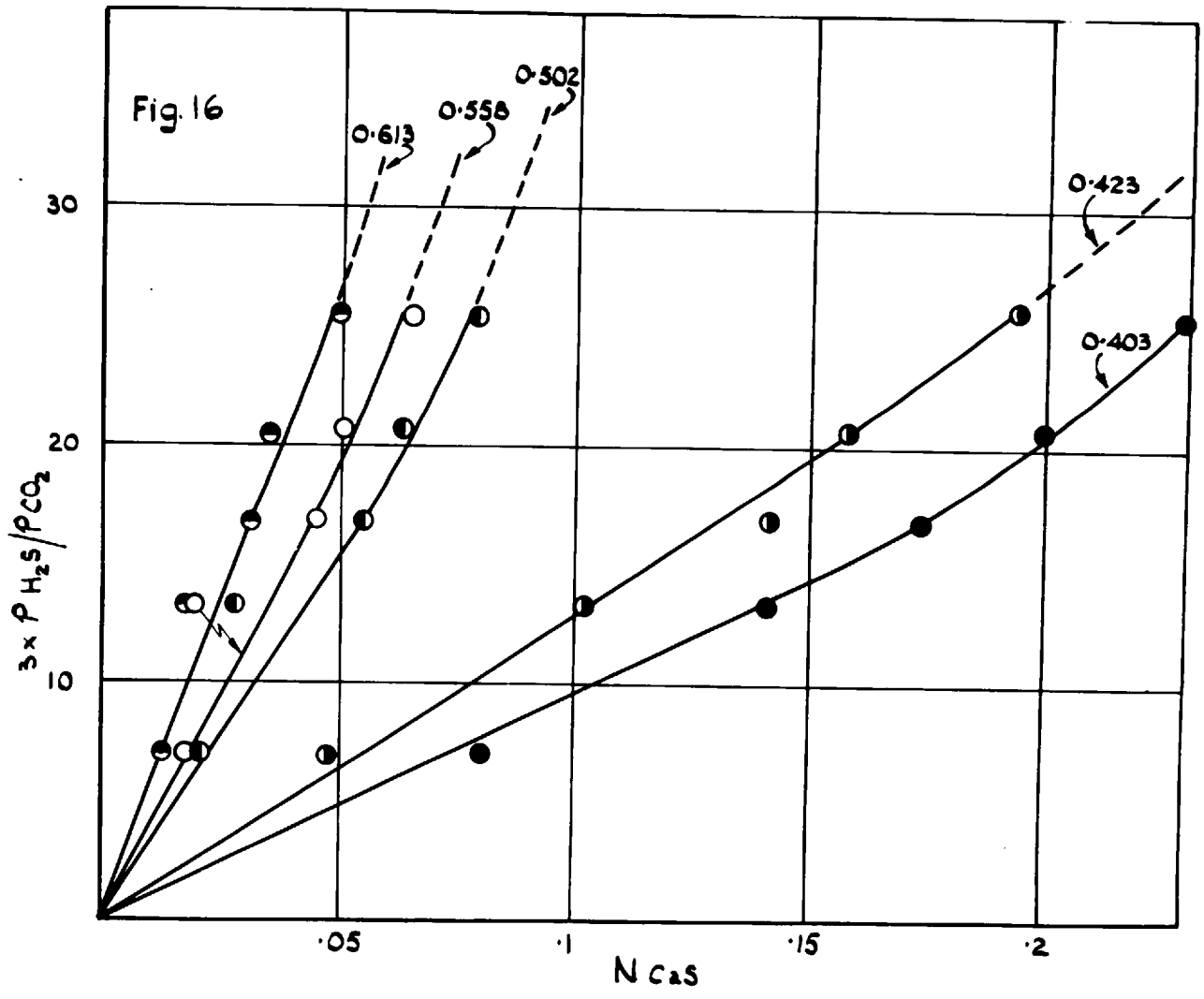


Fig. 14







$$\Delta G^\circ = N_{\text{CaO}} \overline{\Delta G}_{\text{CaO}} + N_{\text{Al}_2\text{O}_3} \overline{\Delta G}_{\text{Al}_2\text{O}_3}$$

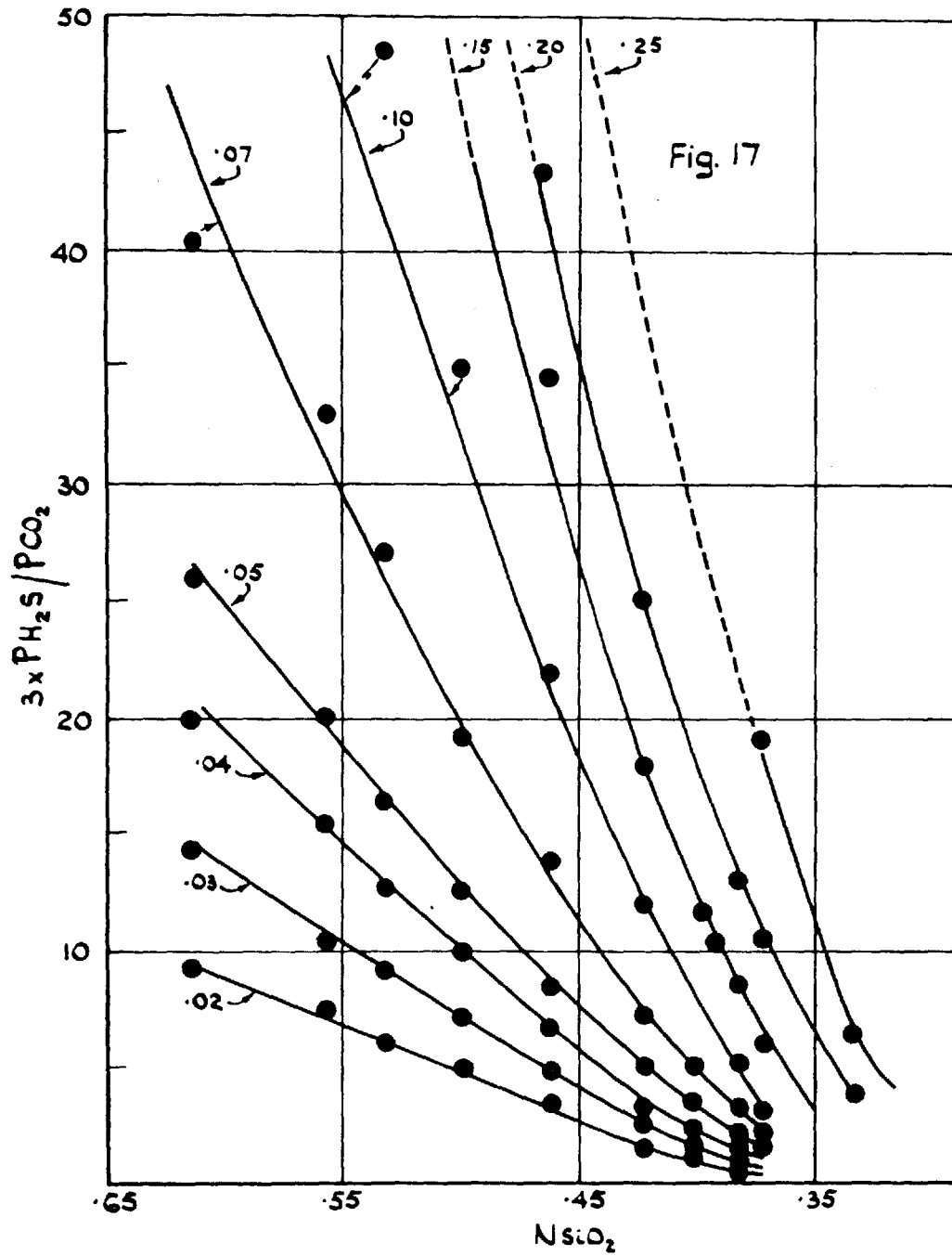
The values calculated in this way at 1500°C are given in Table X and Fig. 27.

(b) Lime-silica melts

(b₁) Solubility limits of CaS

The results of the experiments carried out at 1500° and 1550° are submitted in Tables XI and XII. The range of finishing compositions obtained is shown in Figures 13 and 14, where each point represents a separate sample. All the samples obtained near CaSiO₃, in spite of its m.p. of 1544°C, were clear glasses, showing that the CaS present, together with any excess CaO or SiO₂, was sufficient to bring the melting point of the slag below 1500°C. The results at 1500°C are also fully supported in this region by those obtained at 1550°C.

In Figures 15 and 16, the mole fractions of calcium sulphide ultimately obtained in the melts are shown as a function of the compositions of the ingoing gas mixtures at 1500° and 1550°C. The gas compositions were made of N₂, 50%; H₂S, 8% at 1500°C and 7.4% at 1550°C, the remainder being H₂ and CO₂. Each curve has been drawn through the results obtained with the same initial mixture of CaO and SiO₂ so that all the compositions on each curve have the same mole fraction of silica indicated by the figure at the end of the curve.



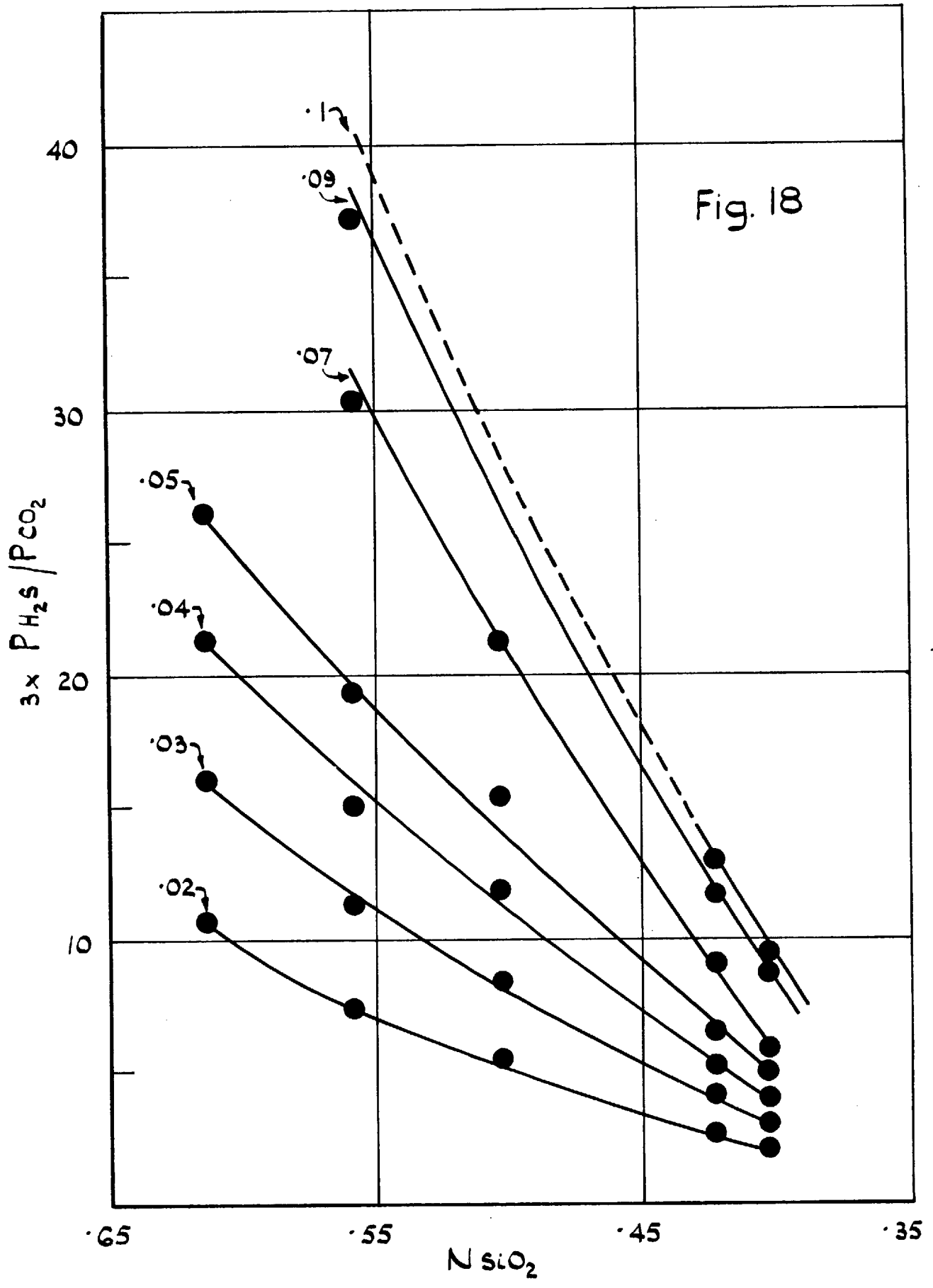
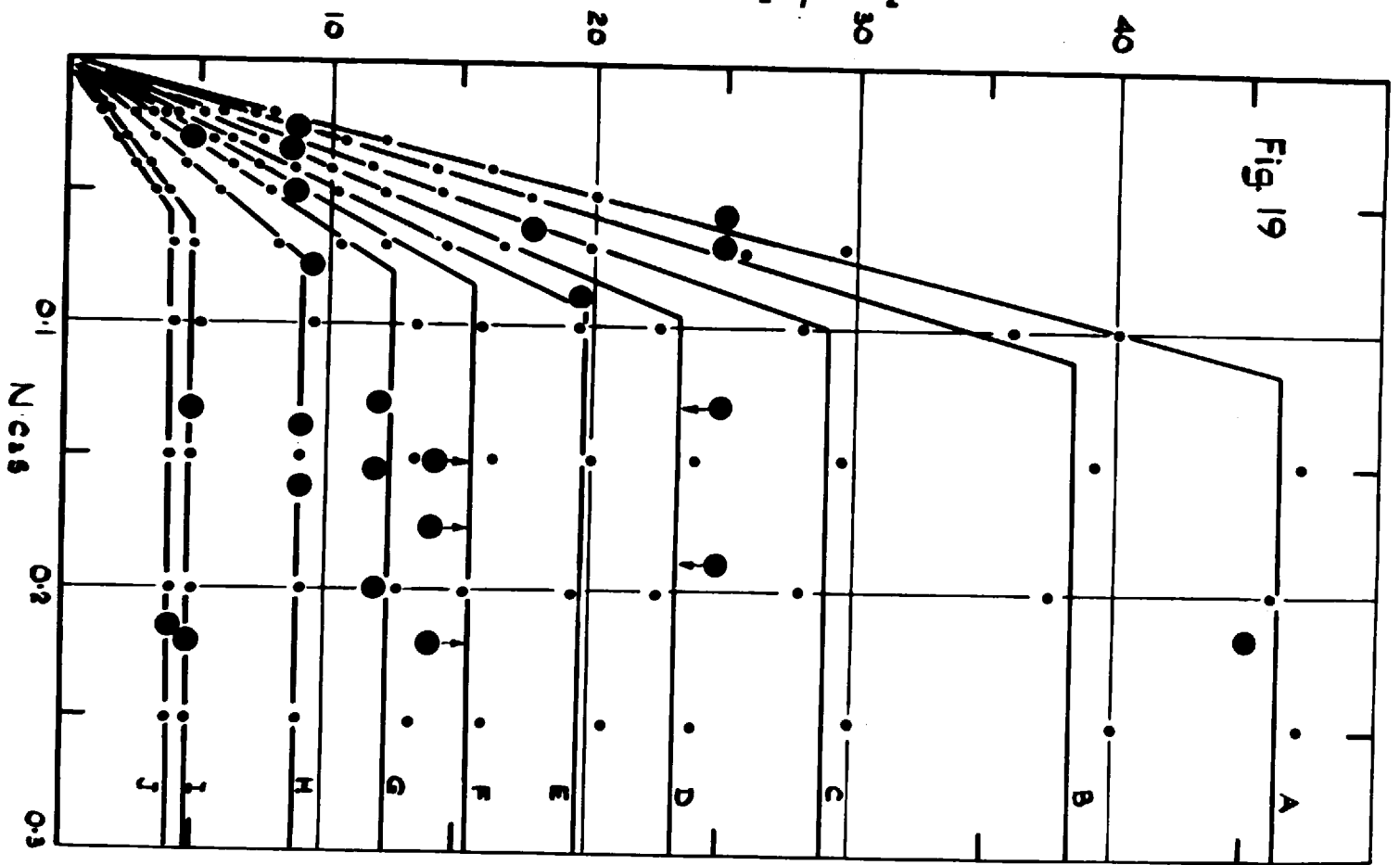
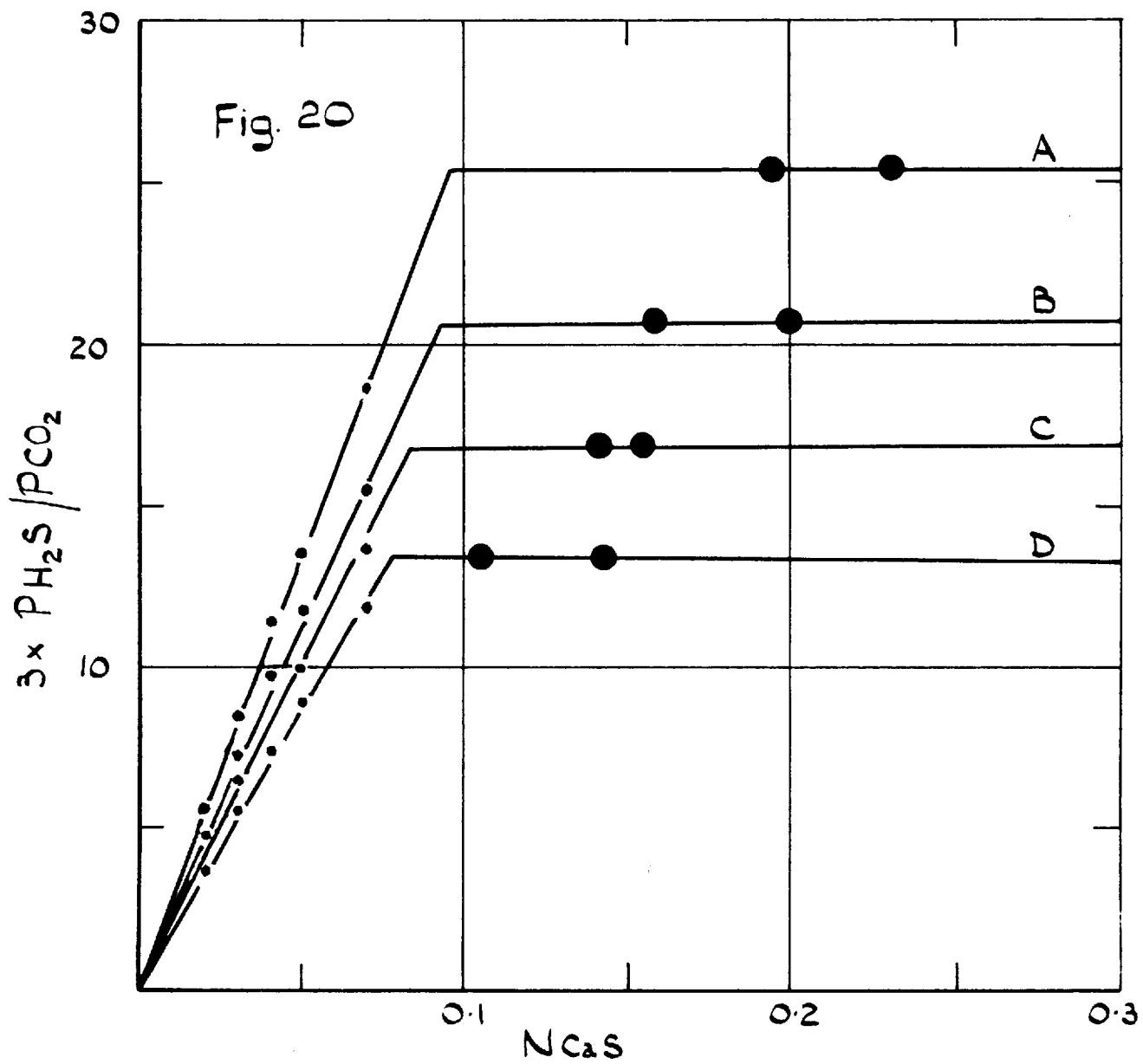


Fig. 18

Figures 17 and 18 for 1500°C and 1550°C have been constructed from the results shown in Figures 15 and 16. These show the gas compositions as a function of the mole fraction of silica for the constant mole fraction of CaS (shown by the figures at the end) in the melt (or the mixtures of CaS and the melt), obtained after the equilibrium had been reached. The points are the values read off the curves drawn in Figures 15 and 16. From the Figures 17 and 18 reading compositions from the Figures 13 and 14, were constructed Figures 19 and 20. These show the gas mixtures in equilibrium with various mole fractions of CaS for melts (or mixtures of melt and CaS) which have the same ratio of lime to silica at the end of each experiment at 1500°C and 1550°C. These mixtures thus lie along the lines A, B, C, etc., of Figures 13 and 14. Saturation limits of CaS in the melts are obtained at and beyond the points where the horizontals in Figures 19 and 20 cut the upward sloping curves. In these Figures the actual experimental points lying on the curves A, B, C, etc., are shown by large filled circles, other points are interpolations obtained from Figures 17 and 18. The solubility limits so obtained are shown by the filled circles on the curves in Figures 13 and 14, and are given in Table XIII. From the scatter of the results, the uncertainties in the lines in Figures 15 and 16, and the uncertainties in the points of intersection in Figures 19 and 20, it is considered that the

$$\frac{3 \times P_{H_2S}}{P_{CO_2}}$$





solubility limits are correct to $\pm 10\%$. The fact that the solubility limits in the $\text{CaO} + \text{SiO}_2$ system should decrease, while that in $\text{CaO} + \text{Al}_2\text{O}_3$ should increase, with increasing CaO concentration in the melt has been dealt with on pages 110 and 111.

The values of γ_{CaS} calculated from these limits at saturation (relative to solid pure CaS) are given in Table XIII, and Figure 21. In this figure solid points and circles represent the values at 1500° and 1550°C respectively. It can be seen from this figure that, within the probable limits of the experimental error, the values at 1500° and 1550°C are approximately equal.

(b₂) Line activities in $\text{CaO} + \text{SiO}_2$ melts.

Line activities in the CaS saturated ternaries $\text{CaO} + \text{SiO}_2 + \text{CaS}$ were obtained using the relationship:

$$a_{\text{CaO}} = \frac{1}{K} \left(\frac{P_{\text{O}_2}}{P_{\text{S}_2}} \right)^{\frac{1}{2}} \quad (4)$$

$(P_{\text{O}_2}/P_{\text{S}_2})^{\frac{1}{2}}$ was obtained experimentally. K was the same as described on page 87 and is equal to 2.75×10^{-3} at 1500°C and 3.27×10^{-3} at 1550°C . The activity values at 1500° and 1550°C are shown in Figures 13 and 14.

ACTIVITY COEFFICIENT CaS

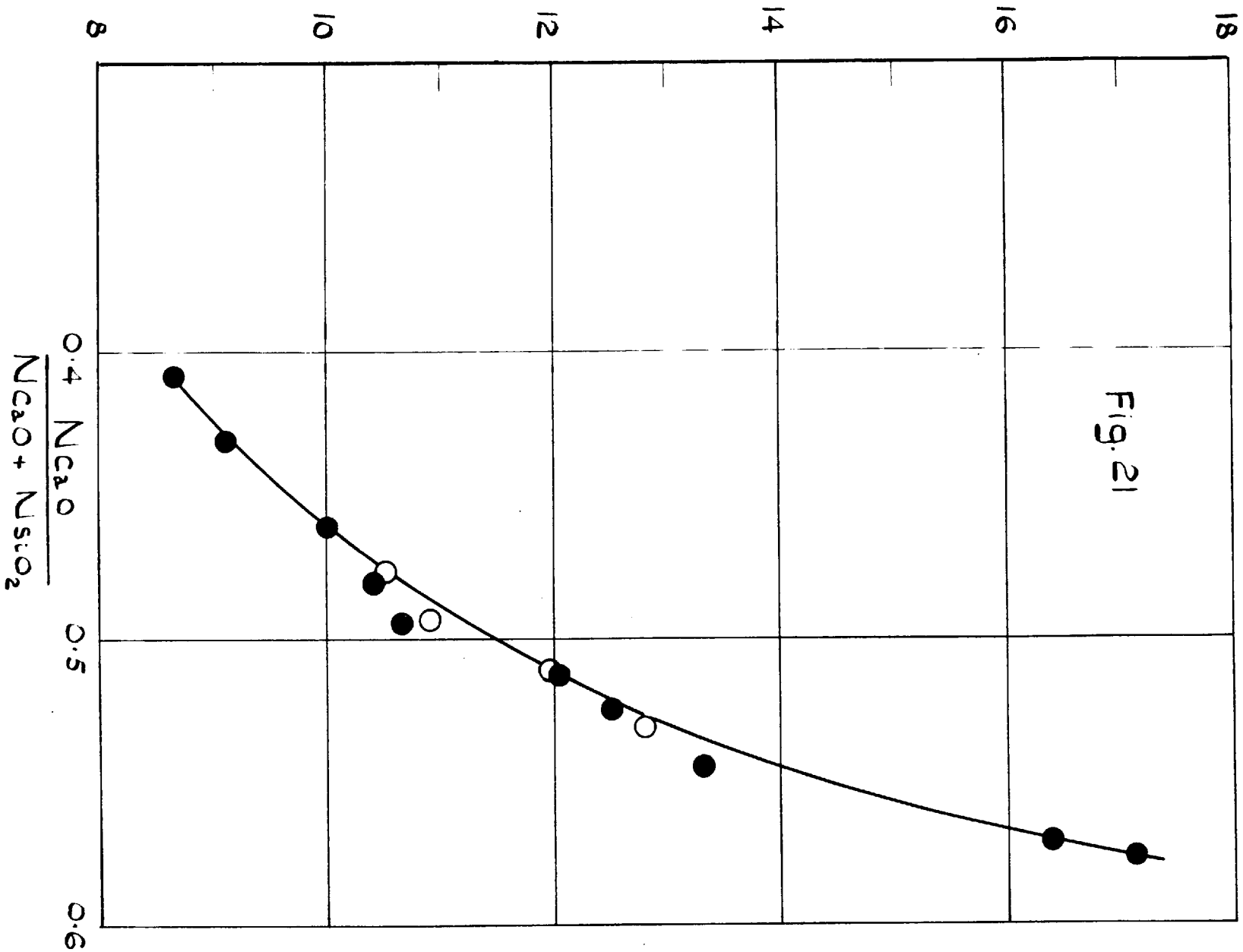
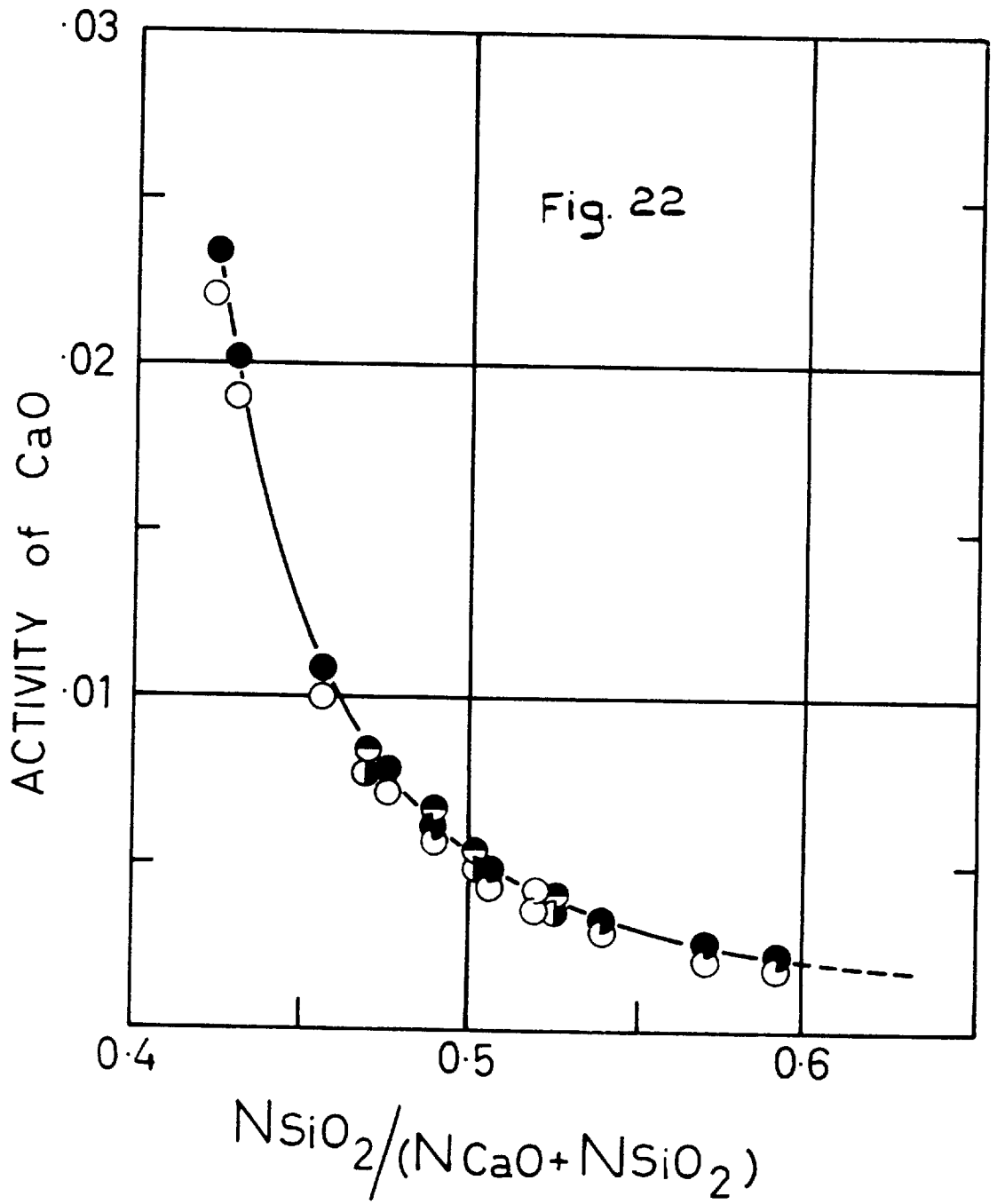


Fig. 21





To estimate the activities in the binary $\text{CaO} + \text{SiO}_2$ melts from these results, it is necessary to make an assumption concerning the way in which either γ_{CaS} or γ_{CaO} varies as N_{CaS} falls from saturation (0.06 to 0.12 of N_{CaS}) to zero. From Figures 19 and 20, it may be seen that N_{CaS} at constant lime to silica ratio is proportional to $(P_{\text{H}_2\text{S}}/P_{\text{CO}_2})$ and hence to $(P_{\text{S}_2}/P_{\text{O}_2})^{\frac{1}{2}}$. It follows that $(\gamma_{\text{CaS}}/a_{\text{CaO}})$ is constant at constant lime to silica ratio. Thus $(\gamma_{\text{CaO}}/\gamma_{\text{CaS}})$ is proportional to N_{CaO} . There are now two reasonable assumptions which lead to slightly different values for lime activities in the binary. One is that γ_{CaO} remains constant and the other is that γ_{CaS} remains constant as N_{CaS} falls to zero. The latter assumption leads to the same lime activities in the binary as in the ternary at the same lime to silica ratio. The former assumption leads to lime activities that are 6-12% greater. It is unlikely that the ratio $\frac{\gamma_{\text{CaS}}}{\gamma_{\text{CaO}}}$ would remain nearly constant (within 6-12%) when calcium sulphide is present at low concentrations and lime is present at much higher concentrations unless both activity coefficients were nearly constant. The assumption of constancy for γ_{CaO} is tantamount to assuming that γ_{CaS} rises by about 6-12% as N_{CaS} falls from saturation to zero. Any suggestion that γ_{CaS} may rise by a large factor between these limits, as in Taylor and Stobo,⁴⁶ is ruled out.

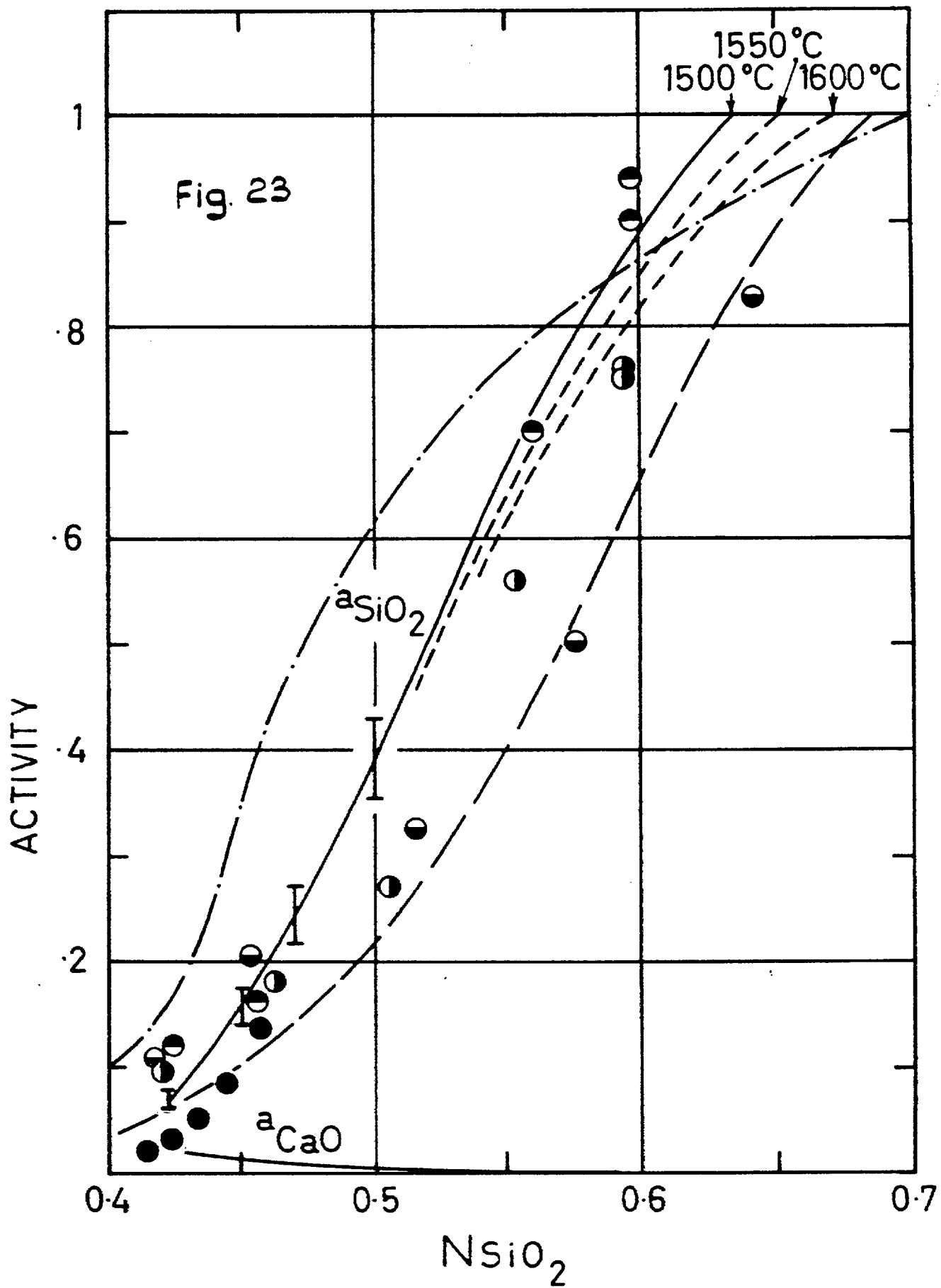


If, for instance, γ_{CaS} were twice as great at low concentrations of CaS than at saturation, the values of a_{CaO} which could be calculated for the binary by the equation

$$a_{CaO} = \frac{\gamma_{CaS} C_S}{32 N.K}$$

described on page 88, would be twice those calculated by equation (4) for the melt of the same CaO to SiO₂ ratio, saturated with CaS. Such large differences in a_{CaO} are quite improbable. The reverse suggestion that γ_{CaS} might be two times less at low concentrations, would lead to much higher lime activities in the ternaries than in the binaries of similar lime to silica ratio; this also is quite improbable.

Since CaS is essentially an inert diluent in CaO + SiO₂ mixtures, it seems most reasonable to assume that a_{CaO} rises proportionally with N_{CaO} , as γ_{CaS} falls to zero. The lime activities calculated on this assumption are shown in Figure 22 together with the values for the saturated ternary mixtures. In this figure the activities are indicated by  at 1500°C, by  at 1550°C in the binary derived as above, and by  at 1500°C and by  at 1550°C in saturated ternaries. The values are also given in Table XIV.



The results derived by Carter and Macfarlane²⁰ from sulphide capacities are not included in Figure 22, because these authors assumed that γ_{CaS} was equal to 12 in all their $\text{CaO} + \text{SiO}_2$ melts, and 16 in their standard lime saturated $\text{CaO} + \text{SiO}_2 + \text{Al}_2\text{O}_3$ slag. If allowance were made for these incorrect assumptions (which were the best that could be made at that time) their results would agree satisfactorily with those derived here, because there is no disagreement over the sulphide capacities.

(b₃) Silica activities in lime-silica melts.

The silica activities have been calculated by using the modified Gibbs-Duhem equation given on page 91 and the measured lime activities, the silica activity being taken as unity at the silica saturation limit shown by the phase diagram.⁵¹ The integration was carried out graphically. Solid silica was taken as the reference state. It was necessary to extrapolate γ_{CaO} to silica saturation as shown in Figure 22 by the broken line. This was best done by a short extrapolation of a plot of $\log \frac{\gamma_{\text{CaO}}}{(1 - N_{\text{CaO}})^2}$ versus N_{SiO_2} , which is a straight line in the region where N_{SiO_2} exceeds 0.54. The silica activity curve so obtained is shown in Figure 23, together with the results of the other workers. In this figure are indicated the results of the present work by a full curve at 1500°C, by dashed curves estimates at 1550°C and 1600°C;

c. . Young et al¹⁸ by a dot-dash curve at 1627°C; of Sanbongi and Omori²² by a heavy dashed curve at 1637°C; of Chipman¹⁹ (recalculated) by solid points at 1600°C; of Kay and Taylor¹⁷ by points \ominus , \oplus , at 1500° and 1550°C respectively, and of Baird and Taylor⁵² by points \ominus at 1550°C. The values of a_{SiO_2} of the present work are also given in Table XIV. From Figure 23 it may be seen that there is a good agreement with the results of Kay and Taylor at 1500°C.

From the values of a_{SiO_2} and a_{CaO} for the melt, which is saturated with Ca_2SiO_4 ($N_{\text{CaO}} \sim 0.58$) it is possible to calculate the free energy of formation of crystalline Ca_2SiO_4 at 1500°C. The value so obtained is -35,860 cal. The error limits ($a_{\text{CaO}} \pm 15\%$ and $a_{\text{SiO}_2} \pm 18\%$) suggest that the error on ΔG° may be between 1 and 2 Kcal. From the heat of formation of Ca_2SiO_4 ⁵³ and the relevant data for entropies,^{54, 55} heat capacities,^{56, 57} and the heat of transformation of quartz to cristobalite,⁵⁷ one can derive the equation

$$\Delta G^\circ = -24,120 - 5.74T \pm 1,000 \text{ cal}$$

This leads to a value of -34,300 cal at 1500°C. There is thus adequate agreement between the results of the activity studies (coupled with phase diagram) and the thermal data on crystalline α - Ca_2SiO_4 . A check on the thermal data

available from e.m.f. measurements made by Benz and Wagner⁵⁸ at 700°C with a special solid cell involving calcium silicates. The value of ΔG° for the formation of $\beta - \text{Ca}_2\text{SiO}_4$ (from quartz) which can be derived from their measurements is $-32,400 \pm 300$ cal, whereas the value for this temperature from thermal data is $-31,500$ cal. It may thus be seen that the ΔG° values from the thermal data are a little too positive.

According to the phase diagram,⁵¹ crystalline CaSiO_3 can be in equilibrium at 1500°C with either of two liquids, with N_{CaO} equal to 0.44 or 0.55. It follows that in each case

$$\Delta G_T^\circ = RT \ln (a_{\text{CaO}} a_{\text{SiO}_2})$$

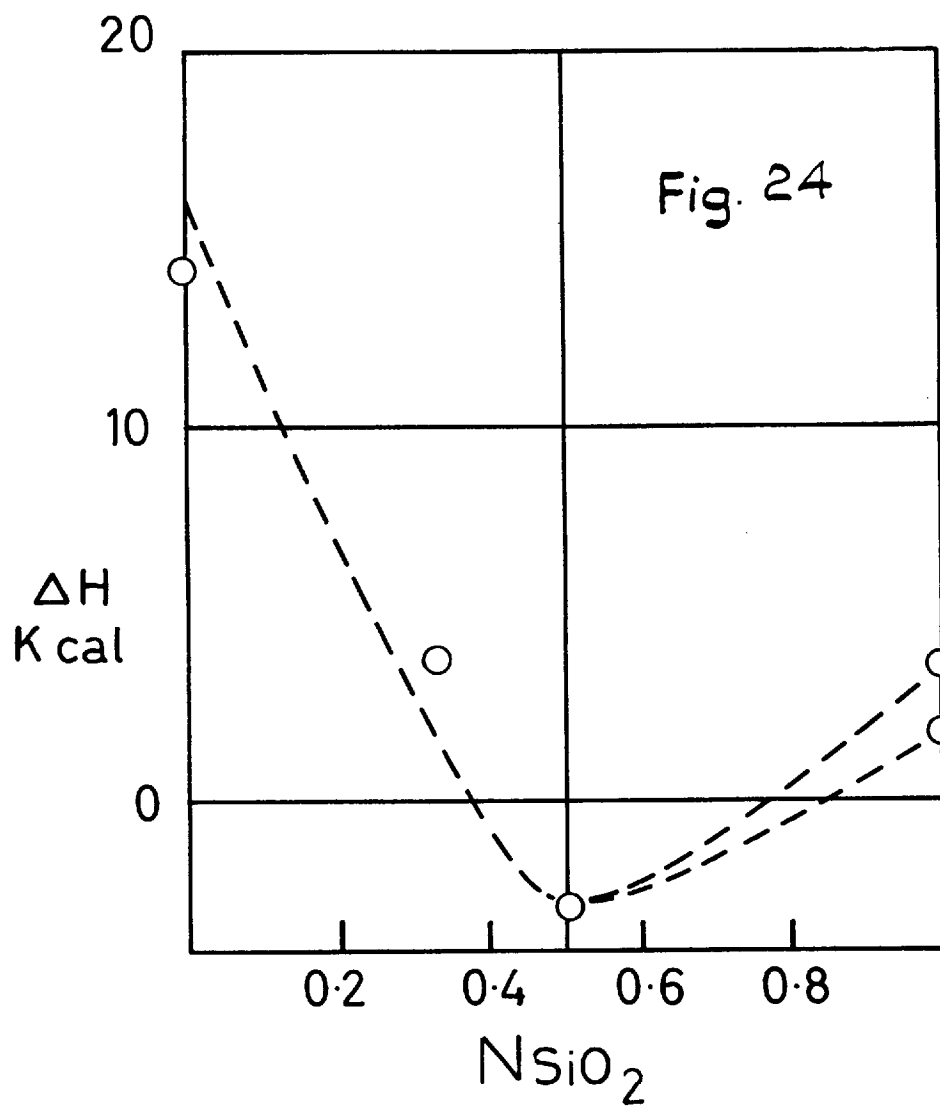
where ΔG_T° is equal to the free energy of formation of crystalline CaSiO_3 from its component oxides. From the activity data the two values for ΔG° are $-22,000$ and $-21,900$ cal whereas the value which can be derived from thermal data,^{55, 56, 57, 59, 60} is $22,050$ cal. The agreement, which is fortuitously good since it is well within the probable limits of error, provides further confirmation of the activity data. It is interesting to note that for CaSiO_3 at 700°C there is complete agreement between the value for ΔG° from the thermal data and that derived from the e.m.f. work of Benz and Wagner.⁵⁸

It is possible to calculate the free energy of formation of liquid CaSiO_3 from the oxides at 1500°C from the thermal data and the entropy of fusion⁶¹, which is $8.1 \text{ cal. deg.}^{-1} \text{ mole}^{-1}$. The value obtained is $-21,680 \text{ cal.}$, which is identical to that derived from the lime and silica activities ($-21,660 \text{ cal.}$).

The question arises as to where the activity curves for silica lie at higher temperatures. The results in Figure 22 show that the activity of lime at $a_{\text{CaO}} = 0.5$ is almost the same at 1550°C as at 1500°C . The free energy data on liquid CaSiO_3 already considered above indicate that the free energies of formation and the activity products (relative to solid CaO and SiO_2) have the following values:

Temperature $^\circ\text{C}$	$\Delta G'$	$a_{\text{SiO}_2} \times a_{\text{CaO}}$
1500	- 21,680	0.00,212
1550	- 22,140	0.00,221
1600	- 22,600	0.00,231

The rate of change of the activity product with temperature, which depends on the value of ΔH° , should be more accurate than the actual values of the product. Thus, if a_{CaO} is the same at 1550°C as at 1500°C , a_{SiO_2} rises by 5% over the 50°C range. If a_{CaO} were to rise by 10%, which

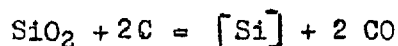


is not impossible in view of possible errors in Figure 22, a_{SiO_2} would fall by 5%. In either event, the change in a_{SiO_2} is small. On the basis of such reasoning, the activity curves for SiO_2 have been drawn in Figure 23 for 1550°C and 1600°C from the silica saturation limits towards the equimolar composition. The probable range in which the activities lie at 1600°C at and beyond this composition is indicated by the four vertical lines.

It seems likely that the activities of silica do not vary as much with temperature as the results of Kay and Taylor¹⁷ suggest. It is possible to construct a rough heat of formation curve for $\text{CaO} + \text{SiO}_2$ melts from crystalline lime and silica from the thermal data already quoted for the two silicates, an estimated entropy of fusion of lime of $5 \text{ cal. deg.}^{-1} \text{ mole}^{-1}$, the heat of fusion of silica 1800 or 3600 cal. mole^{-1} ,²¹ and the assumption that the entropy of fusion of Ca_2SiO_4 is the same as for Fe_2SiO_4 ,⁶² i.e. $14.8 \text{ cal. deg.}^{-1} \text{ mole}^{-1}$. This is shown in Figure 24. It looks very much as though the silica activity coefficient should rise with rising temperature, when N_{SiO_2} falls below about 0.5 ($\overline{\Delta H_{\text{SiO}_2}}$ negative) and that correspondingly the activity coefficient of lime should fall with rising temperatures ($\overline{\Delta H_{\text{CaO}}}$ positive) when N_{CaO} exceeds about 0.5. The values of the partial molar heats in the vicinity of the equimolar composition are so small that

neither activity coefficient can change much with temperature. When, for instance, $\overline{\Delta H}$ is about 3.0 Kcal γ can change only 4% between 1500° and 1600°C.

The activity values published by Chipman¹⁹ have been based on the studies of slag and metal equilibrium



where the silicon is dissolved in iron saturated with carbon. The calculations depend on the free energy change for the reaction



and hence on the free energy of formation of silica. Chipman derived this from the thermal data. It has been recently shown by Ramstad and Richardson⁶⁹ that the free energy of formation so derived is significantly in error at high temperatures, and a new equation has been proposed. When this is used the calculated silica activities become 2.75 times greater than before: it is these values that are shown in Figure 23. The accuracy of the new ΔG° values for SiO_2 is about 2 Kcal, and this corresponds to a factor of 1.7 on the derived values of a_{SiO_2} : the accuracy of the silica activity values proposed here is considered to be some 18%. Thus, the two sets of results are not seriously discordant, although those of Young, et al.¹⁸ and Sanbongi and Omori²² certainly are.

(b₄) The integral free energies of formation of binary CaO + SiO₂ melts.

The integral free energy of formation have been calculated from the partial molar free energies by the equation

$$\Delta G^{\circ} = N_{\text{CaO}} \overline{\Delta G}_{\text{CaO}} + N_{\text{SiO}_2} \overline{\Delta G}_{\text{SiO}_2}$$

The partial molar free energies were obtained by the relation

$$\overline{\Delta G} = RT \ln a$$

The calculated values at 1500°C are given in Table XIV and Figure 27. The dashed extrapolated part is based on the estimated entropy of fusion of Ca₂SiO₄. Thus, the ΔG° value for liquid Ca₂SiO₄ at 1500°C should lie about 3100 cal above the value shown for the crystal in Figure 10. Also shown for comparison are the free energies of formation of crystalline Ca₂SiO₄, by point O from the thermal data and by (1) from the phase diagram and activity data, and of liquid CaSiO₃ by point O derived from the thermal data mentioned earlier.

B. Activities of manganese oxide in aluminate and silicate melts.

The method of obtaining the manganese oxide activities in the melts has been described earlier. The melts studied include the mixtures of the binary $\text{MnO} + \text{Al}_2\text{O}_3$ and of the ternary $\text{MnO} + \text{Al}_2\text{O}_3 + \text{SiO}_2$. The activities so derived, are referred to solid manganous oxide in equilibrium with liquid metal manganese as the standard state.

(a) Manganese oxide activities in the binary $\text{MnO} + \text{Al}_2\text{O}_3$ melts.

The activities have been measured at 1650°C . The results are given in Table XV and Figure 25. Activities with respect to liquid manganese oxide as standard state were also calculated by using the entropy of fusion $\Delta S_f = 5 \text{ cal. deg}^{-1} \text{ mole}^{-1}$ and melting point 1850°C , for manganese oxide.⁷ They are shown in this figure by the thin curve. It has been seen from this figure that the manganese oxide activities with respect to solid manganese oxide have a negative deviation from Raoult's Law below and a positive deviation above $N_{\text{MnO}} = 0.725$, but with respect to liquid MnO , a negative deviation throughout the range studied. Manganese oxide activities⁷ in the $\text{MnO} + \text{SiO}_2$ melts at 1650°C , with respect to solid as well as liquid manganese oxide as standard states, are also shown in this figure, by the dotted curves respectively.

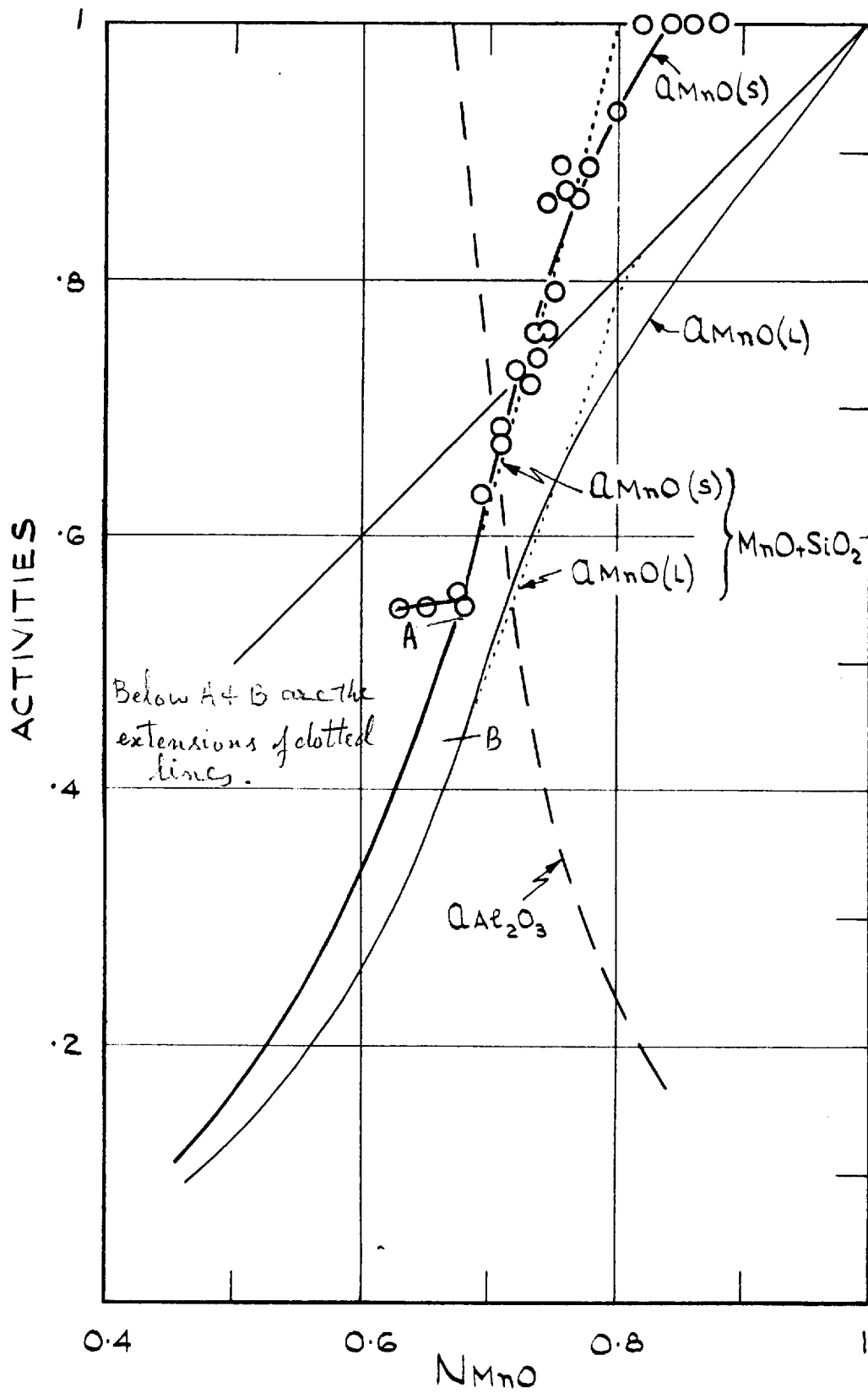


FIG. 25.

It may be seen from the curves in this figure that a_{MnO} in the $\text{MnO} + \text{Al}_2\text{O}_3$ melts is the same as that in the $\text{MnO} + \text{SiO}_2$ melts up to 0.77 mole fraction of manganese oxide, but smaller than the corresponding ones above this mole fraction.

According to the activity data, the melt should be in equilibrium with solid manganese oxide at 0.840 mole fraction of MnO. This agrees well with the sulphide capacity results reported earlier, but not with the phase diagram reported by Hay, White and McIntosh⁶³.

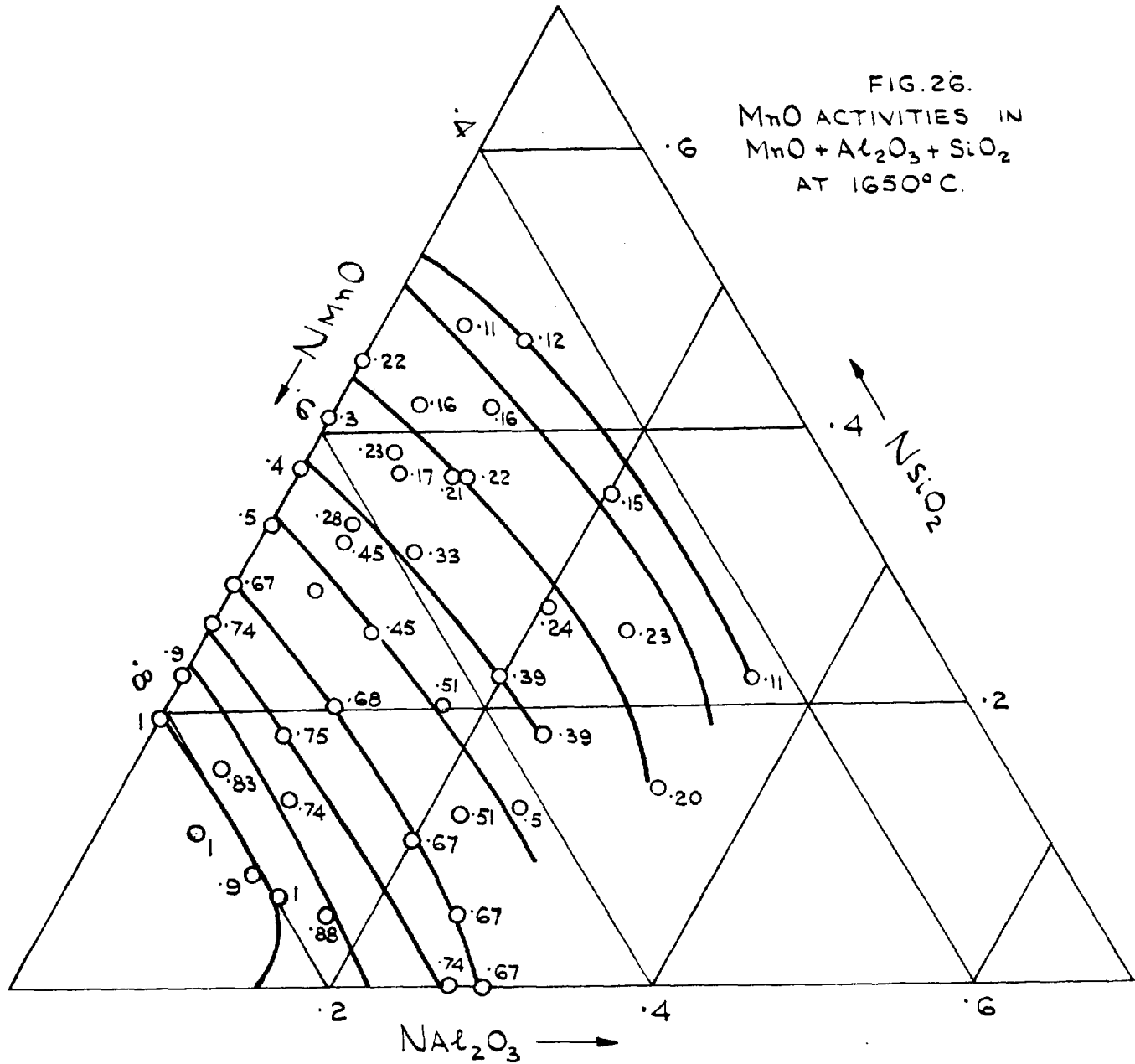
(b) Alumina activities in $\text{MnO} + \text{Al}_2\text{O}_3$ melts.

The alumina activities have been derived by the modified Gibbs-Duhem equation (page 91) using the measured MnO activities and taking the alumina activity to be unity at N_{MnO} of 0.68; according to the phase diagram⁶³ the melt is saturated with alumina at this mole fraction. The reference standard state is solid alumina. The alumina activities, so derived at 1650°C, are given in Table XVI and Figure 25.

(c) Manganese oxide activities in the $\text{MnO} + \text{Al}_2\text{O}_3$
+ SiO_2 melts.

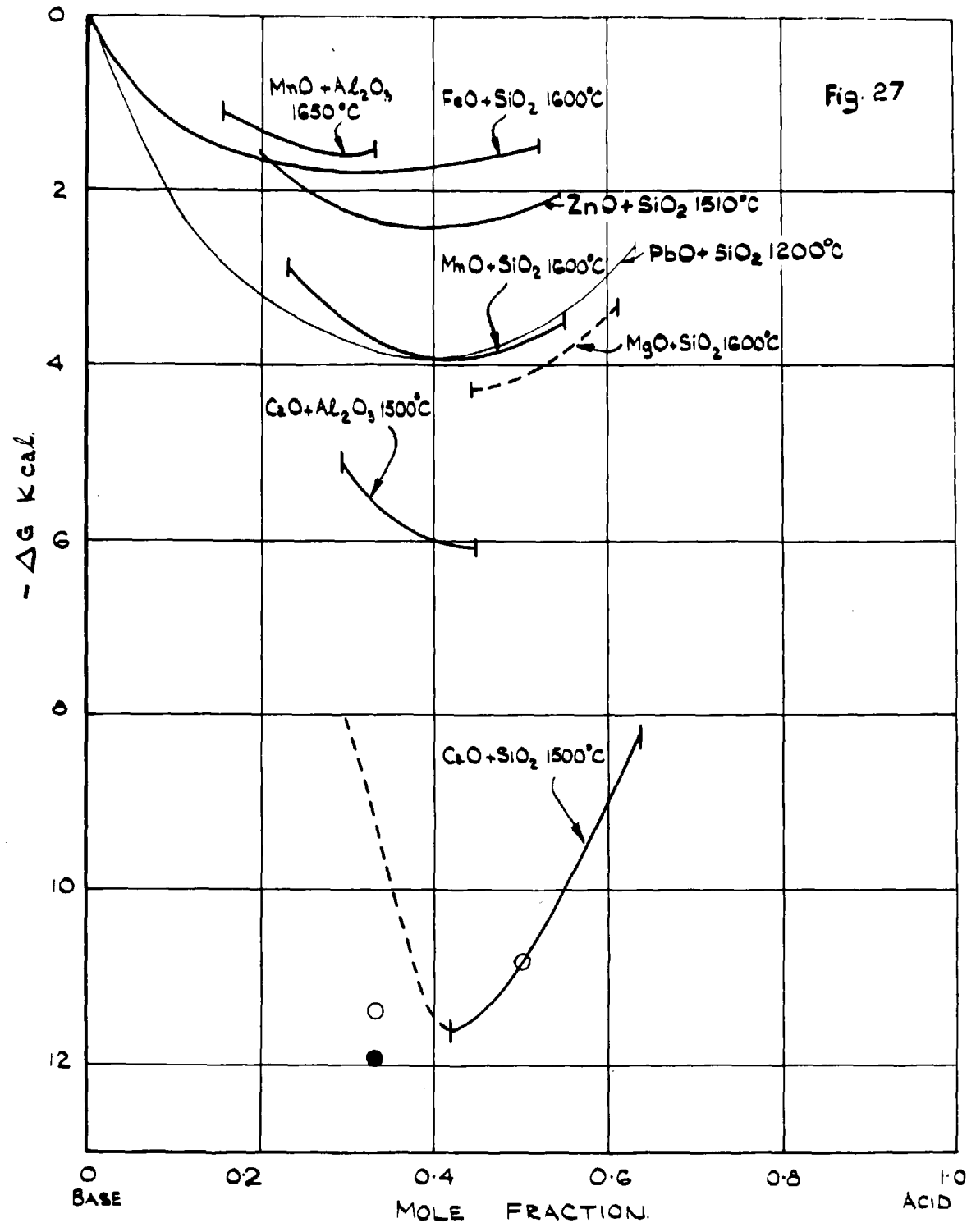
The measured activities in these melts at 1650°C have been submitted in Table XVII and Fig. 26. MnO activities

FIG. 26.
MnO ACTIVITIES IN
 $\text{MnO} + \text{Al}_2\text{O}_3 + \text{SiO}_2$
AT 1650°C.



in the binary MnO + SiO₂ melts are the values reported by Abraham.⁷ It may be seen from this figure that, at constant mole fraction of MnO, when alumina replaces silica, activities of MnO first increase and then start decreasing in the region below N_{MnO} of 0.65, remain constant between 0.67-0.75 N_{MnO} , and first remain constant and then start decreasing at approximately 0.8 N_{MnO} . This sort of variation in manganese oxide activities may be associated with the typical behaviour of alumina, in which it may have both cationic as well as anionic types of reactions. In melts such as MnO + Al₂O₃ + SiO₂ it would be expected to act mostly as cations at high concentrations of silica and as anions at low concentrations, while at intermediate concentrations of silica the two effects should balance each other. Accordingly, at constant mole fraction of MnO in the region below 0.65 N_{MnO} , alumina at its lower concentrations may act as cations and thus increase a_{MnO} while at higher concentrations it may act appreciably as anions, hence decrease a_{MnO} ; between 0.65 - 0.75 N_{MnO} the cationic and anionic types of reactions of alumina may balance each other thereby maintaining a_{MnO} constant, while at about 0.8 N_{MnO} alumina, at low silica concentration, initially may have both cationic and anionic reactions, and therefore constant a_{MnO} , but later on prominently, when the silica concentration is further decreased, alumina may have predominantly anionic reactions, thus decreasing a_{MnO} .

Fig. 27

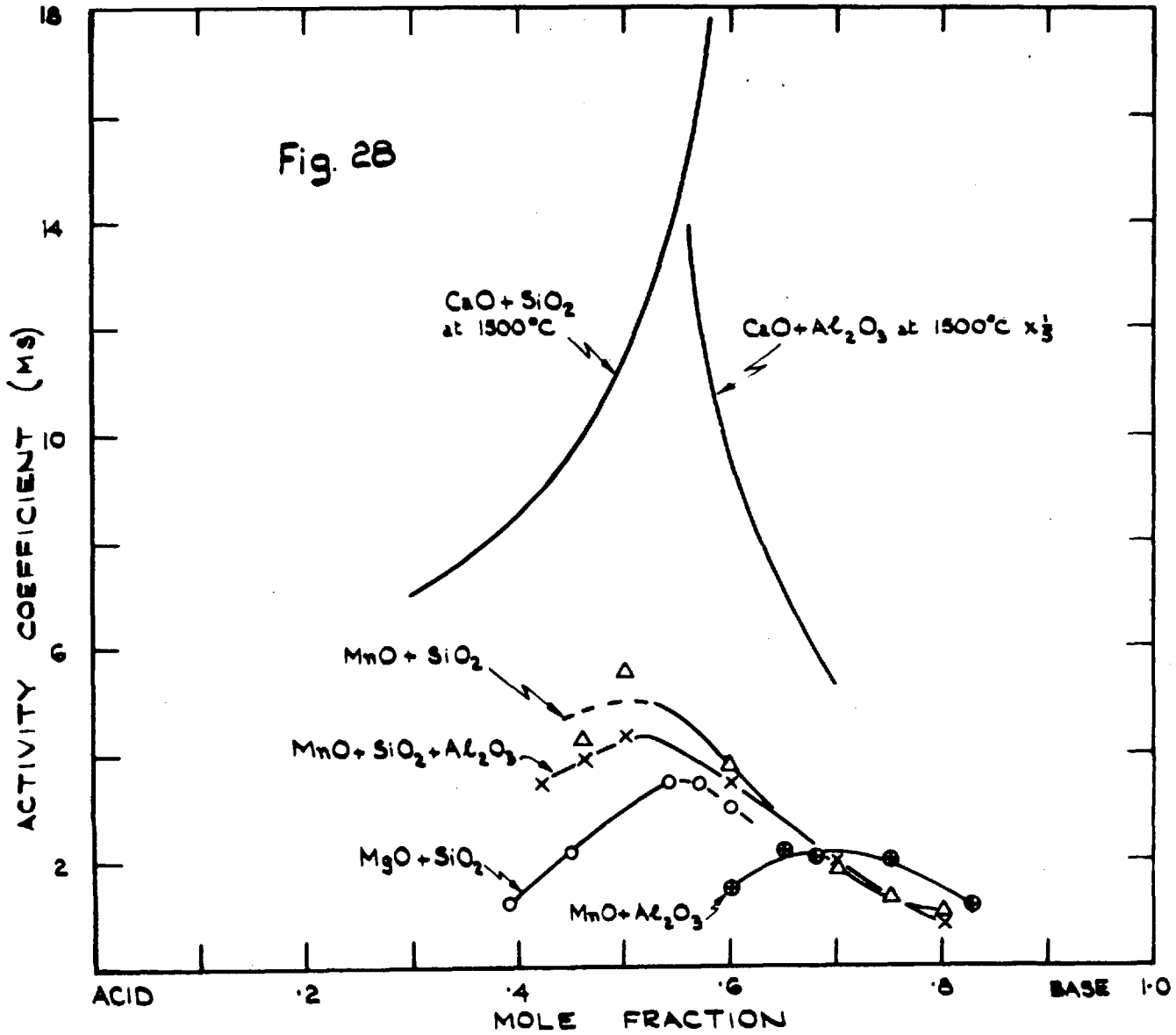


(d) Integral free energies of formation for the binary MnO + Al₂O₃.

The integral free energies of formation ΔG° for these melts, have been calculated at 1650°C, from the activity data using the following relationship:

$$\Delta G^\circ = RT N_{\text{MnO}} \ln a_{\text{MnO}} + RT N_{\text{Al}_2\text{O}_3} \ln a_{\text{Al}_2\text{O}_3}$$

The values are given in Table XVI and Figure 27. Integral free energies of formation for MnO + SiO₂ melts⁷ at 1650°C, FeO + SiO₂⁶⁴ at 1600°C, ZnO + SiO₂ at 1510°C derived by Richardson⁶⁵ from thermal data and the phase diagram and PbO + SiO₂⁶⁶ at 1200°C, are also shown in this figure, for comparison.



Activity Coefficients of sulphides in the aluminate and silicate melts.

The activity coefficients of sulphides at 1650°C in the melts $\text{MnO} + \text{Al}_2\text{O}_3$, $\text{MgO} + \text{SiO}_2$ and $\text{MnO} + \text{Al}_2\text{O}_3 + \text{SiO}_2$ at $N_{\text{SiO}_2}/N_{\text{Al}_2\text{O}_3} = 0.5$, are given in Tables XVIII, XIX and XX and in Figure 28. In this figure are also shown the activity coefficients of CaS in $\text{CaO} + \text{Al}_2\text{O}_3$ and $\text{CaO} + \text{SiO}_2$ melts at 1500°C reported on pages 57 and 62, and that of manganese sulphide⁷ in $\text{MnO} + \text{SiO}_2$ melts at 1650°C. The standard state in each case is pure solid sulphide. It is obvious from the results submitted in this figure that the activity coefficient in each system varies with the composition of the melt. It thus indicates that the activity coefficient of the sulphide should not be assumed to be constant over a wide range of composition of the melt, even for approximate calculation of the activity of the metal oxide. It is also seen from this figure that the activity coefficient of the sulphide in all the melts except $\text{CaO} + \text{Al}_2\text{O}_3$ does not increase with increasing concentrations of SiO_2 or Al_2O_3 . The γ_{CaS} increases in $\text{CaO} + \text{SiO}_2$ melts and decreases in $\text{CaO} + \text{Al}_2\text{O}_3$ with increase in N_{CaO} .

It appears from Figures 27 and 28 that the activity coefficient of the sulphide increases with decreasing integral free energy of the melt and is maximum at minimum ΔG° .

This is obvious from the results obtained in the systems $\text{MnO} + \text{SiO}_2$, $\text{MnO} + \text{Al}_2\text{O}_3$ and $\text{MgO} + \text{SiO}_2$. The difference in behaviour of the activity coefficient of calcium sulphide in $\text{CaO} + \text{SiO}_2$ and $\text{CaO} + \text{Al}_2\text{O}_3$ melts may also be associated with the fact that the measurements for $\text{CaO} + \text{SiO}_2$ have been made on the lime poor side of ΔG° minimum, whereas those for $\text{CaO} + \text{Al}_2\text{O}_3$ for the lime rich side.

Solubility of sulphur dioxide gas at one atmosphere in sulphuric acid and ~~in~~ water mixture was also observed to be minimum at the minimum in the integral free energy of $\text{H}_2\text{SO}_4 - \text{H}_2\text{O}$.⁶⁷ This behaviour has also been reported in the case of Fe-Si alloys⁶⁸ at $1500^\circ - 1650^\circ\text{C}$ where the solubility of hydrogen was found to be minimum at ΔG minimum.

Figure 29 shows the variation of the activity coefficient of manganese sulphide in $\text{MnO} + \text{Al}_2\text{O}_3 + \text{SiO}_2$ melts at 1650°C . The shapes of the iso-activity coefficient curves may also be in accordance with the variation of the free energies of formation of the melt, but no data are available on the free energies of formation for comparison.

The activity coefficient of calcium sulphide in $\text{CaO} + \text{SiO}_2 + \text{Al}_2\text{O}_3$ melts at 1550°C has been shown in Figure 30. In this system also the contours of the iso-activity coefficient may ... be in accordance with the free energies of formation

FIG. 29
 γ/MnS
 $\text{MnO} + \text{SiO}_2 + \text{Al}_2\text{O}_3$
 AT 1650°C.

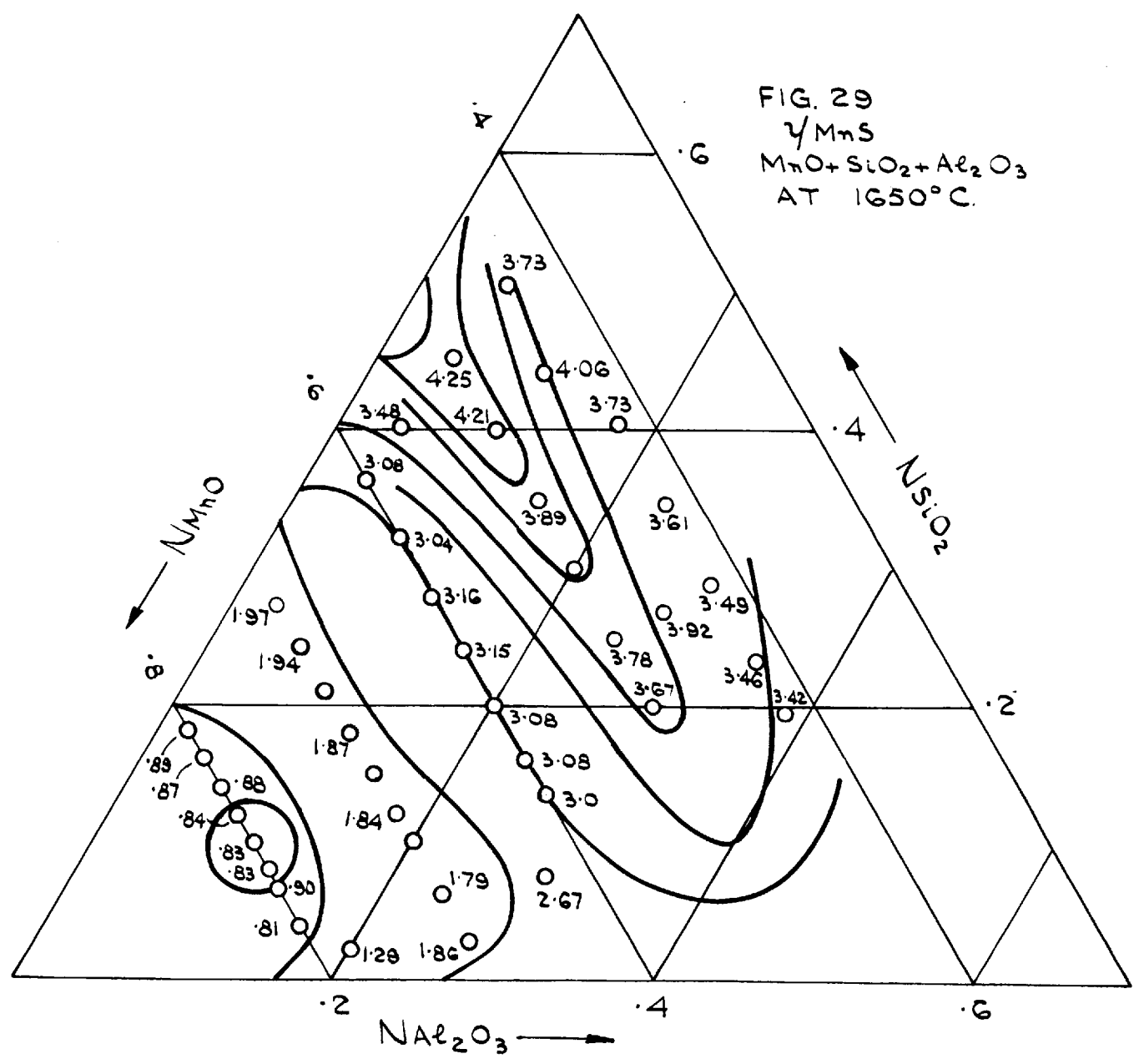
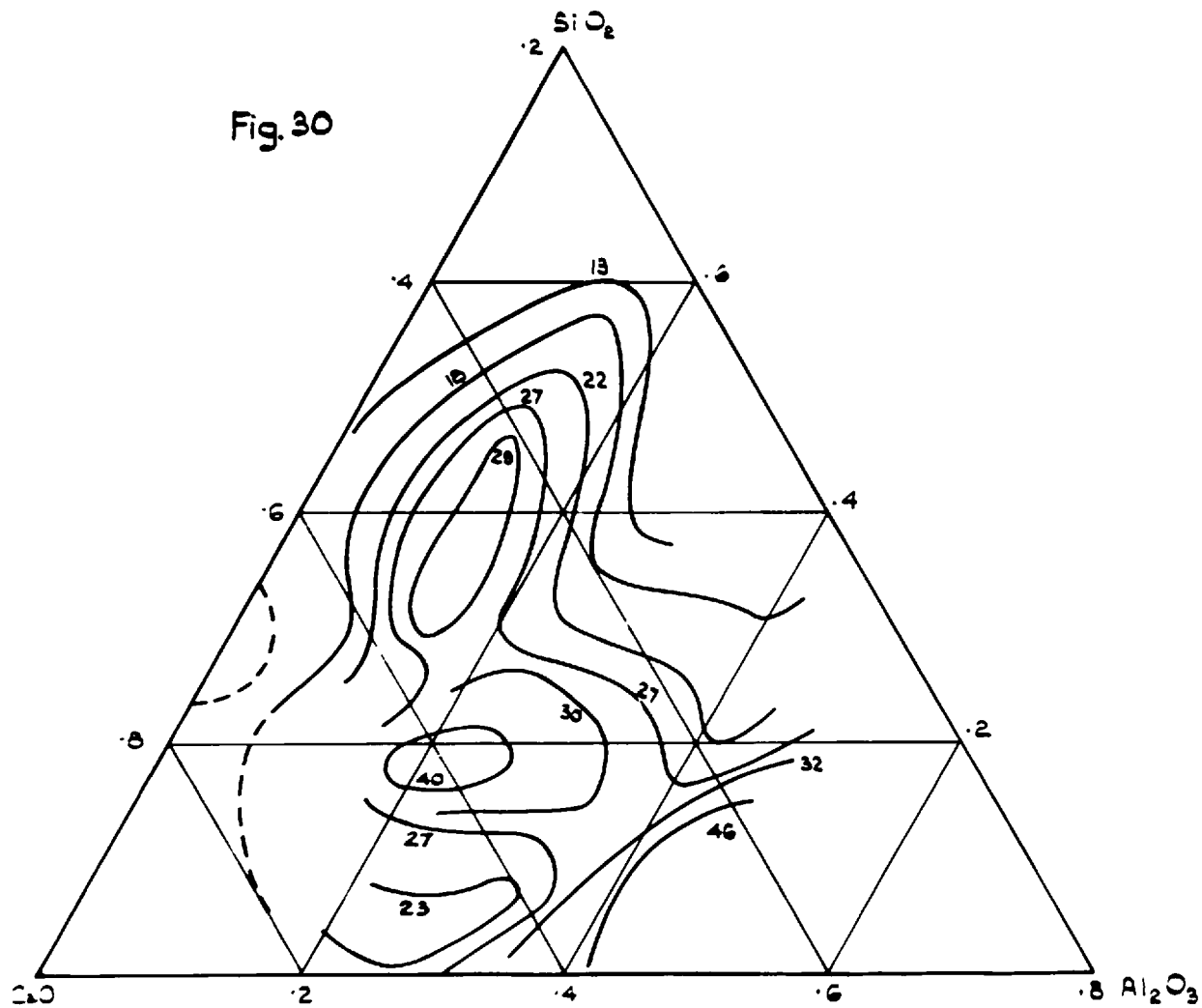


Fig. 30



of the melt. The closed loops may be due to the depressions in the free energies of formation in this region of the melt.

Darken⁶⁷ using the Gibbs-Duhem relationship for a regular ternary melt, has shown that the solubility of a third element in a binary alloy is minimum where there is minimum in the excess integral free energy ΔG^{XS} of the binary. While Richardson and Alcock,⁶⁹ from a consideration of the energetics of a random ternary solution with bond energy and coordination number independent of composition, have derived the following equation for the activity coefficient of a dilute solute S in a mixture of X and Y.

$$\log \gamma_S(X + Y) = N_Y \log \gamma_S(Y) + N_X \log \gamma_S(X) - \frac{\Delta G^{XS}}{RT}(X + Y)$$

$\gamma_S(Y)$ etc., are the activity coefficients of S in (Y) and so on, and $\Delta G^{XS}(X + Y)$ is the integral excess free energy of X + Y at mole fractions of N_X and N_Y . This also leads to the same conclusion that the activity coefficient of a third element should have a maximum value in a binary mixture at a composition which has excess integral free energy at the maximum negative value.

It is interesting to see this type of behaviour in the complex mixtures involved in the present work. As regards the relationship between the solubility of an element and ΔG°

for the melt, it may be said in a general way only that the free energy minima presumably occur at compositions where the various components of the melt may fit together to make the lowest energy structures, indicating a dislike for any other element for association. The high value of the activity coefficient may then indicate that it requires more energy to fit disturbing ions or groups of ions in the melt under such conditions than at compositions where configurations are not so stable.

Results in relation to ideal mixing theory of silicate melts.

Richardson²⁷ has shown that the ideal free energy of formation of a ternary AO + BO + SiO₂ melt can be obtained by adding ideal free energy of mixing ($\Delta G_{\text{mix}}(\text{cations})$) to the weighted sum of the free energies of formation of the two corresponding binaries AO + SiO₂ and BO + SiO₂ of equal silica mole fractions. The ideal free energy of the cation mixing is:

$$\Delta G_{\text{mix}}(\text{cations}) = RT N_{\text{AO}} \ln \frac{N_{\text{AO}}}{N_{\text{AO}} + N_{\text{BO}}} + N_{\text{BO}} \ln \frac{N_{\text{BO}}}{N_{\text{AO}} + N_{\text{BO}}} \quad (1)$$

per mole of the slag when no interactions between cations occur.

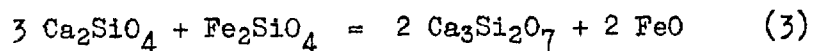
The sum of the free energies of formation of the two binaries

$$\Delta G' = \frac{N_{\text{AO}}}{N_{\text{AO}} + N_{\text{BO}}} \Delta G_{\text{AO}}(\text{bin}) + \frac{N_{\text{BO}}}{N_{\text{AO}} + N_{\text{BO}}} \Delta G_{\text{BO}}(\text{bin}) \quad (2)$$

Using the results for binaries FeO + SiO₂, MnO + SiO₂ and CaO + SiO₂, Richardson and Abraham⁷⁰ calculated the free energies of formation for the ternaries FeO + CaO + SiO₂ and CaO + MnO + SiO₂. There was a good agreement between the calculated values and the experimental ones in the metasilicate region, but negative deviation near the orthosilicate region.

The probable reasons given for the negative deviation were that the anionic matrix may maintain the same structure but there could be an interaction between the cations, which would invalidate the relation (1), or, alternatively, that there could be change in the anionic matrix which would effect the value of $\Delta G'$ in relation (2).

Abraham and Richardson, by assuming that the interactions between cations are negligible (details later) and that there are changes in anionic matrix of the type represented by the equation



calculated the values for the integral free energy of mixing within ± 500 cal of those obtained experimentally. The probability of this reaction from thermodynamic considerations may be seen from the following: the free energies of formation for Ca_2SiO_4 , $\text{Ca}_3\text{Si}_2\text{O}_7$, Fe_2SiO_4 , Mn_2SiO_4 , FeO and supercooled liquid MnO (Figure 27), are -30, -61, -5.4, -11.1, 0 and +1.2 Kcal respectively. Free energy change for the above reaction is -32 Kcal and -19 Kcal if FeO is replaced by MnO . This lends support to the above suggestion.

It has been shown by Meadowcroft⁷¹ that in a melt of single cation phosphates, the anion distribution is a function of the ratio of the metal oxide to phosphorus pentoxide

and of the type of cation present. The anion distribution is related to the shape of heat of formation curve for the system. It was also indicated that for mixtures of two systems which have heat of formation curves close (or similar in shape), heat of mixing is small and anion distribution is mean. Those mixtures for which these curves are far apart (or have different profiles) have substantial heats of mixing and the anionic distribution is anomalous. As the phosphates and silicates are similar in structure, this anomalous anion distribution should occur also in silicates under similar conditions. This also supports the change in the anionic matrix proposed above.

The integral free energy of mixing ΔG_M has been calculated in the system $\text{FeO} + \text{CaO} + \text{SiO}_2$ and $\text{MnO} + \text{CaO} + \text{SiO}_2$ at 1600°C using the ΔG° values in the binary $\text{CaO} + \text{SiO}_2$ as measured in the present work which are different from those used earlier.⁷⁰ The ΔG° values used here for $\text{MnO} + \text{SiO}_2$ ⁷ and $\text{FeO} + \text{SiO}_2$ ⁶⁴ systems have been reported by Abraham.⁷ The results are presented in Figures 31 and 32, where ΔG_M has been shown as a function of N_{FeO} or N_{MnO} at constant CaO to SiO_2 ratios. The thick lines a, b, ... etc., represent the calculated integral free energies of mixing and the corresponding thin lines represent the free energies of mixing compatible with the measured ones. a, b, c and d as shown in

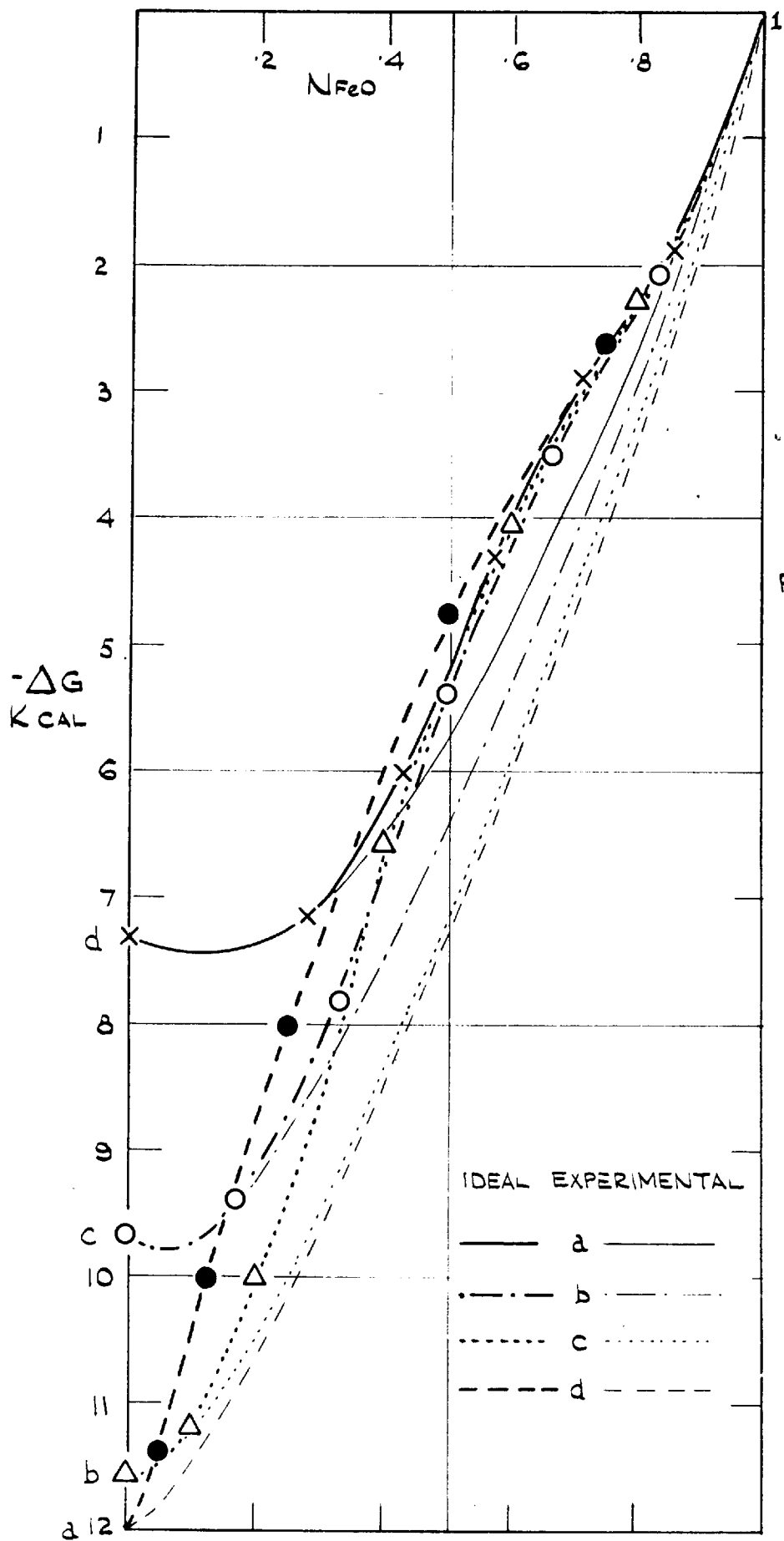


FIG. 31.

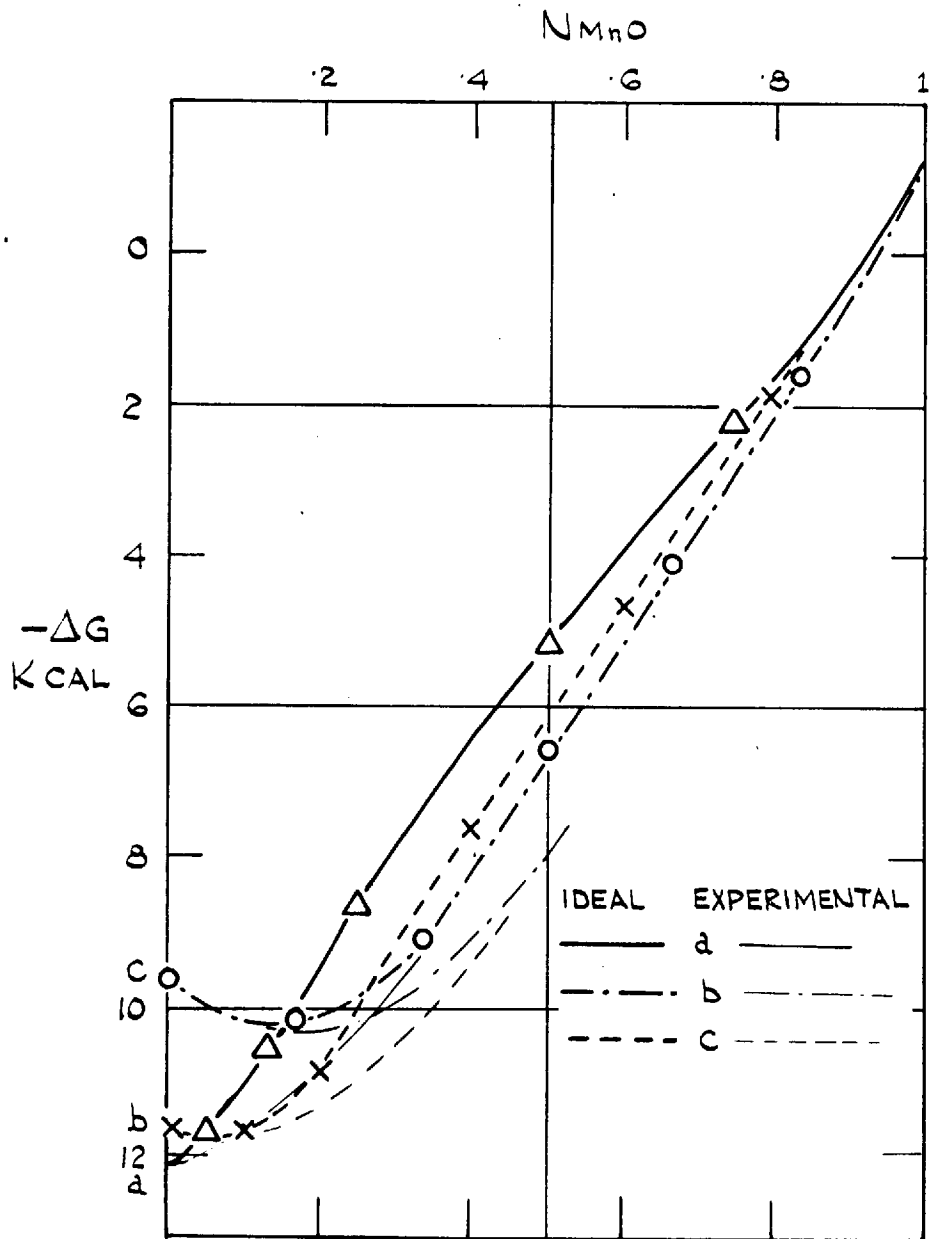


FIG. 32.

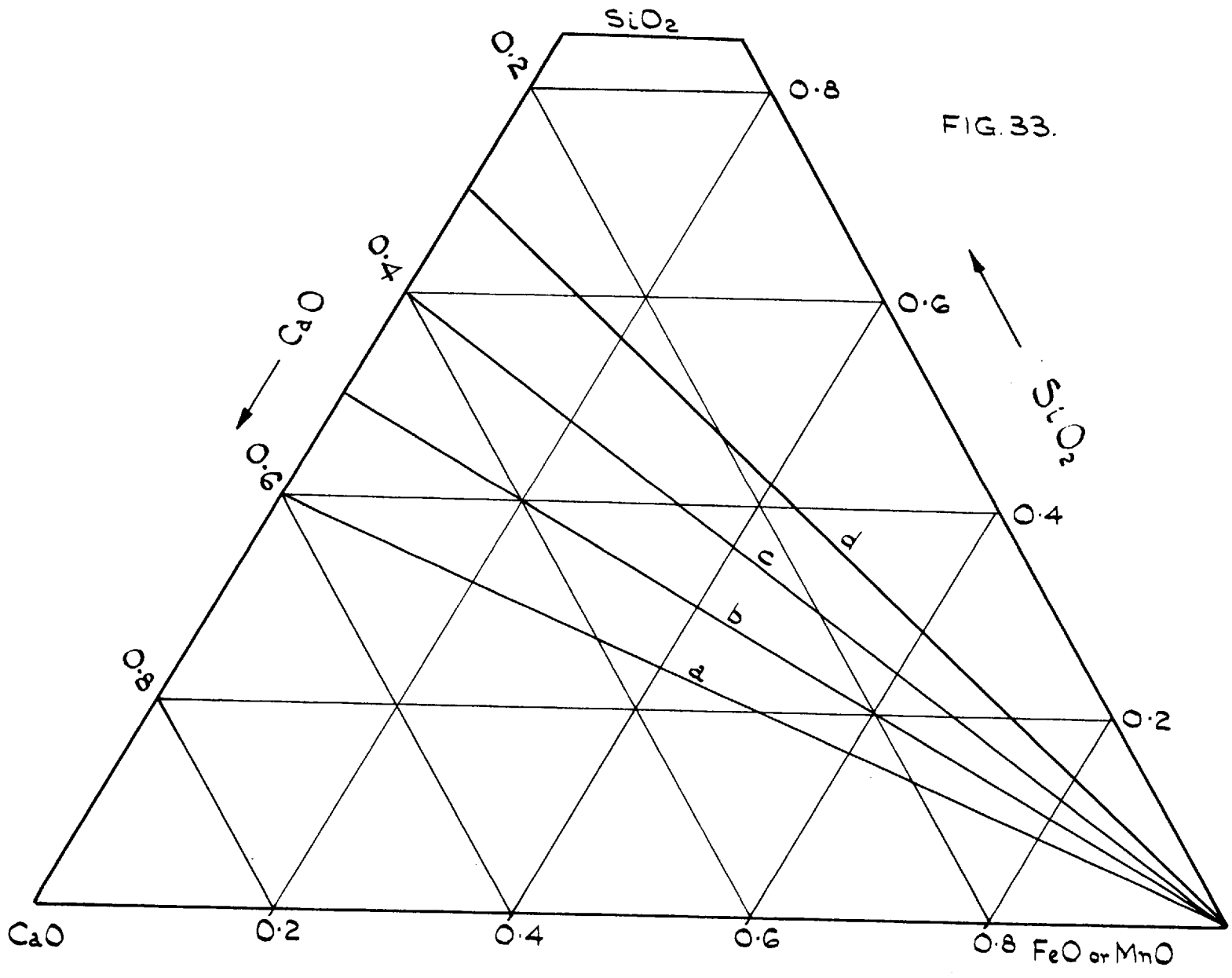
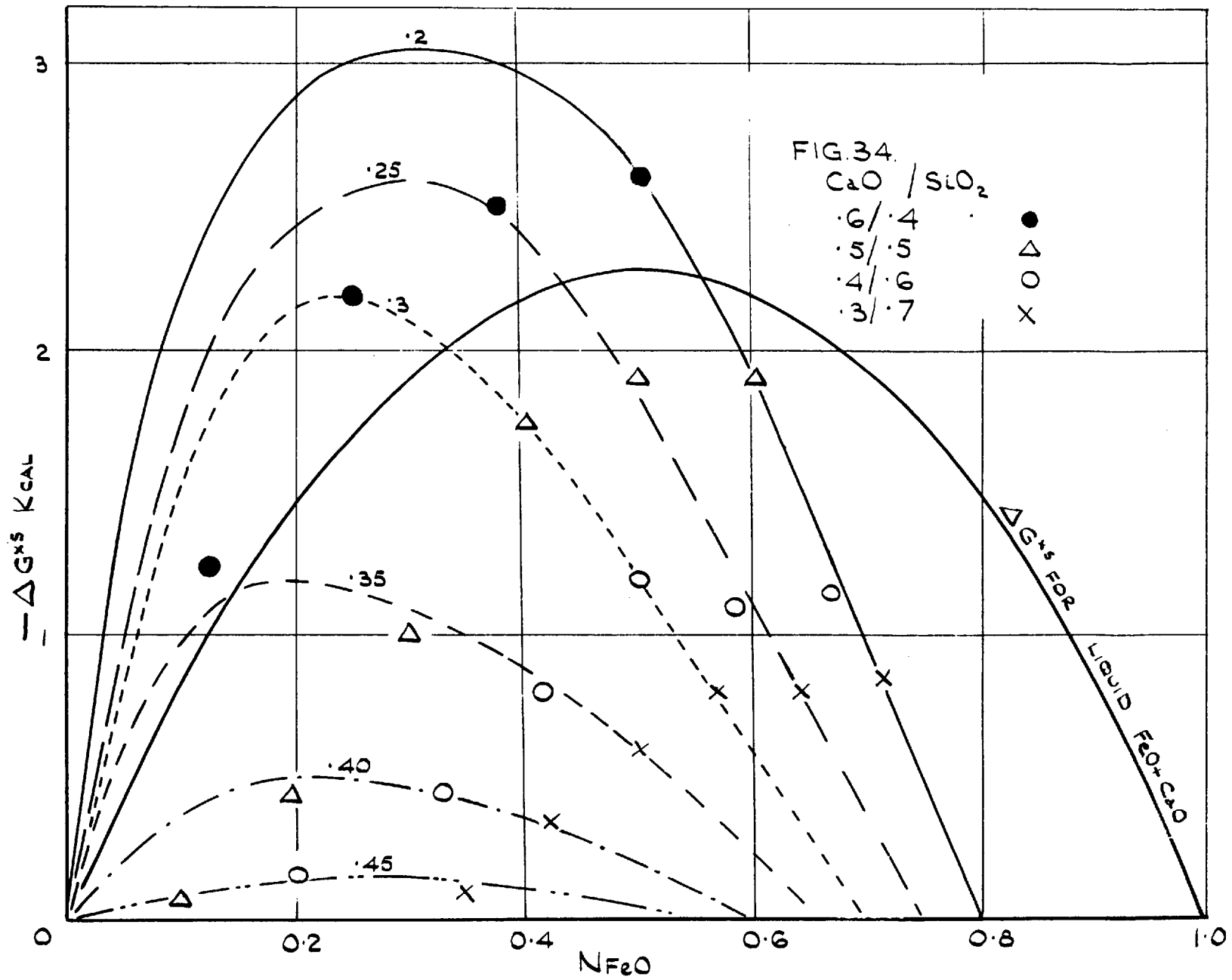


FIG. 33.



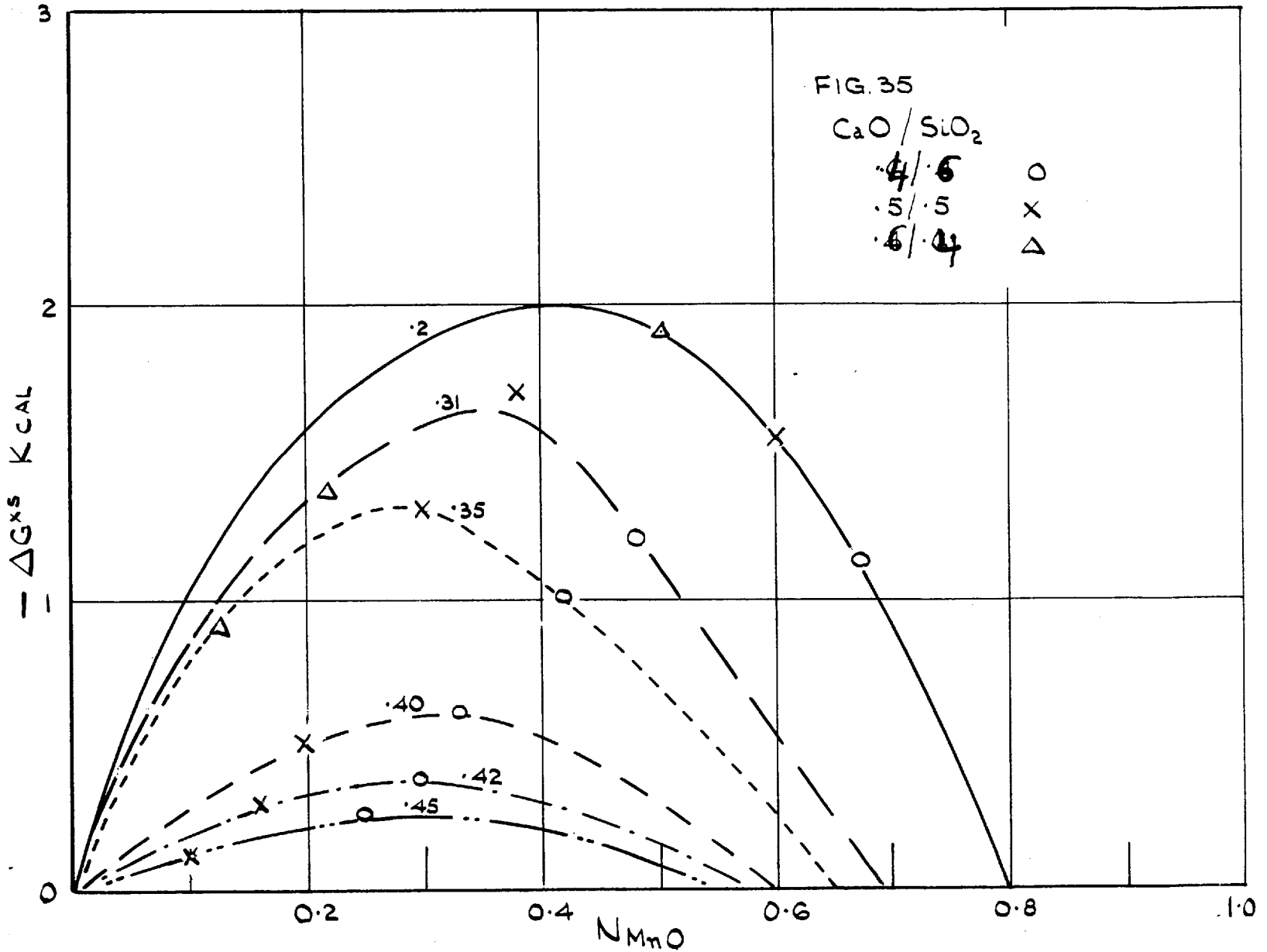


Figure 33, represent the compositions in the ternaries along the constant CaO to SiO₂ ratios; 6/4, 5/5, 4/6 and 3/7. Figures 34 and 35 have been constructed from Figures 31 and 32. Excess integral free energies ΔG^{XS} has been plotted as a function of N_{MnO} for the system MnO + CaO + SiO₂ and of N_{FeO} for the system FeO + CaO + SiO₂ in these figures. Each curve represents the variation in the ΔG^{XS} for a constant mole fraction of SiO₂ shown by the respective figure. The points ~~and~~ represent the values read off from the curves a, b, c and d in Figures 31 and 32. Although the deviation in the Figures 31 and 32 have great effects on the activities, it can be seen from Figures 34 and 35 that the small excess integral free energies could account for these large differences between the ideal and experimental integral free energies. It may also be seen from these figures that the excess integral free energy never exceeds 3 Kcal in FeO + CaO + SiO₂ melts and 2 Kcal in MnO + CaO + SiO₂. It is one Kcal in both cases at $N_{SiO_2} = 0.35$ and continuously decreases with increasing SiO₂ mole fraction and becomes negligible at $N_{SiO_2} = 0.5$. The same has been observed earlier⁷⁰. Abraham,⁷⁰ measured the heats of formation of the crystalline mixed cation silicates and found them ideal to within ± 400 cal. It was implied from this that the interaction between cations such as Ca⁺⁺ and Fe⁺⁺ are negligible, but Lumsden²² attributes the absence of the heat effect in the formation of these isomorphous

solid solutions between Calcium and ferrous silicates to the strain energy due to the disparity between the sizes of calcium and ferrous ions happening to be equal in magnitude but opposite in sign to the heat effect due to the intrinsic interactions between two ions. Meadowcroft⁷³ determined the heats of mixing for phosphate glasses and found small heats of mixing for the pairs Na-Li, Li-Ca, Ca-Zn, where the curves for the heats of formation of phosphates are close in respective pairs, but substantial for Na-Zn which has the heats of formation curves apart. In view of the similarity in structure between silicates and phosphates there should be interactions between cations in silicate glasses under these conditions. ΔG^{XS} could also be calculated from the FeO activity data in the CaO + FeO system reported by Bishop, et al.⁷⁴. This has also been shown in Figure 34. These values, of course, cannot account for the negative deviations observed, as seen from Figure 35. So it appears that the negative deviation is caused by the combined effect of the interactions between cations and also of changes in the anionic matrix.

Nevertheless, ideal mixing theory provides a standard against which the behaviour of the complex slags may be compared. By the application of this simple theory, it is also possible to calculate the free energy of formation in the ternary melts in the metasilicate region reasonably well, and

to make useful predictions in the orthosilicate region if rough allowance is made for cation-cation interactions and for possible changes in the anionic matrix.

APPENDIX

Calculation of the Partial Pressures of Oxygen and Sulphur.

Equilibrium partial pressures of oxygen and sulphur in the gas phase were calculated from the composition of the ingoing gases and the free energies of formation of the various types of gas molecules formed by the interactions at the temperature of the experiment. It was assumed that at high temperatures and moderate pressures, gases obey the ideal gas law, $PV = nRT$. The deviations are smaller than any existing quantitative measurements can detect.⁷⁵ Assumption was also made that the gases reached equilibrium within themselves because at high temperatures reactions between gases occur at almost immeasurably high speeds. Similar calculations have already been made by Fincham³⁴, Davies³ and Abraham⁶ where the gas mixtures were made either of N_2 , H_2 and CO_2 or N_2, H_2, CO_2 and SO_2 . In the present work the gas mixture of different oxygen and sulphur potentials and of components N_2 , H_2 , CO_2 and H_2S were used. The method of calculation is given below.

(i) Calculation of oxygen partial pressures in H_2 , CO_2 and N_2 mixtures.

Only H_2 , H_2O , CO_2 , CO , N_2 and O_2 occur in the significant amounts out of all the gaseous species formed by the interactions of the above gases at the equilibrium temperature.

This may be shown by the thermodynamic data available.⁷⁶

The free energies of formation of H₂O⁷⁷ from H₂ and O₂ and of carbon dioxide⁷⁷ from CO and O₂ within ± 1 Kcal between 1500°C - 1650°C are

$$2\text{H}_2 + \text{O}_2 = 2\text{H}_2\text{O}; \Delta G^\circ = -100,491 + 29.56T - 7043 \log T \quad (1)$$

$$\begin{aligned} 2\text{CO} + \text{O}_2 = 2\text{CO}_2; \Delta G^\circ = & -135,757 + 43.048T \\ & - 0.2089 \times 10^{-3} T^2 \log T \end{aligned} \quad (2)$$

where T is absolute temperature.

The equilibrium constants $K_2 = \frac{P_{\text{CO}_2}}{P_{\text{CO}} \cdot P_{\text{O}_2}^{1/2}}$ for the reaction (2) and $K_3 = \frac{P_{\text{H}_2\text{O}} \times P_{\text{CO}}}{P_{\text{H}_2} P_{\text{CO}_2}}$ for the reaction

$$\text{H}_2 + \text{CO}_2 = \text{H}_2\text{O} + \text{CO} \quad (3)$$

at appropriate temperatures were obtained by the relationship $\Delta G^\circ = -RT \ln K$. p indicates the partial pressure at the equilibrium.

Now, by substituting the required oxygen partial pressure in K_2 the quantity $P_{\text{CO}}/P_{\text{CO}_2}$ is obtained, and from K_3 and (2)

$$P_{\text{H}_2}/P_{\text{H}_2\text{O}} = \frac{P_{\text{CO}}}{P_{\text{CO}_2}} \cdot \frac{1}{K_3}$$

and

$$P_{\text{CO}} = P_{\text{H}_2\text{O}}$$

From the stoichiometry

$$P_{CO_2(i)} = P_{CO} + P_{CO_2}$$

$$P_{H_2(i)} = P_{H_2} + P_{H_2O}$$

where the subscript (i) indicates the partial pressure in the ingoing gas mixture

$$\begin{aligned} \therefore \frac{P_{H_2(i)}}{P_{CO_2(i)}} &= \frac{P_{H_2} + P_{H_2O}}{P_{CO} + P_{CO_2}} \\ &= \frac{P_{H_2O} (P_{H_2}/P_{H_2O} + 1)}{P_{CO} (1 + \frac{P_{CO_2}}{P_{CO}})} \\ &= \frac{\frac{P_{CO}}{P_{CO_2}} \times K_3 + 1}{(1 + P_{CO_2}/P_{CO})} \end{aligned} \quad (4)$$

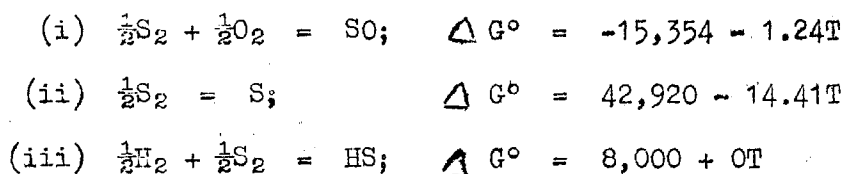
Thus, from the required oxygen partial pressure, the values of $P_{H_2(i)}/P_{CO_2(i)}$ can be calculated. The individual values of $P_{H_2(i)}$ and $P_{CO_2(i)}$ could also be calculated as it was always arranged to have

$$P_{N_2(i)} = P_{H_2(i)} + P_{CO_2(i)} = 0.5$$

It should be noted that all the partial pressures were measured in atmospheres. By changing the ratio $P_{H_2(i)}/P_{CO_2(i)}$ the partial pressure of oxygen can be varied over the required range.

- (ii) Calculations of oxygen and sulphur partial pressures in gas mixtures consisting of either N₂, H₂, CO₂ and SO₂ or N₂, H₂, CO₂ and H₂S.

In the case of the above gas mixtures, in addition to N₂, CO, CO₂, H₂ and H₂O, the species containing sulphur also needed to be considered. They are S₂, S, SO₂, SO, SO₃, H₂S, HS, COS, CS, CS₂, S₈ and S₆. The free energies³⁰ of formation of S₈, S₆, SO₂, SO₃, H₂S and CS₂ from S₃ at one atmosphere pressure are known to within ± 1 Kcal, and that of COS to within ± 3 Kcal. The free energies³⁰ of formation of S, SO and HS are in doubt by more than ± 10 Kcal. Recently Dewing and Richardson¹¹ have revised the values for the dissociation energies of SO and S₂. These values are considered more reliable and hence are used in the present calculations. The free energy of formation of HS was also corrected to suit this new value for the dissociation energy of S₂. The revised values for these species reported by Abraham⁶ are



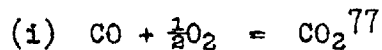
Rough calculations based on available thermodynamic data have shown that at the temperatures used in this work (1500° - 1650°C):

- (i) the partial pressure of CS₂ can never be more than about 10⁻³ of the total sulphur pressure,
- (ii) the partial pressure of SO₃ can never be more than about 10⁻² of the total sulphur pressure even at oxygen partial pressure of one atmosphere,
- (iii) the partial pressures of S₆ and S₈ are less than 10⁻¹⁰ of the total sulphur pressure,
- (iv) the partial pressure of CS can never be more than 10⁻⁴ of the total pressure of sulphur.

Consequently, the only species containing sulphur to be considered here, were S₂, S, SO, SO₂, COS, H₂S and HS.

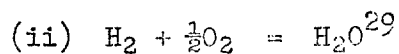
The method of calculation.

The equilibrium constants at the required temperature T°K were first calculated from the standard free energy changes of the respective reactions, as follows:



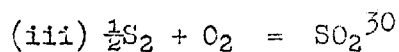
$$\Delta G^\circ = -67,878.5 + 21.524T - 0.10,445 \times 10^{-3} T^2 \log T$$

$$K_1 = \frac{P_{\text{CO}_2}}{P_{\text{CO}} \times P_{\text{O}_2}^{\frac{1}{2}}}$$



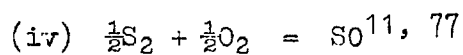
$$\Delta G^\circ = -50,245.5 + 14.73T - 3,521.5 \log T$$

$$K_2 = \frac{p_{H_2O}}{p_{H_2} \cdot p_{O_2}^{\frac{1}{2}}}$$



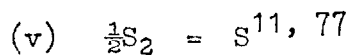
$$\Delta G^\circ = -86,620 + 17,31T$$

$$K_3 = \frac{p_{SO_2}}{p_{S_2}^{\frac{1}{2}} p_{O_2}}$$



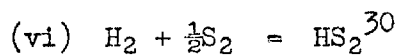
$$\Delta G^\circ = -15,354 - 1.24T$$

$$K_4 = \frac{p_{SO}}{p_{S_2}^{\frac{1}{2}} p_{O_2}^{\frac{1}{2}}}$$



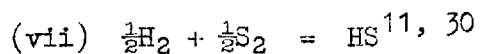
$$\Delta G^\circ = 42,920 - 14.41T$$

$$K_5 = \frac{p_S}{p_{S_2}^{\frac{1}{2}}}$$



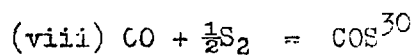
$$\Delta G^\circ = -21,580 + 11.805T$$

$$K_6 = \frac{p_{HS_2}}{p_{H_2} \times p_{S_2}^{\frac{1}{2}}}$$



$$\Delta G^\circ = 8,000 + 0T$$

$$K_7 = \frac{p_{HS}}{p_{H_2}^{1/2} p_{S_2}^{1/2}}$$



$$\Delta G^\circ = -22,860 + 18.70T$$

$$K_8 = \frac{p_{COS}}{p_{CO} p_{S_2}^{1/2}}$$

The desired oxygen and sulphur partial pressures p_{O_2} and p_{S_2} at equilibrium were selected. The values of p_{SO_2} , p_{SO} and p_S were calculated from the known values of K_3 , K_4 , K_5 , p_{O_2} and p_{S_2} at $T^\circ K$.

$$(ix) \quad p_{SO_2} = K_3 p_{O_2} \cdot p_{S_2}^{1/2}; \quad p_{SO} = K_4 p_{O_2}^{1/2} \cdot p_{S_2}^{1/2};$$

$$p_S = K_5 p_{S_2}^{1/2}$$

The values of p_{H_2O} , p_{H_2S} and p_{HS} were calculated in terms of p_{H_2} from K_2 , K_6 and K_7 , and p_{S_2} and p_{O_2} at $T^\circ K$.

$$(x) \quad p_{\text{H}_2\text{O}} = K_2 p_{\text{O}_2}^{\frac{1}{2}} p_{\text{H}_2}; \quad p_{\text{H}_2\text{S}} = K_6 p_{\text{S}_2}^{\frac{1}{2}} p_{\text{H}_2};$$

$$p_{\text{HS}} = K_7 p_{\text{S}_2}^{\frac{1}{2}} p_{\text{H}_2}^{\frac{1}{2}}$$

The values of p_{COS} and p_{CO_2} were calculated in terms of p_{CO} from K_8 , K_1 , p_{O_2} and p_{S_2} at $T^\circ\text{K}$.

$$(xi) \quad p_{\text{COS}} = K_8 p_{\text{S}_2}^{\frac{1}{2}} p_{\text{CO}}; \quad p_{\text{CO}_2} = K_1 p_{\text{O}_2}^{\frac{1}{2}} p_{\text{CO}}$$

As the total pressure is one atmosphere;

$$(xii) \quad p_{\text{N}_2} + p_{\text{H}_2} + p_{\text{H}_2\text{O}} + p_{\text{CO}_2} + p_{\text{CO}} + p_{\text{SO}_2} + p_{\text{S}_2} + p_{\text{S}} + p_{\text{H}_2\text{S}} \\ + p_{\text{HS}} + p_{\text{SO}} + p_{\text{COS}} = 1.$$

In the case of the gas mixture consisting of N_2 , H_2 , CO_2 and SO_2 ; the source of oxygen is CO_2 and SO_2 , and this oxygen can combine with hydrogen only. By the relation (ii) the total number of oxygen atoms combined with hydrogen is equal to the total number of H_2O molecules produced, i.e. $n_{\text{H}_2\text{O}} = 2n_{\text{O}_2}$. By equation (i) the number of CO molecules produced is equal to the number of oxygen atoms that came out of CO_2 . So the number of CO molecules is equal to the total number of oxygen atoms released from SO_2 and CO_2 minus the number of CO atoms consumed in COS formation and minus the number of oxygen atoms released from SO_2 only. So it can be seen from the stoichiometry that:

$$(xiii) \quad p_{CO} = p_{H_2O} - (4p_{S_2} + p_{SO} + 2p_{H_2S} + 2p_{HS} + 3p_{COS} + 2p_S)$$

By substituting the values of the right hand terms from (ix), (x) and (xi) p_{CO} was obtained in terms of p_{H_2}

(xiv) Similarly, by substituting the value of p_{CO} in (xi) p_{CO_2} and p_{COS} were obtained in terms of p_{H_2} .

(xv) If $\sum C$ is the sum of all the partial pressures of the gases containing one atom of carbon, $\sum H_2$ the sum of the partial pressures of the gases containing two atoms of hydrogen and $\sum S$ the sum of the partial pressures of all the gases containing one sulphur atom, then

$$\sum C = p_{CO_2} + p_{CO} + p_{COS}$$

$$\sum H_2 = p_{H_2} + p_{H_2O} + p_{H_2S} + \frac{1}{2}p_{HS}$$

$$\sum S = p_{H_2S} + p_{COS} + p_{HS} + 2p_{S_2} + p_{SO_2} + p_{SO} + p_S$$

These quantities are directly proportional to the number of carbon, hydrogen and sulphur atoms in the mixture. Throughout this work the partial pressure of nitrogen in the ingoing gas mixture was made equal to the sum of the partial pressures of the other three gases, i.e. H_2 , CO_2 and SO_2

$$p_{N_2(i)} = p_{CO_2(i)} + p_{H_2(i)} + p_{SO_2(i)}$$

consequently,

$$\sum N_2 = p_{N_2} = \sum C + H_2 + \sum S$$

The values of $\sum H_2$, $\sum S$ and $\sum C$ are all known in terms of p_{H_2} . So the value of p_{N_2} was calculated in terms of p_{H_2} .

(xvi) By substituting the values of different terms (some in terms of p_{H_2}) in equation (xii) and by solving the quadratic equation so obtained in terms of p_{H_2} and $\sqrt{p_{H_2}}$ the value of $\sqrt{p_{H_2}}$ and p_{H_2} were determined. From this $\sum C$, $\sum H_2$ and $\sum S$ were calculated.

(xvii) The partial pressures in the ingoing mixture corresponding to selected equilibrium oxygen and sulphur partial pressures were given by:

$$p_{CO_2(i)} = \frac{\sum C}{\sum C + \sum H_2 + \sum S + \sum N_2}$$

$$p_{H_2(i)} = \frac{\sum H_2}{\sum C + \sum H_2 + \sum S + \sum N_2}$$

$$p_{SO_2(i)} = \frac{\sum S}{\sum C + \sum H_2 + \sum S + \sum N_2}$$

$$p_{N_2(i)} = 0.5$$

The partial pressures of the gases in the ingoing gas mixtures and the corresponding equilibrium sulphur and oxygen partial pressures derived in this way by using the electronic computer for calculation, are listed in Table A. All the partial pressures are expressed in atmospheres.

(xiiiA) When the gas mixture consisted of N_2 , H_2 , H_2S and CO_2 the procedure for calculation up to (xii) was the same. But the source of oxygen in this case is only CO_2 and the total number of oxygen atoms must be equal to the sum of the number of carbon monoxide molecules and the number of COS molecules by the relation (i) and so

$$p_{CO} = 2n_{O_2} + n_{H_2O} + 2n_{SO_2} + n_{SO} - n_{COS}$$

$$\therefore p_{CO} = 2p_{O_2} + p_{H_2O} + 2p_{SO_2} + p_{SO} - p_{COS}$$

By substituting the value of p_{COS} in terms of p_{CO} from (xi) the value of p_{CO} was calculated in terms of p_{H_2} .

(xivA) By substituting the value of p_{CO} so obtained in (xi) the value of p_{CO_2} and p_{COS} were obtained in terms of p_{H_2} .

(xv) If $\sum C$ is the sum of all the partial pressures of the gases containing one atom of carbon, $\sum H_2$ the sum of the partial pressures of the gases containing two atoms of hydrogen originally present in hydrogen gas $H_{2(i)}$; and $\sum H_2S$ the sum of the partial pressures of the gases containing two hydrogen atoms

originally present in $H_2S(i)$, then

$$\sum C = p_{CO_2} + p_{CO} + p_{COS}$$

$$\sum H_2 = p_{H_2} + p_{H_2O} - \frac{1}{2}p_{HS} - p_{SO_2} - 2p_{S_2} - p_{SO} - p_S - p_{COS}$$

$$\sum H_2S = p_{SO_2} + 2p_{S_2} + p_{SO} + p_S + p_{HS} + p_{H_2S} + p_{COS}$$

(By the relation (vi) $H_2S \rightarrow H_2 + \frac{1}{2}S_2$, the number of hydrogen molecules from $H_2S(i)$ must be equal to the number of sulphur atoms).

These quantities are directly proportional to the number of CO_2 , H_2 and H_2S molecules in the mixture. Throughout this work the partial pressure of nitrogen in the ingoing gas mixture was made equal to the sum of the partial pressures of the other three gases, i.e. H_2 , H_2S and CO_2

$$p_{N_2(i)} = p_{CO_2(i)} + p_{H_2(i)} + p_{H_2S(i)}$$

$$\text{Consequently } \sum N_2 = p_{N_2} = \sum H_2 + \sum H_2S + \sum C$$

The values of $\sum H_2$, $\sum H_2S$ and $\sum C$ were all known in terms of p_{H_2} and so the value of p_{N_2} was found in terms of p_{H_2} .

(xviiA) By substituting the values of different terms (some in terms of p_{H_2}) in the (xii) and by solving the quadratic equation so obtained in terms of p_{H_2} and $\sqrt{p_{H_2}}$, the value of $\sqrt{p_{H_2}}$ and p_{H_2} were found. From this the values of $\sum H_2$, $\sum H_2S$ and $\sum C$ were calculated.

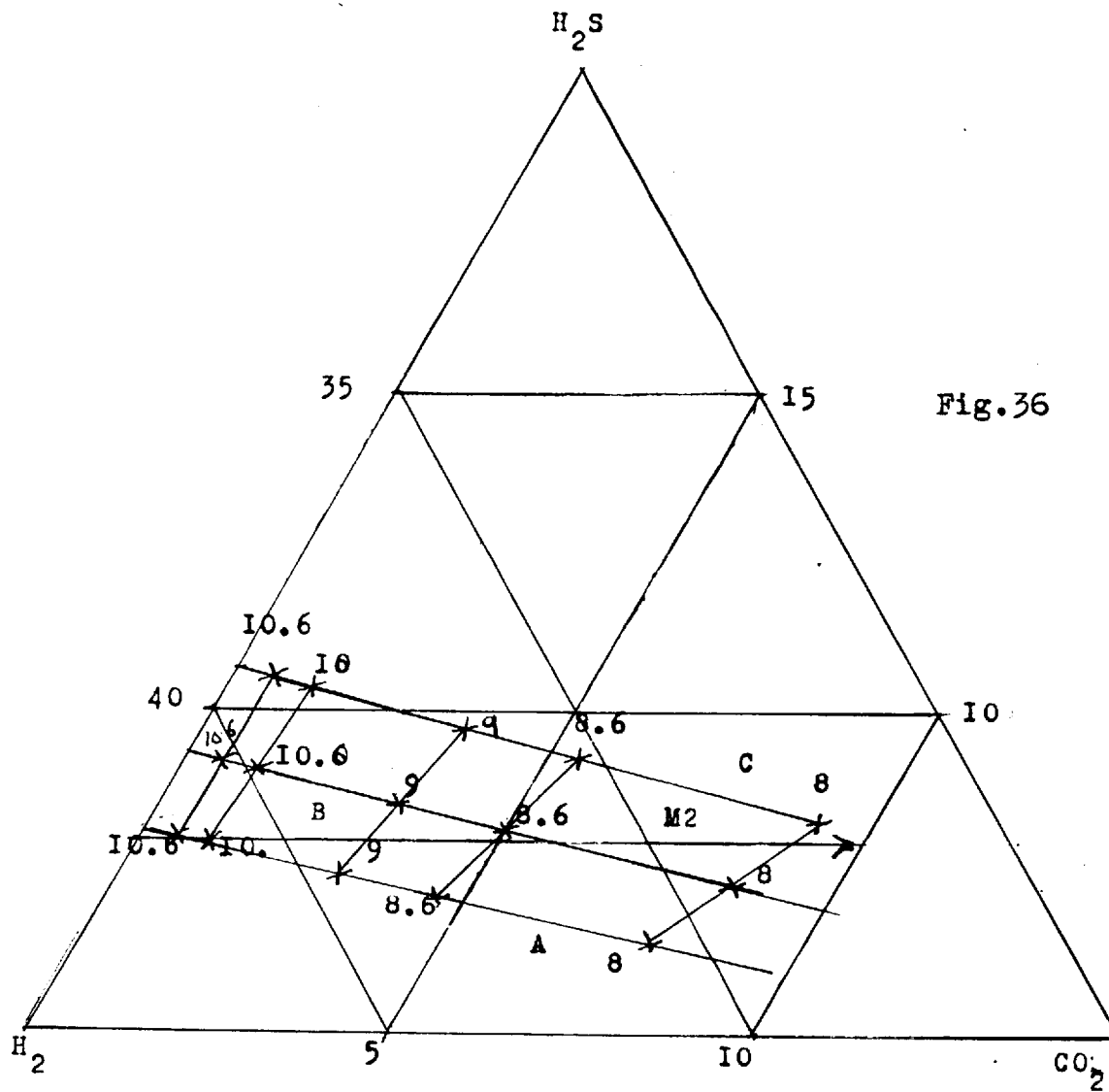


Fig.36

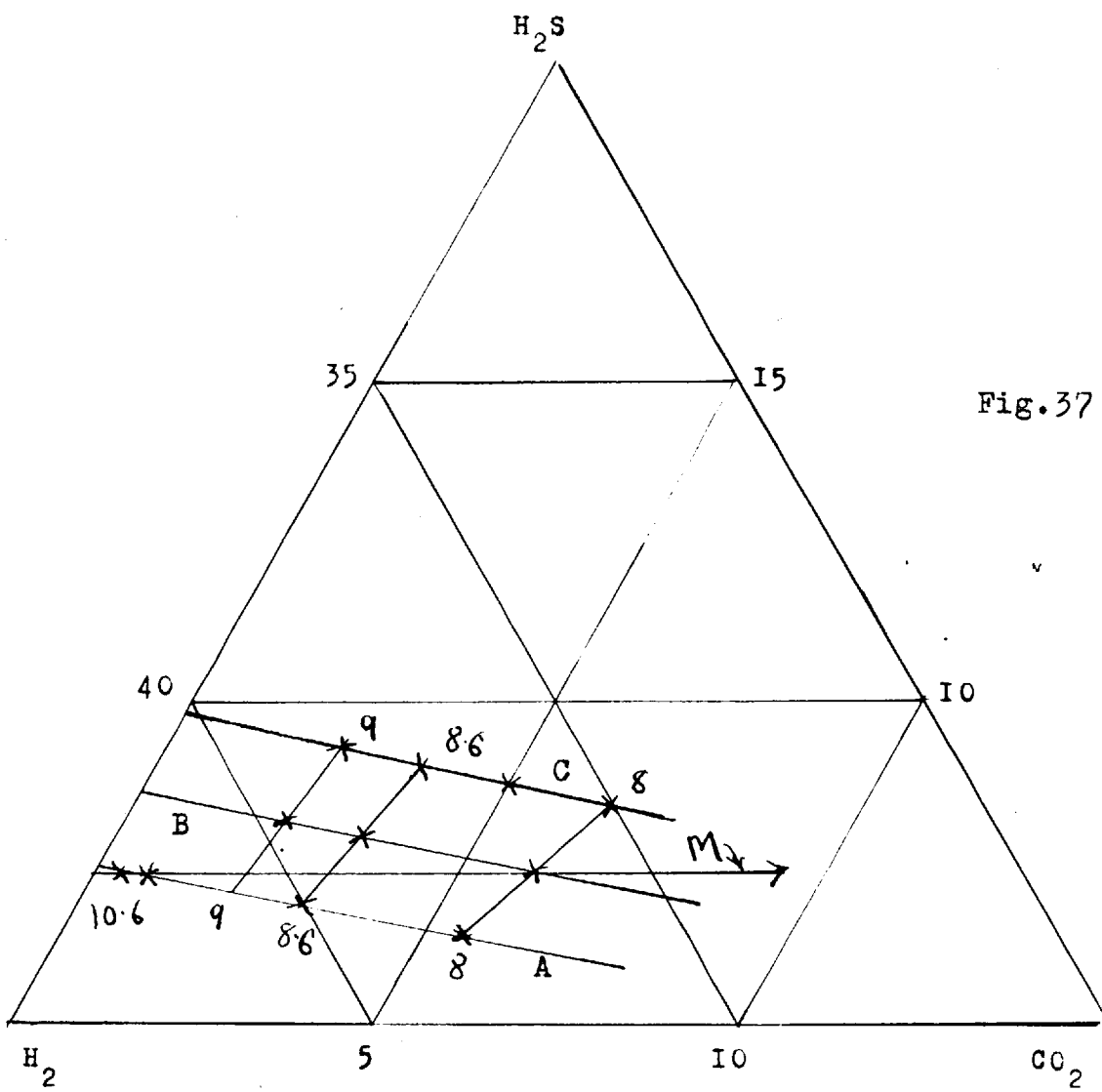


Fig.37

(xciiA) The ingoing partial pressures corresponding to selected equilibrium oxygen and sulphur pressures were given by.

$$P_{CO_2(i)} = \frac{\sum C}{\sum C + \sum H_2 + \sum H_2S + \sum N_2}$$

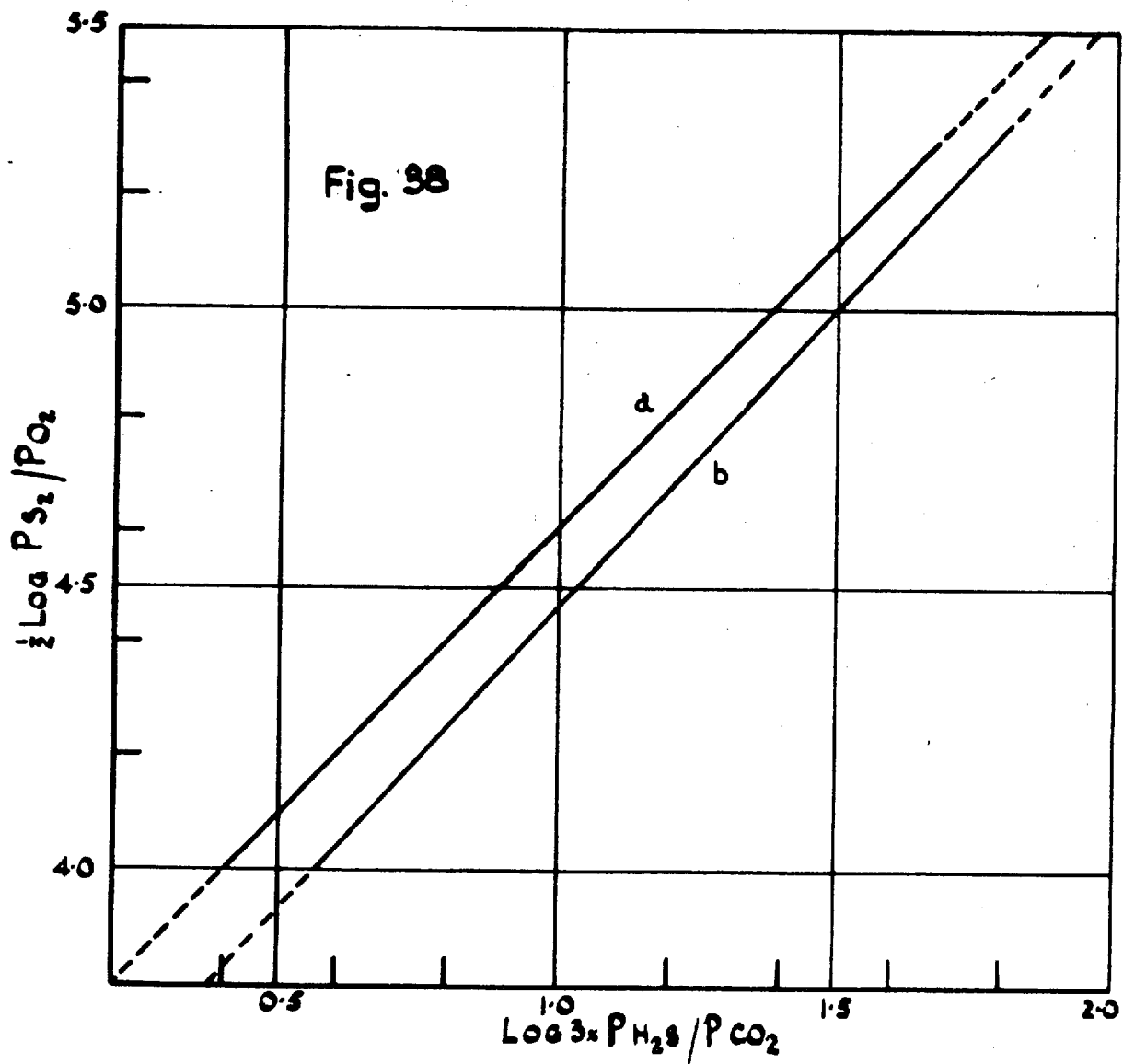
$$P_{H_2(i)} = \frac{\sum H_2}{\sum H_2 + \sum H_2S + \sum C + \sum N_2}$$

$$P_{H_2S(i)} = \frac{\sum H_2S}{\sum H_2 + \sum H_2S + \sum C + \sum N_2}$$

$$P_{N_2(i)} = 0.5$$

The partial pressures are in atmospheres. The calculations are quite rigid and no assumptions are involved. The uncertainties are due to those in the free energy equations.

The partial pressures of the gases in the ingoing gas mixtures and the corresponding equilibrium sulphur and oxygen partial pressures obtained by this method are listed in Table B., and Figures 36 and 37. In these figures $N_2 = 50\%$ in each mixture is kept constant and each point represents a logarithm of P_{S_2}/P_{O_2} ratio (shown by figures 8, 8.6, 9, etc.) given by certain initial gas composition. The initial gas compositions for the same partial pressure of sulphur are observed to lie on a straight line, i.e. the lines A, B and C in the Figures 36 and 37, represent the partial pressures of sulphur, 10^{-2} , $10^{-1.9}$, $10^{-1.8}$ atm., respectively. The same



ratios of P_{S_2}/P_{O_2} obtained by different gas compositions are also seen to lie on a straight line. The intersections of these straight lines with any line representing a constant proportion of $H_2S(i)$ (in the figure shown by M_2 and M), in the ingoing gas mixtures should represent the different P_{S_2}/P_{O_2} ratios given by these straight lines.

Now a plot between the P_{S_2}/P_{O_2} ratios and the $P_{H_2(i)}/P_{CO_2(i)}$ ratios of these intersections can be constructed which will give a relation between P_{S_2}/P_{O_2} and $P_{H_2(i)}/P_{CO_2(i)}$ along a constant proportion of $H_2S(i)$. Such plots between $\frac{1}{2} \log P_{S_2}/P_{O_2}$ and $\log P_{H_2(i)}/P_{CO_2(i)}$ at $1500^\circ C$ for 8% H_2S and at $1550^\circ C$ for 7.4% are shown by a and b respectively in Figure 38. From this figure the required composition of ingoing gas mixture can be obtained for any desired P_{S_2}/P_{O_2} ratio.

TABLE A

The equilibrium oxygen and sulphur pressures
calculated from the partial pressures of
the gases in the ingoing mixture.

<u>Temperature</u>	<u>P_{H₂(i)}</u>	<u>P_{CO₂(i)}</u>	<u>P_{SO₂(i)}</u>	<u>P_{N₂(i)}</u>	<u>P_{O₂}</u>	<u>P_{S₂}</u>
1650°C	0.154	0.326	0.02	0.50	1.115 x 10 ⁻⁶	1.839 x 10 ⁻⁴
1650°C	0.260	0.220	0.02	0.50	1.112 x 10 ⁻⁷	2.709 x 10 ⁻³
1650°C	0.157	0.333	0.01	0.50	1.072 x 10 ⁻⁶	5.013 x 10 ⁻⁵
1650°C	0.355	0.135	0.01	0.50	1.020 x 10 ⁻⁸	9.696 x 10 ⁻⁴
1650°C	0.364	0.116	0.02	0.50	1.038 x 10 ⁻⁸	2.958 x 10 ⁻³
1500°C	0.115	0.382	0.003	0.50	1.816 x 10 ⁻⁷	3.872 x 10 ⁻⁶
1500°C	0.134	0.346	0.02	0.50	1.069 x 10 ⁻⁷	4.255 x 10 ⁻⁴
1500°C	0.151	0.3294	0.02	0.50	7.248 x 10 ⁻⁸	7.837 x 10 ⁻⁴
1500°C	0.375	0.115	0.01	0.50	4.190 x 10 ⁻¹⁰	5.862 x 10 ⁻⁴
1500°C	0.480	0.010	0.01	0.50	7.775 x 10 ⁻¹²	2.456 x 10 ⁻⁴
1500°C	0.470	0.020	0.01	0.50	1.495 x 10 ⁻¹¹	2.644 x 10 ⁻⁴
1500°C	0.460	0.020	0.02	0.50	4.037 x 10 ⁻¹¹	1.109 x 10 ⁻³
1500°C	0.470	0.010	0.02	0.50	2.576 x 10 ⁻¹¹	1.033 x 10 ⁻³
1500°C	0.479	0.001	0.02	0.50	1.610 x 10 ⁻¹¹	9.712 x 10 ⁻⁴
1500°C	0.4799		0.02	0.50	1.533 x 10 ⁻¹¹	9.712 x 10 ⁻⁴

TABLE B

The equilibrium oxygen and sulphur pressures
calculated from the partial pressures
of the gases in the ingoing gas mixtures.

Temperature	Composition of the ingoing gas					
	$P_{N_2(i)}$	$P_{H_2(i)}$	$P_{CO_2(i)}$	$P_{H_2(i)}$	P_{S_2}	P_{O_2}
1500°C	0.50	0.075	0.03	0.395	10^{-2}	10^{-11}
1500°C	0.50	0.079	0.010	0.410	10^{-2}	10^{-12}
1500°C	0.50	0.080	0.005	0.415	10^{-2}	$10^{-12.6}$
1500°C	0.50	0.064	0.079	0.356	10^{-2}	10^{-10}
1500°C	0.50	0.071	0.046	0.383	10^{-2}	$10^{-10.6}$
1500°C	0.50	0.105	0.006	0.389	$10^{-1.8}$	$10^{-12.6}$
1500°C	0.50	0.073	0.086	0.340	$10^{-1.9}$	$10^{-9.9}$
1500°C	0.50	0.083	0.092	0.325	$10^{-1.8}$	$10^{-9.8}$
1500°C	0.50	0.085	0.034	0.380	$10^{-1.9}$	$10^{-10.9}$
1500°C	0.50	0.093	0.054	0.353	$10^{-1.8}$	$10^{-10.4}$
1500°C	0.50	0.090	0.012	0.400	$10^{-1.9}$	$10^{-11.9}$
1500°C	0.50	0.097	0.036	0.366	$10^{-1.8}$	$10^{-10.8}$
1500°C	0.50	0.104	0.013	0.384	$10^{-1.8}$	$10^{-11.8}$
1550°C	0.50	0.064	0.056	0.380	10^{-2}	10^{-10}
1550°C	0.50	0.069	0.031	0.400	10^{-2}	$10^{-10.6}$
1550°C	0.50	0.071	0.020	0.410	10^{-2}	10^{-11}
1550°C	0.50	0.073	0.007	0.420	10^{-2}	10^{-12}
1550°C	0.50	0.074	0.0034	0.423	10^{-2}	$10^{-12.6}$
1550°C	0.50	0.084	0.066	0.350	$10^{-1.8}$	$10^{-9.8}$
1550°C	0.50	0.090	0.037	0.370	$10^{-1.8}$	$10^{-10.4}$
1550°C	0.50	0.093	0.024	0.380	$10^{-1.8}$	$10^{-10.8}$
1550°C	0.50	0.073	0.060	0.370	$10^{-1.9}$	$10^{-9.9}$
1550°C	0.50	0.079	0.034	0.390	$10^{-1.9}$	$10^{-10.5}$
1550°C	0.50	0.031	0.022	0.400	$10^{-1.9}$	$10^{-10.9}$
1550°C	0.50	0.074	0.021	0.400	$10^{-1.96}$	$10^{-10.96}$

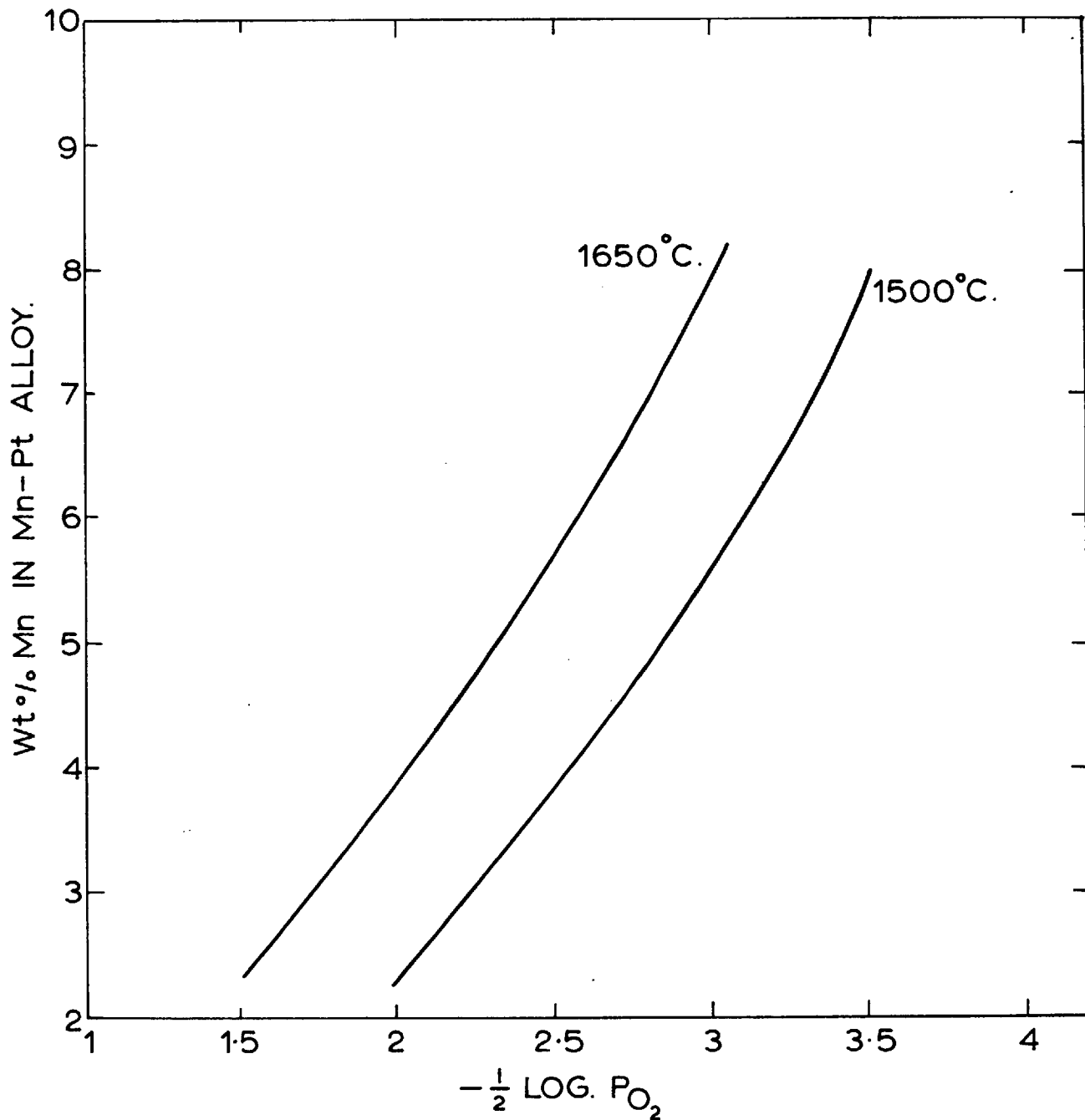


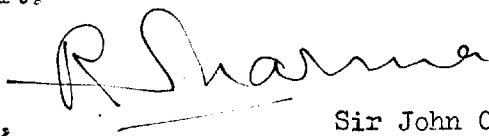
FIG. 39. RELATION BETWEEN Mn CONTENTS OF Mn-Pt ALLOYS IN EQUILIBRIUM WITH PURE MnO AND PARTIAL PRESSURES OF OXYGEN.

Acknowledgements

The author wishes to express his sincere gratitude to Prof. F. D. Richardson for his constant supervision and interest throughout this work. He also wishes to thank Dr. A. J. Lindsey and Dr. D. H. Houseman for their general interest in the work.

His thanks are due also to his colleagues at Sir John Cass College and the Nuffield Research Group and in particular to Dr. P. S. Rogers for valuable suggestions and discussions.

He is also indebted to Colombo plan authorities, BISRA, and Governors and Principal of Sir John Cass College for the financial support.



Nuffield Research Group,
Imperial College of Science
and Technology,
London, S.W.7.

Sir John Cass College,
Aldgate,
London, E.C.3.

References

1. Fincham and Richardson; Proc. Roy. Soc. A, 1954, 223, ~~45~~.
2. Richardson and Fincham; J. Iron and Steel Inst., 1954, 178, 4.
3. Davies; Thesis, University of London, 1955.
4. St. Pierre and Chipman; Trans. A.I.M.E. 1956, 206, 1474.
5. Carter and MacFarlane; J. Iron and Steel Inst. 1957, 185, 54.
6. Abraham; Thesis, University of London, 1959.
7. Abraham, Davies and Richardson; J. Iron and Steel Inst.
1960, 196, 309.
8. Abraham and Richardson; Ibid 1960, 196, 313-317.
9. Flood and Grietheim; Ibid 1952, 171, 64.
10. Osborne, De Varies, Gee and Kraner; J. Metals, 1954, 7, 33.
11. Dewing and Richardson; Trans. Farad. Soc., 1958, 54, 679.
12. Mac. Caffery and Oesterle; Trans. Am. Inst. Min. Metall. Eng.
1923, 69, 606.
13. Glaser; Zbl. Mineralogie, 1926, A, 81.
14. Filler and Darken; Trans. Am. Inst. Min. Metall. Eng.
1952, 194, 253.
15. Chipman, "Physical Chemistry of Process Metallurgy",
44; vol 7, part I, 1959, A.I.M.E. Symp. Inter science
publishers.
16. Rankin and Wright; Phase Diagrams for Ceramists (modified).
The American Ceramic Society Columbus, Ohio, 1956, 48.
17. Kay and Taylor; Trans. Farad. Soc., 1960, 56, 1372.
18. Yang, et al; "Physical Chemistry of Steel Making" 1958, 63,
New York, J. Willey, and Sons. Inc.

19. Langenberg, et al; "Physical Chemistry of Steel Making",
J. Willey, and Sons. Inc. New York 1958 . 65. 67.
20. Carter and Macfarlane; J. Iron and Steel Inst. 1957, 185, 62.
21. Richardson; "Physical Chemistry of Melts", Inst. Min.
Metall., London, 1953, 75-95.
22. Sanbongi and Omori; Scie. Rep. Tohoku, University. A.
1959, 11, 244.
23. Turkdogan; J. Iron and Steel. Inst. 1956, 182, 74.
24. Stuckel and Cucubinsky; Trans. A.I.M.E. 1954, 200, 353.
25. Turkdogan and Hancock; Trans. I.M.M. 1958, 67, 573.
26. Barton; Private communication.
27. Richardson; Trans. Farad. Soc. 1956, 52, 1312.
28. Rosenqvist; Trans. A.I.M.E. 1951, 191, 535-540.
29. U.S. Bur. Standard; "Selected Values of Chemical
Thermodynamic Properties", circular 500 series, 111, 1952.
30. Richardson and Jeffes; J. Iron and Steel Inst. 1952,
171, 165-175.
31. British Oxygen Co; Private communication.
32. Distillers Co. Ltd; Private Communication.
33. Honey Will and Stein Co; . Private communication.
34. Finchan; Thesis, University of London, 1952.
35. Finchan and Richardson; J. Iron and Steel. Inst. 1952, 172, 53.
36. Alcock and Richardson; Nature. 1951, 168, 661.
37. Dewing and Richardson; J. Iron and Steel Inst. 1960,
195, 56 - 58.
38. Mehta; Private communication.

39. Shigeo, Aramaki and Rustum Roy; J. Am. Ceramic Soc. May 1962, 239.
40. Tromel; "Physical Chemistry of Steel Making ". J. Willey and Sons. Inc., New York. 1958, 77 - 78.
41. Kozakevitch; Revue de Metallurgie, Fevrier, 1960, 57, 149.
42. Richardson and Jeffes; J. Iron and Steel Inst. 1948, 160, 267.
43. Richardson and Jeffes; Ibid. 1952, 171, 162.
44. Fisher and Spitzer; "Archiv, für das Eisenhüttenwesen" 29, 1958, 535.
45. Schenck, Froberg, Gammel; Ibid. 31 Jan. 1960, 11 - 17.
46. Taylor and Stobo; J. Iron and Steel Inst. 1954, 178, 360-367.
47. Rankin and Wright; Amer. J. Scie. 1915, (4)39, 1-79.
48. Coughlin; J. Am. Chem. Soc. 1956, 78, 5479 - 5482.
49. King; J. Phys. Chem. 1955, 59, 218 - 219.
50. Bennicksen; Ibid, 1955, 59, 220 - 221.
51. Rankin and Wright; Phase diag. for Ceramists, Columbus, Ohio, 1956, 48.
52. Baird and Taylor; Trans. Farad. Soc. 1958, 54, 527.
53. King; A. Amr. Chem. Soc. 1951, 73, 656 - 658.
54. Todd; Ibid., 32 77 - 3278.
55. U.S. Bur. Standard "Selected Values of Chemical Thermo-
dynamic Properties", circular 500, I, 1952.
56. Kelley; U.S. Bur. Mines. Bull. No. 477, 1950 Ibid No. 584, 1960.
57. Humphrey and King; J. Am. Chem. Soc. 1952, 74, 2041 - 42.
58. Benz and Wagner; J. Phys. Chem. 1961, 65, 1308 - 1311.
59. Torgeson and Sahama; J. Am. Chem. Soc. 1948, 70, 2156-60.
60. Wagner; Zeitschrift für Anorganische Und allgemaine chemie; 1932, 208, 1 - 22.

61. Krack and Neuvoneu. Private communication.
62. Orr; J. Am. Chem. Soc., 1953, 75, 528 - 529.
63. Hay, White and McIntosh; J. West. Scot. I.S.I. 1934, 42, 99.
64. Schutman and Ensio; Trans. A.I.M.E. 1951, 141, 401.
65. Richardson and Pillay; Trans. Inst. Min. Met. London.
1956-57, 66, 309.
66. Richardson and Webb; Trans. Inst. Min. Met. London.
1954-55, 64, 529.
67. Darken; J. Am. Chem. Soc., 1950, 72, 2909.
68. Liang, Bever, Floe; Trans. Am. Inst. Min. Met. Eng. 1946,
167, 395.
69. Richardson and Alcock; Acta Metallurgia, 1958, 6, 385.
70. Abraham and Richardson; "Phys. Chem. Proc. Metallurgy. A.I.M.E.
Interscience Publishers, 1959, Part I. p. 263.
71. Meadowcroft; Thesis, University of London, 1962.
72. Lumsden; Discussion Farad. Soc. "The Structure of Ionic Melts".
1962.
73. Meadowcroft; Private Communication.
74. Bishop, et al; J. Metals April 1953, 185.
75. Goodeve; Discussion Farad. Soc., 1948, 4, 9.
76. Quill (Editor); Chemistry and Metallurgy of Misc. Materials,
Thermodynamics, New York Mac Graw-Hill Book Co., New York,
1950.
77. National Bureau of Standards U.S.; "Selected Values of
Chemical Thermodynamic Properties;" Series II, 1947 - 1949.